Climate Assessment for 2000

Jay H. Lawrimore,* Michael S. Halpert,+ Gerald D. Bell,+ Matthew J. Menne,*
Bradfield Lyon,# Russell C. Schnell,@ Karin L. Gleason,* David R. Easterling,*
Wasila Thiaw,+ William J. Wright,& Richard R. Heim Jr.,*
David A. Robinson,** and Lisa Alexander++

ABSTRACT

The global climate in 2000 was again influenced by the long-running Pacific cold episode (La Niña) that began in mid-1998. Consistent with past cold episodes, enhanced convection occurred across the climatologically convective regions of Indonesia and the western equatorial Pacific, while convection was suppressed in the central Pacific. The La Niña was also associated with a well-defined African easterly jet located north of its climatological mean position and low vertical wind shear in the tropical Atlantic and Caribbean, both of which contributed to an active North Atlantic hurricane season. Precipitation patterns influenced by typical La Niña conditions included 1) above-average rainfall in southeastern Africa, 2) unusually heavy rainfall in northern and central regions of Australia, 3) enhanced precipitation in the tropical Indian Ocean and western tropical Pacific, 4) little rainfall in the central tropical Pacific, 5) below-normal precipitation over equatorial east Africa, and 6) drier-than-normal conditions along the Gulf coast of the United States.

Although no hurricanes made landfall in the United States in 2000, another active North Atlantic hurricane season featured 14 named storms, 8 of which became hurricanes, with 3 growing to major hurricane strength. All of the named storms over the North Atlantic formed during the August–October period with the first hurricane of the season, Hurricane Alberto, notable as the third-longest-lived tropical system since reliable records began in 1945. The primary human loss during the 2000 season occurred in Central America, where Hurricane Gordon killed 19 in Guatemala, and Hurricane Keith killed 19 in Belize and caused $200 million dollars of damage.

Other regional events included 1) record warm January–October temperatures followed by record cold November–December temperatures in the United States, 2) extreme drought and widespread wildfires in the southern and western Unites States, 3) continued long-term drought in the Hawaiian Islands throughout the year with record 24-h rainfall totals in November, 4) deadly storms and flooding in western Europe in October, 5) a summer heat wave and drought in southern Europe, 6) monsoon flooding in parts of Southeast Asia and India, 7) extreme winter conditions in Mongolia, 8) extreme long-term drought in the Middle East and Southwest Asia, and 9) severe flooding in southern Africa.

Global mean temperatures remained much above average in 2000. The average land and ocean temperature was 0.39°C above the 1880–1999 long-term mean, continuing a trend to warmer-than-average temperatures that made the 1990s the warmest decade on record. While the persistence of La Niña conditions in 2000 was associated with somewhat cooler temperatures in the Tropics, temperatures in the extratropics remained near record levels. Land surface temperatures in the high latitudes of the Northern Hemisphere were notably warmer than normal, with annually averaged anomalies greater than 2°C in parts of Alaska, Canada, Asia, and northern Europe.

*National Climatic Data Center, NOAA, Asheville, North Carolina.
+Climate Prediction Center, NCEP/NWS/NOAA, Washington, D.C.
#International Research Institute for Climate Prediction, Lamont-Doherty Earth Observatory, Palisades, New York.
@Climate Monitoring and Diagnostics Laboratory, NOAA, Boulder, Colorado.
&National Climate Centre, Australian Bureau of Meteorology, Melbourne, Australia.

**Department of Geography, Rutgers University, New Brunswick, New Jersey.
++Hadley Centre for Climate Prediction and Research, Met Office, Bracknell, United Kingdom.
Corresponding author address: Jay H. Lawrimore, National Climatic Data Center, NESDIS/NOAA, 151 Patton Avenue, Asheville, NC 28801-5001.
©2001 American Meteorological Society

Table of Contents

1. Introduction

This is the 11th in a series of annual climate assessments written to summarize the state of the earth's climate. It provides a comprehensive summary of the global climate system in 2000 with analyses of significant events and associated impacts that occurred in all regions of the globe. While this report should prove valuable as a record of the significant climate events and atmospheric dynamics that have influenced weather and climate during the past year, it also places the state of the earth's climate in historical perspective. The instrumental record provides evidence of a climate that is highly variable and a climate that is noticeably different than it was at the start of the last century. As such, this assessment includes recent analyses of trends in temperature, precipitation, and trace gases that are part of the global climate system.

Produced by the National Climatic Data Center for the first time, this assessment was developed through a cooperative effort that included scientists from the Climate Prediction Center, the Climate Monitoring and Diagnostics Laboratory, the Australian Bureau of Meteorology, the United Kingdom Met Office, the International Research Institute for Climate Prediction, and Rutgers University. Numerous data sources were used in the analyses contained within this report, including 1) land surface temperature and precipitation data from the Global Historical Climatology Network (Peterson and Vose 1997; Vose et al. 1992) and the United States Historical Climatology Network (Easterling et al. 1996), 2) surface temperature data from a land–sea blended dataset developed in the United Kingdom (Jones et al. 2001), 3) gridded analyses from the National Centers for Environmental Prediction–National Center for Atmospheric Research (NCEP–NCAR) Climate Data Assimilation System/ 50-Year Reanalysis (Kistler et al. 2001), 4) satellite data, and 5) ship reports. It should be noted that the large number of different data sources preclude the use of one standard base period.

Included in this report is a review of global climate variations, an examination of oceanic and atmospheric anomalies in the global Tropics and extratropics, an analysis of selected significant regional climate highlights, and a review of trace gases in the atmosphere. Section 2 contains an analysis of the Pacific cold episode (La Niña) that was present again in 2000. La Niña is discussed first in this year's assessment to emphasize the importance of the El Niño–Southern Oscillation (ENSO) on weather and climate throughout the world. Issues and trends related to global temperature and precipitation are addressed in section 3. Regional climate highlights are discussed in section 4, including a review of record heat, extreme drought, and destructive wildfires in the United States as well as an active North Atlantic hurricane season. There is also discussion of extreme winter weather in Mongolia, continuing drought in the Middle East and the Greater Horn of Africa, heavy rainfall and flooding in southern Africa and Southeast Asia, a deadly heat wave and drought in southern Europe, and strong storms in western Europe. A summary of significant events in South America and Australia is also part of this section.

In section 5, an assessment of various trace gas concentrations and trends is presented. This includes a discussion on the Antarctic ozone hole as well as atmospheric concentrations of carbon dioxide, methane, carbon monoxide, halocarbons, and stratospheric water vapor. As in previous assessments, the final section of this report contains seasonal maps of temperature anomalies, precipitation percentiles, and 500-hPa heights and anomalies, which are referenced throughout the report. While each section is essentially self-contained, there is frequent cross-referencing between sections.

2. Continuation of Pacific cold episode (La Niña)

a. Overview

Cold episode (La Niña) conditions again prevailed in the tropical Pacific throughout 2000, continuing the long-running episode that began in mid-1998. During this 2.5-yr period there has been considerable seasonal variability in the strength and extent of the accompanying oceanic and atmospheric anomalies (Fig. 1). These cold episode conditions have been strongest during the 1998–99, 1999–2000, and 2000–01 Northern Hemisphere (NH) winter seasons, followed by a weakening of the cold episode during the following NH spring seasons (Fig. 1c). The cold episode has been weakest during June–September (JJAS) 1999 and 2000 before subsequently reintensifying during October–December.

The evolution toward the 1998–2001 cold episode began over the central and eastern equatorial Pacific in early 1998, as 1) the oceanic thermocline (approximated by the depth of the 20°C isotherm) became shallower than normal, 2) the subsurface ocean temperatures dropped, and 3) the volume of anomalously

warm water accompanying the 1997–98 El Niño decreased and became increasingly confined to the near-surface region (Bell et al. 1999). These conditions set the stage for a rapid transition to below-normal sea surface temperatures (SSTs) over the central and east-central equatorial Pacific during the first week of May 1998, and the establishment of a mature cold episode by July 1998.

The periods of mature cold episode conditions during both 1999 and 2000 are indicated by the persistence of an anomalously shallow 20°C isotherm depth across the eastern equatorial Pacific (Fig. 1a), and below-average SSTs over the central equatorial
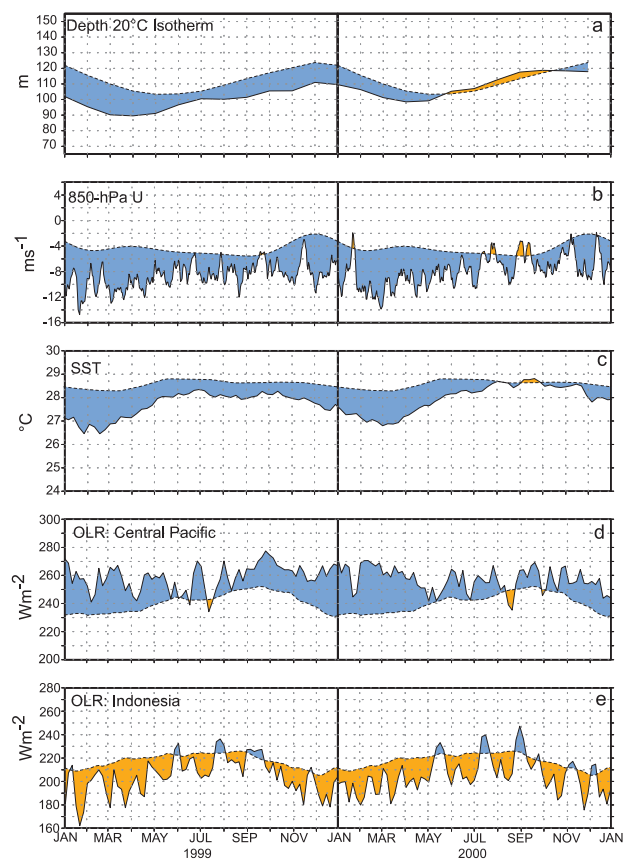

FIG. 1. Monthly time series of (a) the depth of the 20°C isotherm (m), (b) 850-hPa zonal wind speed (m s^{-1}), (c) SST (°C), (d) OLR (W m^{-2}) over the central Pacific, and (e) OLR (W m^{-2}) over Indonesia. Values are determined by averaging over the region bounded by 5°N–5°S and in (a) 180°–100°W, in (b) and (d) 150°E–150°W, in (c) 160°E–160°W, and in (e) 90°–140°E. The solid curve in all panels shows the monthly mean values and the dashed curve shows the climatological mean. The anomalies are shown shaded, with orange (blue) shading indicating positive (negative) anomalies, except for in (d) and (e) where the shading convention is reversed. The climatology and anomalies are computed with respect to the 1979–95 base period.

Pacific (Fig. 1c). Characteristic atmospheric features that accompanied these oceanic conditions throughout this period included 1) enhanced low-level equatorial easterly winds across the central and west-central equatorial Pacific (Fig. 1b), 2) suppressed tropical convection [indicated by positive anomalies of outgoing longwave radiation (OLR)] across the central and eastern equatorial Pacific (Fig. 1d), and 3) enhanced tropical convection (indicated by negative OLR anomalies) throughout Indonesia and the western Pacific (Fig. 1e).

In contrast, both JJAS 1999 and 2000 featured a return toward near-normal SSTs over the central equatorial Pacific (Fig. 1c) and a return to near-average depth of the oceanic thermocline over the equatorial Pacific (Fig. 1a). The low-level wind (Fig. 1b) and tropical convection anomalies (Figs. 1d,e) also weakened considerably during these periods. This return toward near-normal conditions was most pronounced during JJAS 2000.

The atmospheric anomalies during JJAS of both 1999 and 2000 also exhibited considerable intraseasonal variability in association with strong Madden–Julian oscillation (MJO) activity with a period of approximately 45 days. This MJO activity was particularly prominent during JJAS 2000, and contributed to periodic reversals in the sign of the low-level wind and tropical convection anomalies typically associated with the La Niña. In contrast, the reintensification of cold episode conditions during October–December of both 1999 and 2000 was accompanied by a strengthening and increased persistence of the La Niña–related atmospheric wind and convection anomalies, and by a corresponding reduction in the strength of the MJO.

b. Precipitation impacts

Many areas of the world experienced precipitation anomalies during 2000 (Fig. 2) that were consistent with past cold episodes (Ropelewski and Halpert 1989, also see section 3c). The largest and most persistent positive precipitation anomalies were observed over Indonesia, the eastern half of the tropical Indian Ocean, southeastern Asia, northern Australia, and the western and central subtropical South Pacific (area labeled South Pacific convergence zone). Above-average rainfall was also observed in the Amazon Basin and over southeastern Africa. This enhanced rainfall occurred during the rainy season in each of these areas, in association with a La Niña–related enhancement of the local monsoon system.

In contrast, significantly below-average rainfall was recorded over the central and west-central tropi-

cal Pacific throughout the year, in response to the La Niña–related suppression of tropical convection in that region. In the extratropics, the Gulf coast of the United States also experienced well below-average rainfall during the year, with the largest deficits occurring during January through July. This area has experienced long-term dryness beginning in late 1998 in association with the persistent La Niña episode.

c. Equatorial Pacific Ocean sea surface and subsurface temperatures

With the exception of JJA 2000 (Figs. 3e,f) the La Niña–related patterns of seasonal SSTs reflected an enhanced cold tongue extending westward from the west coast of South America to the vicinity of the date line (Figs. 3a,c and 3b,d). Accompanying this cold tongue was a westward retreat of the 28°C isotherm to near 160°E, which is 30° west of its climatological mean position near 170°W. The 28°C temperature represents the approximate threshold for deep tropical convection over the central equatorial Pacific (Gadgil et al. 1984), and the decrease in SSTs below this level was consistent with the persistent pattern of suppressed convective activity previously noted in this region.

This anomalous westward extension and strengthening of the equatorial cold tongue is further highlighted by a persistent pattern of below-average SSTs (more than 1.0°C below normal) across the central and eastern Pacific during both December-February (DJF) and March–May (MAM) (Figs. 3b,d). After diminishing during June–August (JJA), these negative SST anomalies reappeared during the September–November (SON) season (Figs. 3g,h), and by December 2000 SSTs again averaged more than 1°C below normal over the central equatorial Pacific (*Climate Diagnostics Bulletin,* December 2000, their Fig. T18). Farther west, the cold episode conditions were accompanied by anomalously warm SSTs (averaging 0.5°–1.0°C above normal) throughout the western tropical Pacific. Similar SST anomaly patterns also prevailed throughout the Pacific basin during the preceding mid-1998–99 period (Bell et al. 2000).

The subsurface temperature structure is a fundamental component of La Niña (and El Niño) episodes. An examination of the subsurface thermal structure during January–May 2000 indicates that the anomalously cold ocean temperatures extended down to approximately 175-m depth across the central and eastern equatorial Pacific (Figs. 4a,b), while anomalously warm ocean temperatures were evident over the western Pacific between approximately 50 and 400 m. These subsurface temperature anomalies reflected an increased slope of the oceanic thermocline, and resulted from the characteristic La Niña–related pattern of strong oceanic upwelling over the eastern half of the Pacific and increased downwelling over the western Pacific.
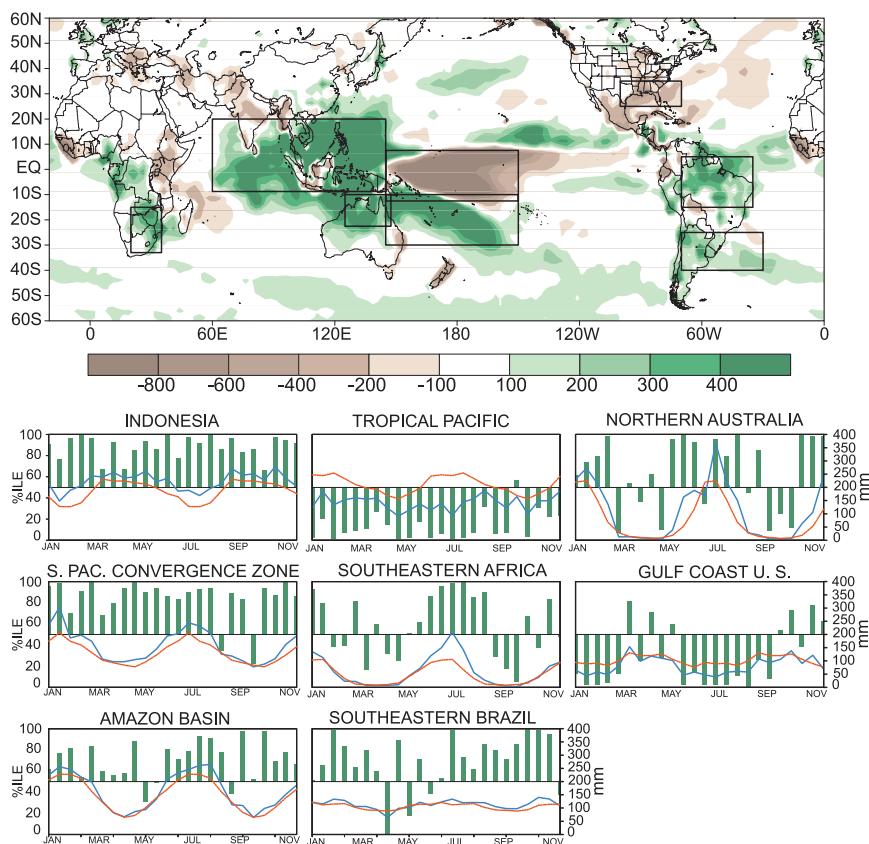
FIG. 2. January–December 2000 accumulated precipitation anomaly (top), and regional area-averaged estimates of monthly mean precipitation amounts (mm, blue lines) and precipitation percentiles (%, bars) during 2000 for the eight boxed regions shown in top panel. The monthly precipitation climatology (mm, dashed, red lines) is the 1979–95 base period monthly means. The percentiles are labeled on the left-hand vertical axis and totals are labeled on the right-hand vertical axis. Precipitation amounts are obtained by merging raingauge observations and satellite-derived precipitation estimates (Janowiak and Xie 1999).

FIG. 3. Seasonal SST (left) and anomaly (right) for (a), (b) DJF 1999–2000, (c), (d) MAM 2000, (e), (f) JJA 2000, and (g), (h) SON 2000. Contour interval is 1°C, with the 0.5°C anom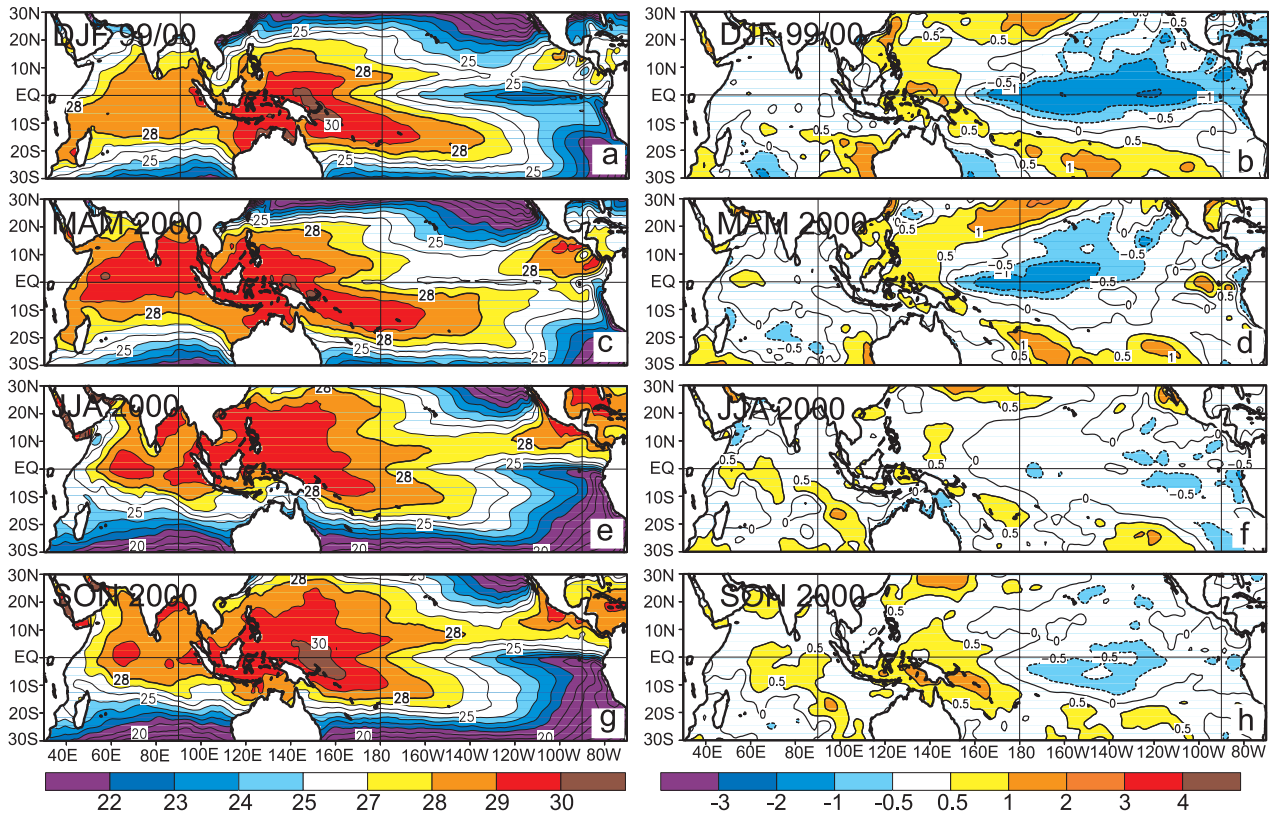aly contour included. Anomalies are departures from the 1961–90 adjusted optimal interpolation (OI) climatology (Smith and Reynolds 1998).

The weakening of the cold episode during JJA and subsequent strengthening during SON is also evident in the pattern of subsurface temperature anomalies (Figs. 4c,d, respectively), which indicate a disappearance of negative anomalies over the eastern Pacific during JJA, and a redevelopment of these anomalies
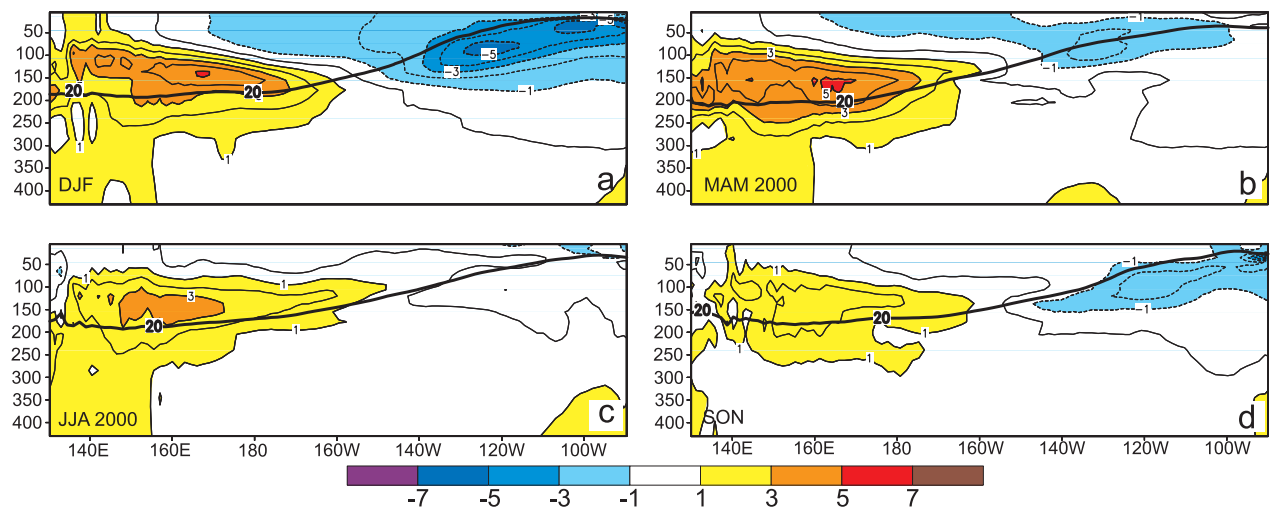

FIG. 4. Equatorial depth–longitude section of ocean temperature anomalies for (a) DJF 1999–2000, (b) MAM 2000, (c) JJA 2000, and (d) SON 2000. Contour interval is 1°C. The dark line is the 20°C isotherm. Data are derived from an analysis system that assimilates oceanic observations into an oceanic GCM (Behringer et al. 1998). Anomalies are departures from the 1983–92 base period means.

during SON. This reintensification of the cold episode was also consistent with the lack of an eastward progression of the anomalously warm water from the western to the eastern Pacific during the period.

d. Tropical convection

The distribution and intensity of tropical convection represents a primary forcing on the atmospheric circulation via its direct modulation of the wind and mass fields throughout the global Tropics and subtropics. During the La Niña episode, enhanced convection (indicated by negative anomalies of OLR shown in green) prevailed across the climatologically convective regions of Indonesia and the western equatorial Pacific (Fig. 5), and suppressed convection dominated the central Pacific (indicated by positive OLR anomalies shown in brown).

This overall pattern of anomalous equatorial convection was most pronounced during the DJF (Fig. 5a) and MAM (Fig. 5b) seasons, was less prominent during JJA (Fig. 5c) as the cold episode weakened, and then reintensified during SON (Fig. 5d). During DJF and MAM the monsoon systems over both southeastern Africa and the Amazon Basin (see sections 4c,e) were also enhanced, which contributed to enhanced convection and precipitation (Fig. 2) in these areas.

e. Atmospheric circulation

1) Pacific basin

Many of the prominent atmospheric circulation features that persisted throughout 2000 in the Tropics and subtropics were also common to the mid-1998–99 period, and to past Pacific cold episodes. These atmospheric anomalies were most pronounced during the DJF, MAM, and SON seasons and least pronounced during JJA. In the Tropics, the La Niña–related anomaly features included 1) upper-level westerly wind anomalies across the central and eastern Pacific (Fig. 5), 2) lower-level easterly wind anomalies across the central and western Pacific (Fig. 6), 3) enhanced ascending motion and convective activity over the western Pacific and Indonesia, and 4) anomalous descending motion and suppressed convective activity over the central Pacific. These conditions reflected an enhanced equatorial Walker circulation across the Pacific basin, a well-known feature of Pacific cold episodes.

In the meridional direction, the circulation featured anomalous equatorward flow in the upper troposphere over the central tropical Pacific (Fig. 5), as well as anomalous upper-tropospheric convergence and anomalous lower-level divergence (implied by the
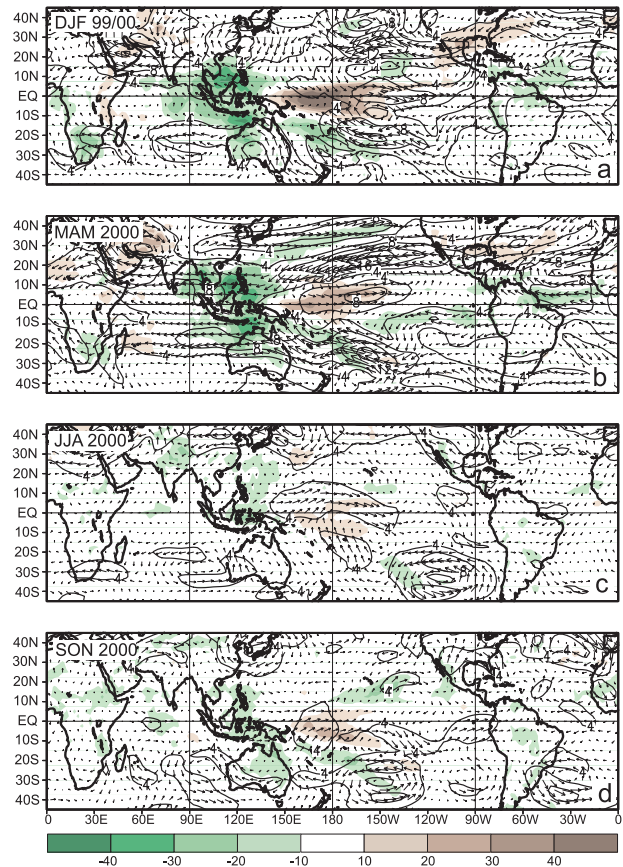

Fig. 5. OLR anomalies (shaded) and 200-hPa vector wind anomalies and isotachs for (a) DJF 1999–2000, (b) MAM 2000, (c) JJA 2000, and (d) SON 2000. Contour interval for isotachs is 4 m s^{-1}. Shading interval for OLR anomalies is 10 W m^{-2}. Anomalies are departures from the 1979–95 base period monthly means.

anomalous OLR pattern in Fig. 5). These conditions reflected a suppressed Hadley circulation, which is another well-known feature of Pacific cold episodes.

The above wind patterns were also consistent with cyclonic streamfunction anomalies [indicated by negative (positive) anomalies in the Northern (Southern) Hemisphere] in the subtropics of both hemispheres (Fig. 7), which flanked the region of suppressed tropical convection over the central and east-central Pacific. These cyclonic anomalies reflected an amplification of the mid-Pacific troughs in both hemispheres and a confinement of the low-latitude ridges to the heavy-convection region of the western Pacific and Australia (Fig. 7b).

2) Upper-tropospheric anticyclonic anomaly pattern in the subtropics

Outside the Pacific sector, upper-tropospheric anticyclonic circulation anomalies [indicated by positive
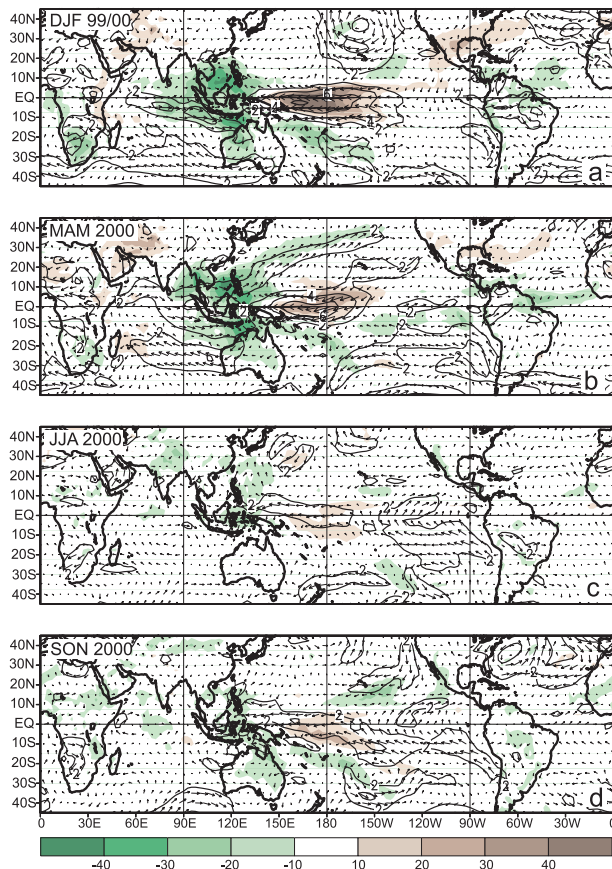
FIG. 6. OLR anomalies (shaded) and 850-hPa vector wind anomalies and isotachs for (a) DJF 1999–2000, (b) MAM 2000, (c) JJA 2000, and (d) SON 2000. Contour interval for isotachs is 2 m s⁻¹. Shading interval for OLR anomalies is 10 W m⁻². Anomalies are departures from the 1979–95 base period monthly means.

FIG. 7. Seasonal 200-hPa streamfunction (contours) and anomalies (shaded) during (a) DJF 1999–2000, (b) MAM 2000, (c) JJA 2000, and (d) SON 2000. Units are 1.0×10-6 m^2 s⁻¹. Contour interval is 10. In the Northern Hemisphere, positive (negative) values indicate an anticyclonic (cyclonic) circulation. In the Southern Hemisphere, negative (positive) values indicate a cyclonic (anticyclonic) circulation. Anomalies are departures from the 1979–95 base period means.

(negative) streamfunction anomalies in the Northern (Southern) Hemisphere] were also evident in the lower- and middle-latitudes of both hemispheres during December 1999–May 2000 (Figs. 7a,b). This global-scale anomaly pattern is the leading mode of atmospheric variability, and explains approximately 43% of the total interannual and interdecadal variance between 40°N and 40°S (Mo and Kousky 1993). It also explains approximately 60% of the local interannual and interdecadal variance in the vicinity of the subtropical ridges outside of the Pacific basin. This mode is strongly controlled by the ENSO cycle, with the pattern of tropical convection typical of La Niña conditions favoring the anticyclonic streamfunction anomalies shown in Figs. 7a,b. Similar anomaly patterns were also prominent throughout the mid-1998–99 period of cold episode conditions (Bell et al. 1999). This anomaly pattern was considerably weaker and

less coherent during JJA (Fig. 7c) and SON 2000 (Fig. 7d), before reemerging throughout the global subtropics in January 2001(*Climate Diagnostics Bulletin,* January 2001, their Fig. T22) as mature cold episode conditions became reestablished for a third consecutive DJF season.

3. Climate and global change issues

a. Surface temperature

Global surface temperatures are based on data from a network of more than 1000 land-based observing stations (Peterson and Vose 1997) and a blended sea surface temperature dataset derived from a combination

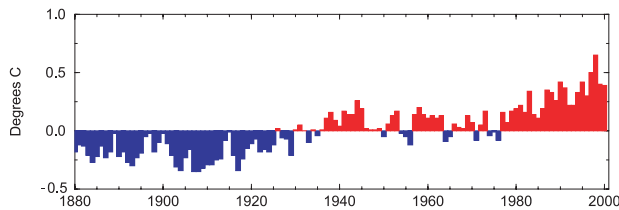FIG. 8. Global mean annual surface temperature anomalies (°C) 1880–2000. Anomalies are departures with respect to an 1880-1999 base period and include both land and sea surface temperature observations.

FIG. 9. Global mean monthly surface temperature anomalies (°C) 1991–2000. Anomalies are departures from a 1961–90 base period and include both land and sea surface temperature observations.

of satellite observations and ship and ocean buoy measurements (Reynolds and Smith 1994; Smith et al. 1996; Quayle et al. 1999). Preliminary analyses indicate that the 2000 mean global surface temperature was 0.39°C above the long-term (1880–1999) average, 0.01°C less than the 1999 average temperature, and 0.26°C less than the warmest year on record (1998).

The year 2000 was the sixth warmest since the start of the global record (Fig. 8). The 5 warmest years all occurred in the preceding 10 years and include, in decreasing order, 1998, 1997, 1995, 1990, and 1999. When viewed as a linear trend, mean global surface temperatures have warmed at a rate approximately 0.06°C per decade during the twentieth century. Since 1977, however, the rate of increase has been closer to 0.2°C per decade (Karl et al. 2000).

The close of the calendar year 2000 also brought an end to the decade of the 1990s (1991–2000). Monthly temperatures are frequently expressed as a departure from the monthly average for the 30-yr period preceding the current decade (WMO 1983). For the 1990s, this "normals" reference period was 1961–90. A graph of monthly temperature anomalies for the past decade calculated with respect to the 1961–90 base period (Fig. 9) illustrates the remarkable warmth of the 1990s. Average monthly temperatures rarely fell below the mean of the preceding 30 years. The virtually uninterrupted series of positive temperature anomalies peaked with a record high monthly anomaly in February 1998 during the height of the 1997–98 El Niño episode as part of an unprecedented string of record temperature anomalies. New monthly global temperature records were established each month from May 1997 through August 1998 (Karl et al. 2000).

Even though the Pacific cold episode persisted in 2000, globally averaged SSTs ranked as fourth warmest for the period 1880–2000 (Fig. 10a). However, the presence of cooler than average conditions across
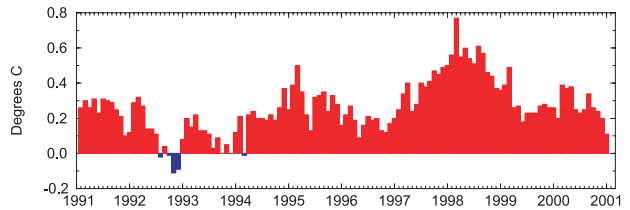
much of the tropical Pacific is reflected in the mean SST anomalies for the tropical latitude band 20°N–20°S. SSTs in this region were the 24th warmest, 0.18°C above the long-term mean (Fig. 10c). In contrast, SSTs averaged over the latitude bands 20°–90°N and 20°–90°S ranked as second and third warmest, respectively (Figs. 10b and 10d).

Globally averaged land surface temperatures were the sixth warmest in 2000 (Fig. 11a) with anomalous warmth most pronounced in the Northern Hemisphere. Land areas north of the equator were 0.75°C above the long-term mean (Fig. 11b), while temperatures in the Southern Hemisphere were only 0.14°C above average (Fig. 11c).

The geographic distribution of mean annual temperature anomalies, with respect to the 1961–90 base period, is shown in Fig. 12. Cooler than average SSTs

FIG. 10. Mean annual sea surface temperature anomalies (°C): (a) global, (b) 20°–90°N, (c) 20°S–20°N, and (d) 90°–20°S. Anomalies are departures from an 1880–1999 base period.

FIG. 11. Mean annual land surface temperature anomalies (°C): (a) global, (b) Northern Hemisphere, and (c) Southern Hemisphere. Anomalies are departures from an 1880–1999 base period.
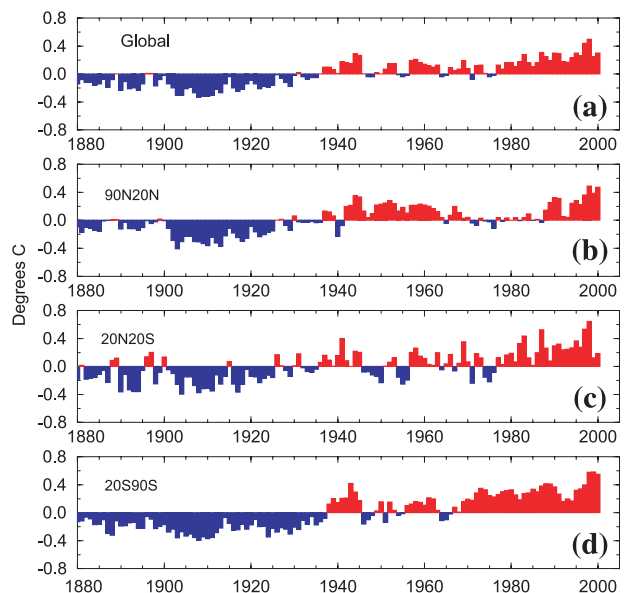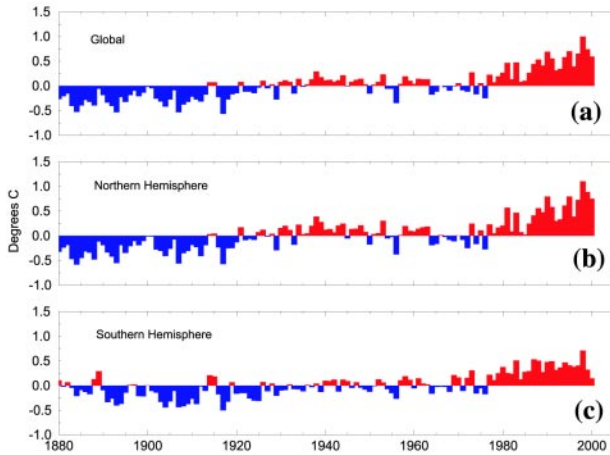

FIG. 12. Mean annual surface temperature anomalies (°C) for 2000. Anomalies are departures from a 1961–1990 base period.

were observed across much of the equatorial Pacific throughout the year. Although negative SST anomalies in this region moderated somewhat at midyear, a general decrease in SSTs occurred during the last few months of the year (Figs. 85, 87). Cooler than average SSTs also were present across portions of the Southern Ocean and off the west coast of North America.

Most of the earth's land surface experienced temperatures that averaged above the 30-yr mean in 2000, most notably in many areas of the mid- and high latitudes of the Northern Hemisphere. Positive anomalies were especially evident in these regions during boreal winter (DJF) and spring (MAM) when essentially all of North America and Eurasia were well above the seasonal average (Figs. 81, 83), in some areas by 4°C or more. This unusual warmth was associated with an anomalous large-scale circulation pattern featuring above-normal heights in the most anomalously warm regions (Figs. 82, 84).

While cooler than average temperatures replaced warmer conditions by year's end in some of these regions (Figs. 85, 87), the annual mean across most Northern Hemisphere land areas was above normal. Temperatures were approximately 1.3°C above normal in Europe, ranking as the warmest over the period of record. Annual mean temperatures across Southern Hemisphere land areas were characterized by smaller anomalies including regions of negative temperature anomalies in portions of western and northern Australia and Argentina. For the continent as a whole, South America averaged near its 1961–90 mean in 2000.
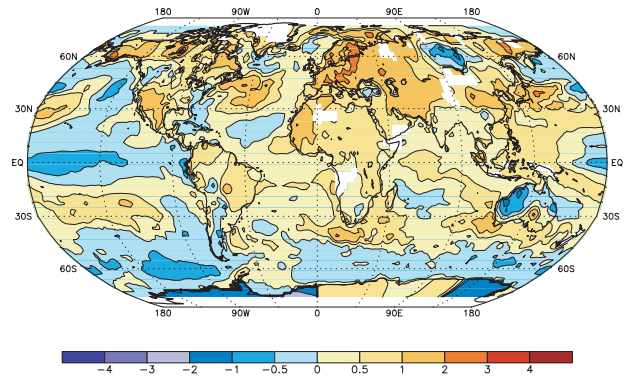
b. Tropospheric–stratospheric temperatures

1) TROPOSPHERE

Lower-troposphere temperature data were collected by the Microwave Sounding Unit (MSU) on NOAA's *TIROS-N* polar-orbiting satellites and adjusted for time-dependent biases by National Aeronautics and Space Administration and the Global Hydrology and Climate Center at the University of Alabama in Huntsville. Temperature estimates in the lower troposphere have been made since 1979 via channel 2R, which has a peak in its weighting function near 750 hPa (Spencer and Christy 1992). MSU estimates indicate global lower-troposphere temperatures remained slightly below average in 2000, 0.06°C less than the 1979–98 mean, similar to temperatures recorded in 1999 (Fig. 13). La Niña conditions, which were present throughout 1999 and persisted for much of 2000 (see section 2a), contributed to a global annual lower-troposphere temperature that was below the 20-yr average for the second year in a row.

To a first approximation the MSU 2R tropospheric temperature anomaly pattern (Fig. 14) is similar to the 1999 anomaly pattern (Bell et al. 2000) with both years reflecting the influence of La Niña conditions. Relatively cold temperatures characterize the global Tropics, except for the Near East through the Indian subcontinent. The lingering effects of the 2.5-yr La Niña are evident in that for 2000, the tropical third of the globe (20°N–20°S) was 0.29°C below the 1979–98 average. Temperatures were only slightly warmer than average from 30°N–30°S. In the Southern Hemisphere south of 30°S, lower-troposphere temperatures were near average to below average for the year. Similar to temperature patterns at the surface, lower-tropospheric temperatures were above average in the NH midlatitudes (+0.16°C), while the high latitudes

(60°–90°N) were the most anomalously warm, 0.51°C above average in 2000.

The presence of strong La Niña conditions early in the year clearly affected tropospheric temperatures in the equatorial eastern Pacific during January–June (Fig. 15a). A broad area of below-average temperatures, with some anomalies less than –1.0°C were measured in the eastern equatorial Pacific. Also evident are the affects of a weakening cold episode (in JJAS) on lower-troposphere temperatures in the July–December average (Fig 15b).

A prominent feature during the last six months of 2000 was a large area of much-above-average temperatures stretching from the Labrador Sea to Scandinavia. The largest anomalies were centered over Scandinavia and widely exceeded 2.0°C in association with above-average 500-hPa heights (Figs. 86, 88). Temperatures were notably warmer than normal during the last two months of the year. Consistent with the negative phase of the North Atlantic oscillation (NAO), above-average heights stretched from Greenland to the high latitudes of the North Atlantic (*Climate Diagnostics Bulletin,* December 2000). A pronounced southward shift of the mean North Atlantic jet stream accompanied this circulation pattern contributing to persistent above-average temperatures in the lower troposphere and at the surface (also see section 3a).

Record warm surface temperatures in the United States during the first half of 2000 (see section 4a) were also reflected in anomalously warm lower-troposphere temperatures during January–June. Temperatures remained anomalously warm throughout the first six months of 2000 and led to a 6-month year-to-date lower-troposphere anomaly over the United States of +1.04°C, the warmest January–June in the 22-yr MSU record.

The anomalously warm temperatures were associated with above-normal 500-hPa heights over the United States (Figs 82, 84). Circulation throughout much of the first half of 2000 featured below-normal heights across the high latitudes of the North Atlantic Ocean basins which reflected a positive phase of the North Atlantic oscillation, with the NAO index strongest in DJF 1999–2000. The strength and persistence of the positive phase of the NAO was a primary contributing factor to the record warmth.

The general agreement between lower-troposphere and surface temperatures in regions such as the United States and western Europe in 2000 is not clearly evident in all regions of the world when comparing surface and lower-troposphere anomaly patterns. There appear to be large differences between the troposphere (Fig. 14) and the surface temperature anomaly patterns (Fig. 12) in some regions. The lower-troposphere anomalies over the Tropics are negative while the surface anomalies are positive over most tropical land areas. A part of this apparent discrepancy can be attributed to the differences in base periods, 1961–90 for the land surface data, and 1979–98 for the MSU 2R. Since the global land surface temperatures for the 1961–78 period are relatively cold compared to the 1979–98 period, the land surface anomalies are positively biased compared to the MSU 2R anomalies.

However, differences in surface and lower-troposphere temperatures not explained by differing base periods are also evident in the 22-yr period
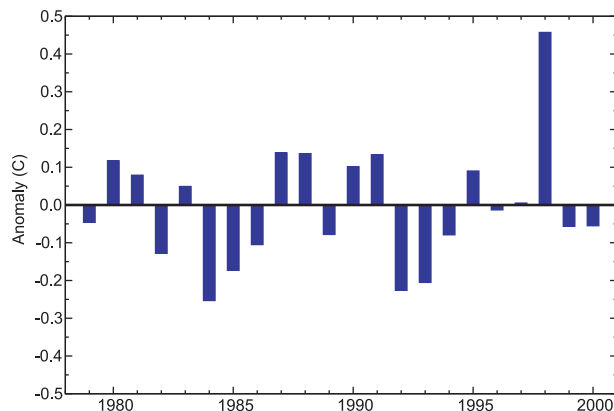
FIG. 13. Annual global-tropospheric temperature anomalies (°C) derived from the MSU channel 2R. Anomalies are departures from the 1979–98 base period means. (Data provided by the University of Alabama in Huntsville.)

FIG. 14. Annual tropospheric temperature anomalies (°C) during 2000, derived from channel 2R of the MSU. Anomalies are departures from the 1979–98 base period means. (Data provided by the University of Alabama in Huntsville.)

(a) **JANUARY–JUNE 2000**

(b) **JULY–DECEMBER 2000**

Fig. 15. Mean tropospheric temperature anomalies (°C) for (a) January–June 2000 and (b) July–December 2000 derived from the MSU channel 2R. Anomalies are departures from the 1979–98 base period means. (Data provided by the University of Alabama in Huntsville.)
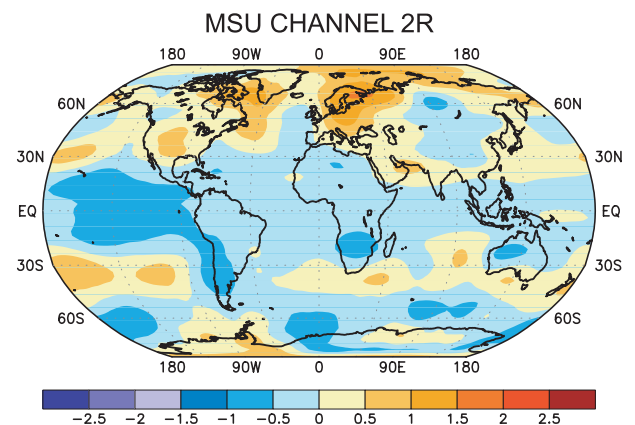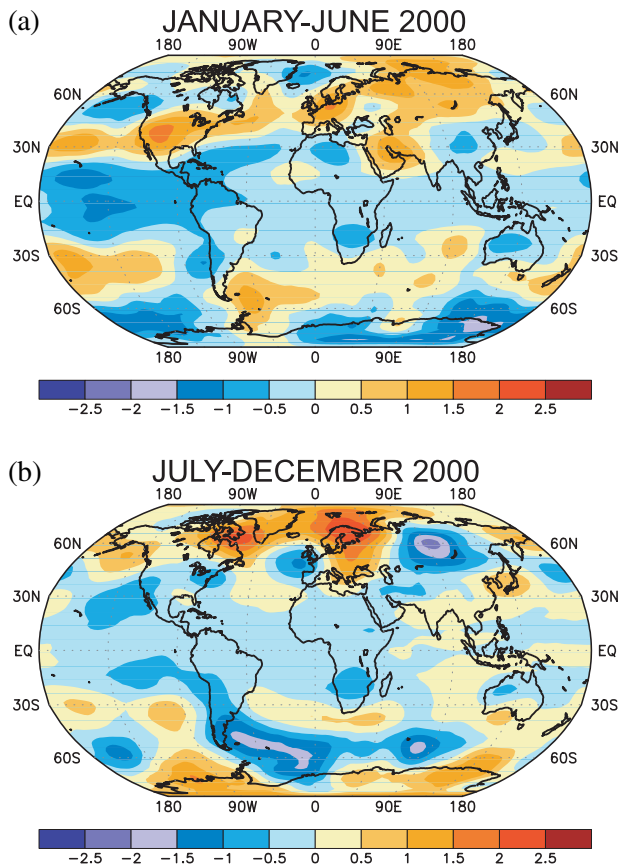
MSU–in situ record. The 1979–2000 global trend in lower troposphere temperature is only slightly positive (+0.04°C per decade), while global surface temperatures have increased more rapidly (+0.14°C per decade) during the same period. Regional comparisons of lower-troposphere and surface temperatures reveal good agreement in some parts of the world and differences in others. Figure 16 contains annually averaged anomalies and smoothed time series for several regions from 1979 to 2000 for the MSU lower-troposphere data as well as a blended dataset of land and sea surface temperatures (Jones et al. 2001).

Trends and year-to-year variability in lower-troposphere and surface temperatures are very similar in North America, Europe, and Australia. The 22-yr trends are identical in North America, and they differ by only 0.02°C per decade in Europe, with temperatures in the troposphere increasing at a slightly higher rate. Temperatures in Australia show little trend

in either dataset. There is also good agreement between the MSU-derived data and in situ data in regions not shown here such as the North Atlantic, South Atlantic, southwest Pacific, and eastern Russia and Alaska.

But while year-to-year temperature variations are similar in central Asia, with increasing surface and lower troposphere trends throughout the period, the surface temperature trend is almost twice as large as the temperature increase in the lower troposphere. There is little or no trend in the MSU-derived temperatures in Africa and Arabia as well as in South America, but the in situ trends are significantly different than zero in these two regions: +0.20°C per decade and +0.12°C per decade, respectively. Trends in the tropical east Pacific differ, but neither trend is significantly different than zero. Trends in other regions, not shown here, such as the southeast Pacific, Indian Ocean, Antarctica, and the tropical west Pacific, also differ.

Although the reasons for these differences cannot yet be fully explained, possible causes include low in situ sampling density in some regions, possible discontinuities in the satellite record, and real differences between temperature trends at the two levels (National Research Council 2000). Real differences in temperature trends may be due to influences that create differences most notable during the relatively short 22-yr sampling period. The decoupling of surface and lower-troposphere temperatures due to temperature inversions, variations in circulation that have a greater influence on surface temperatures in some regions, and differences attributable to the effects of ENSO and volcanic emissions have all been suggested as possible explanations. As the length of the two time series increases during the coming decades, any naturally occurring fluctuations that may create regional differences between lower troposphere and surface temperatures in the short term may average out when viewed within the context of a time series two or three times as long (National Research Council 2000).

2) Lower stratosphere

Lower-stratospheric temperatures are measured from MSU channel 4, which has a peak in its weighting function from 70 to 100 hPa. The estimated global lower stratosphere temperature in 2000 was 0.60°C less than the 1984–1990 average, the second coldest temperature in the 22-yr record (Fig. 17). After small increases in the two years following the record coldest year of 1996, temperatures cooled to near-record levels again in 1999 and 2000.
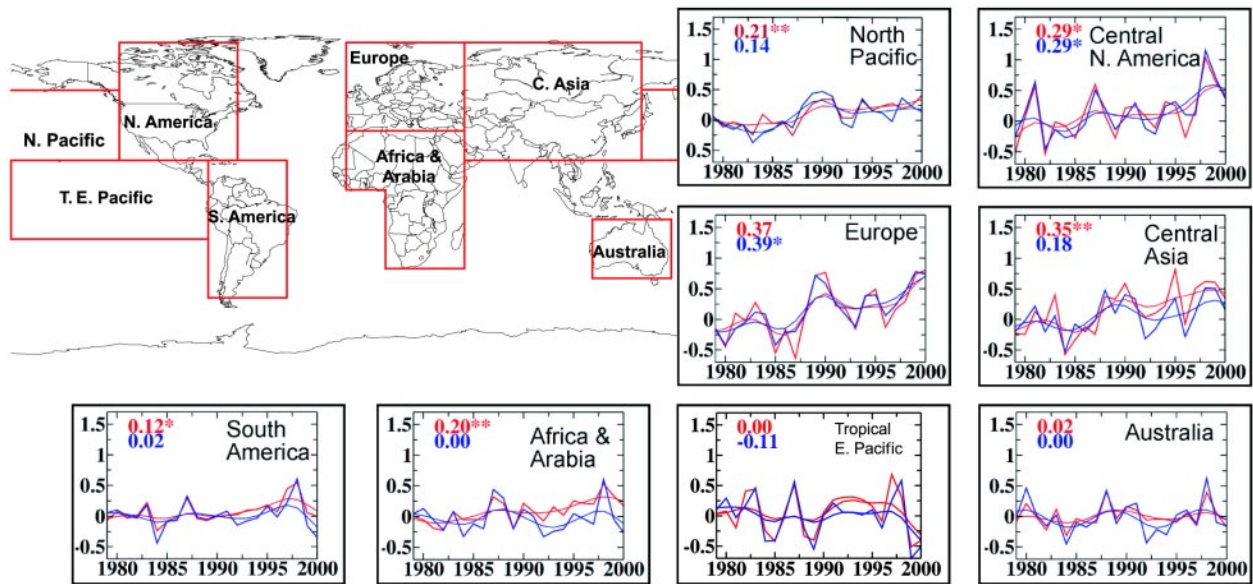
FIG. 16. Annual temperature anomalies and smoothed time series for land surface (red lines) and lower troposphere (blue lines). Decadal trends are indicated in upper-left-hand corner. Trends significant at the 95% confidence limit are indicated by asterisks, and trends significant at 99% are indicated by double asterisks. [Surface anomalies were calculated from Jones et al. (2001) and lower-troposphere anomalies were provided by the University of Alabama in Huntsville.]

Temperatures have remained below average in each of the past eight years with above-average temperatures recorded only in the years heavily influenced by the volcanic eruptions of Mount Pinatubo (1991) and El Chichón (1982). An increase in temperature was observed immediately after these eruptions, followed by a rapid decrease in temperature. Although year-to-year changes in stratospheric temperature are partly determined by natural changes in the environment, the large decrease in stratospheric temperatures observed during the 22 years of satellite record are consistent with the expected effects from increasing atmospheric concentrations of carbon dioxide and water vapor as well as decreases in stratospheric ozone (Houghton et al. 1995).

Stratospheric temperatures were well below average in most regions of the world with the largest negative anomalies recorded in the high-latitude regions of the Northern Hemisphere and middle latitudes of both hemispheres. But although annually averaged temperatures were below average, warmer-than-average conditions were generally observed in the Tropics during the first six months of the year (Fig. 18a). Temperatures in the 20°N–20°S latitude band were +0.34°C above average during the January–June period. The largest and most widespread positive anomalies were recorded in the eastern half of the tropical Pacific in association with La Niña conditions, which persisted through much of

the first half of 2000 (see section 2a). Average stratospheric temperatures in the eastern equatorial Pacific were less typical of a La Niña episode (see Bell and Halpert 2000, their section 3) during the last half of the year (Fig. 18b). The July–December average temperature in the Tropics was 1.23°C below average, the coolest such 6-month period on record.

In contrast, much warmer-than-average stratospheric temperatures were observed over Antarctica during July–December. Unlike recent years, when
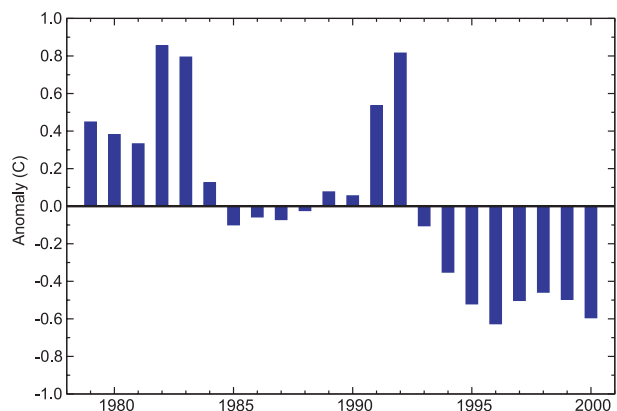

FIG. 17. Annual global-stratospheric temperature anomalies (°C) derived from the MSU channel 4. Anomalies are departures from the 1984-90 base period means. (Data provided by the University of Alabama in Huntsville.)

temperatures were from 3° to 6°C below the 1984–90 average during October and November, temperatures in 2000 were as much as 4.8°C above average (Fig. 19). The warmer-than-average temperatures were associated with an atypical early end to the Antarctic ozone hole in 2000.

Temperatures in the lower stratosphere are closely coupled to ozone through dynamics and photochemistry. For each of the past five years, October–November temperatures have been below average across Antarctica, favoring the persistence of the polar vortex and polar stratospheric clouds (PSCs) that act to deplete Antarctic ozone. Polar stratospheric clouds lead to ozone depletion by enhancing the production and lifetime of reactive chlorine.

The polar vortex and the area of very cold air were both large and developed early in the Southern Hemisphere winter of 2000 (JJA). But the anomalously warm stratospheric temperatures rose above the criti-cal PSC temperature (less than −78°C at 70 hPa) in October and were also associated with a significant reduction in the magnitude and areal extent of the polar vortex in October and November (*Climate and Diagnostics Bulletin,* October 2000). These factors led to an earlier end to the Antarctic ozone hole in 2000 (also see section 5a).

c. Global precipitation

Globally averaged annual precipitation over land areas was 3.9% above the 1961–90 mean making 2000 the third wettest year on record. As in 1999, precipitation patterns were influenced to a great degree by La Niña teleconnections (see section 2b). Unusually wet conditions prevailed in the western tropical Pacific westward into the Indian Ocean in association with La Niña. Parts of southern Africa and most of South America received above normal precipitation, and heavy monsoonal rainfall in Southeast Asia led to the worst flooding in decades. Much of central and northern Europe also received unusually heavy annual rainfall amounts in 2000 (see sections 4d and 4e).

Many areas of the world suffered from drought conditions in 2000, including much of southeastern Europe, the Middle East, and an area stretching from central Asia through northern China. Drought conditions also prevailed over parts of eastern Africa, and into and around the western Indian subcontinent. In the United States, the persistence of warmer and drier-than-normal conditions in southern and western areas of the country led to one of the worst wildfire seasons in over 50 years (see sections 4a–d).
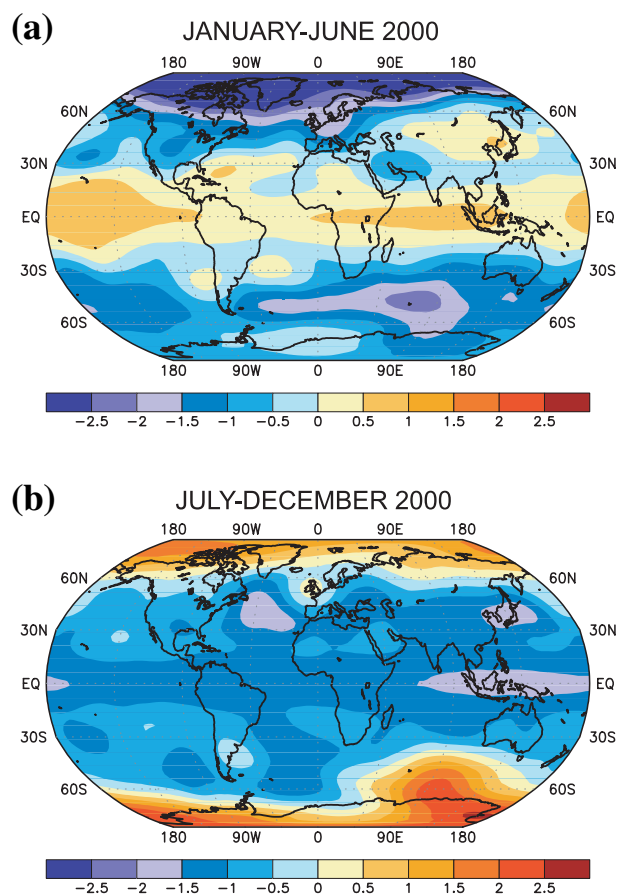
Fig. 18. Mean stratospheric temperature anomalies (°C) for (a) January–June 2000 and (b) July–December 2000 derived from the MSU channel 4. Anomalies are departures from the 1984–90 base period means. (Data provided by the University of Alabama in Huntsville.)
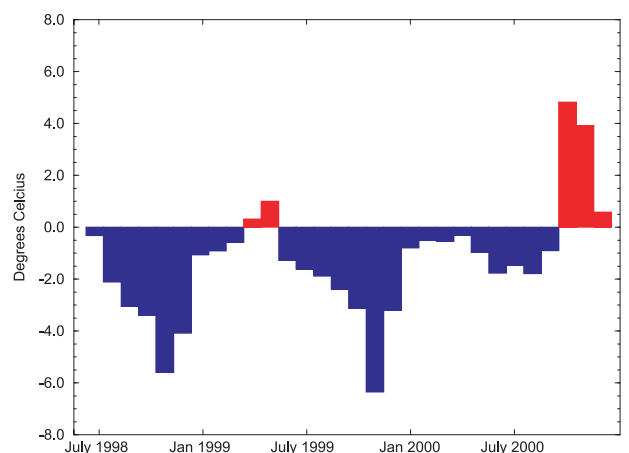
Fig. 19. Monthly lower-stratospheric temperature anomalies (°C) for the polar region (60°–90°S) derived from the MSU channel 4. Anomalies are departures from the 1984–90 base period means. (Data provided by the University of Alabama in Huntsville.)

Precipitation totals averaged within latitude bands and displayed as percent departures from normal illustrate regional differences in annual precipitation (Figs. 20a–f). In the high latitudes of the Northern Hemisphere (85°–55°N) annual precipitation was the second highest on record, exceeded only by totals measured in 1990 (Fig. 20a). Above normal precipitation was also recorded in the Tropics (10°N–10°S), the Southern Hemisphere (SH) subtropics (10°–30°S) and the SH midlatitudes (30°–55°S) (Figs. 20d–f). The continuing influence of La Niña contributed to above-normal precipitation in east equatorial areas of South America as well as the western equatorial Pacific contributing to an average in the Tropics that was 7.1% above normal. The largest average anomaly occurred in the SH subtropics, where precipitation was more than 15% above average. Heavy rainfall, much of it associated with tropical cyclones, fell across the northern half of Australia as well as parts of southern Africa. Precipitation was also above normal in parts of the subtropical areas of South America (see sections 4c and 4f and Figs. 81, 83, 85, 87).

Conversely, precipitation was slightly below normal in the NH midlatitudes (55°–30°N) and NH subtropics (30°–10°N). Drier-than-normal conditions in the southern United States, southern Europe, and the Mediterranean as well as parts of Asia contributed to an average anomaly that was 2.6% below normal in the NH midlatitudes. Precipitation in the NH subtropics averaged 2.3% below normal.

Precipitation totals averaged within latitude bands also reveal notable long-term trends, particularly north of 30°N (Fig. 20). As the climate changes, particularly if it warms appreciably, it is expected that the hydrologic cycle will also change, in part due to an increase in the water-holding capacity of the atmosphere (Houghton et al. 1995). The increase in temperature observed over the past century can be associated with a change in the hydrologic cycle, which has led to an increase in precipitation in many mid- and high-latitude regions of the world with instances of drier than normal conditions in some

regions. Rates of increase on the order of 10% and 5% per century occurred since 1900 in the 85°–55°N and 30°–55°N latitude bands, respectively (Figs. 20a,b). There is also evidence to suggest that much of the increase in mid- to high-latitudes arises from increased autumn and early winter precipitation in much of North America (Groisman and Easterling 1994) and Europe (Houghton et al. 1995).

Although changes in precipitation have not been uniform, there has been an increase in mid- to high-latitude precipitation and a notable decrease in sub-tropical precipitation during the twentieth century (Fig. 21). There are sometimes large, but spatially consistent, patterns of decrease across the tropical and subtropical regions, and increases in most other areas. Some of the largest tropical decreases have occurred in the Sahel region in Africa contributing to long-term drought from the 1960s to the mid-1990s. This region, however, has seen an increase in precipitation in the most recent years to a level approximately that of the twentieth century average.
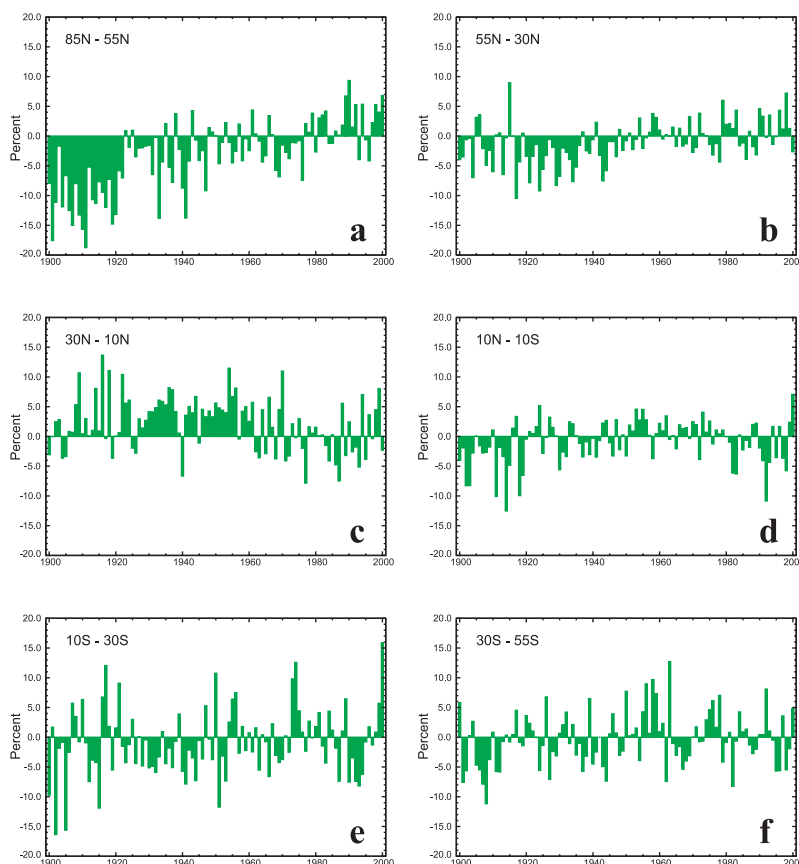

FIG. 20. Annual in situ precipitation anomalies within six latitude bands as percent departures from the 1961–90 average. (Source: Global Historical Climatology Network.)
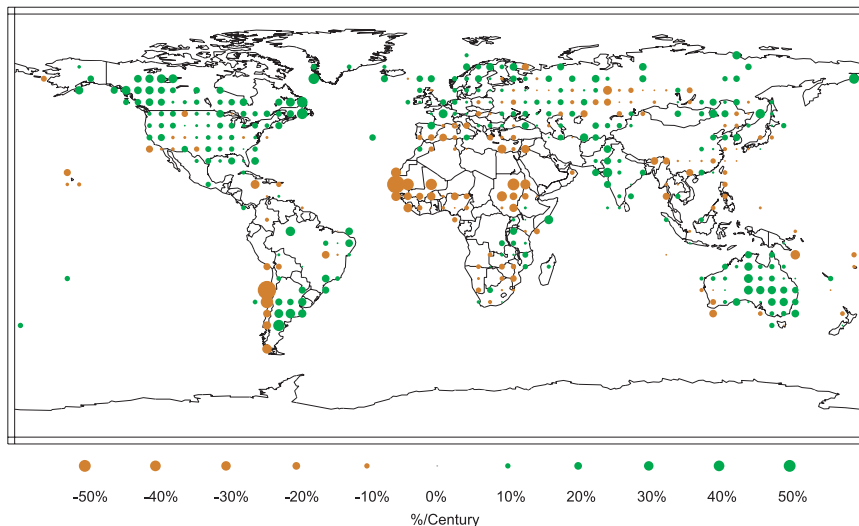
FIG. 21. Annual in situ precipitation trends during the twentieth century. Precipitation anomalies in physical units were calculated for each station based on 1961–90 normals and averaged into 5° × 5° grid cells. Calculation of grid cell trends required at least 66% of the years without missing data and at least 3 yr of data within each decade except the first and last. (Source: Global Historical Climatology Network.)

d. Northern Hemisphere snow cover

Annually averaged Northern Hemisphere snow cover extent was below average for the fourth consecutive year in 2000, continuing a pattern of reduced hemispheric snow cover that began in the late 1980s. Hemispheric snow cover was the fourth least extensive in the 31 years of reliable records and was below the 1966–2000 mean in every month except September and November (Fig. 22). (A total of 12 months were missing from the 1968–71 period, requiring the omission of these years from the computation of the annual values.) Eurasian snow cover extent in 2000 was below the long-term mean in all months except January and the September–November period, while snow cover extent over North America (including Greenland) was below average in all months except September. This low snow cover extent coincided with annually averaged temperatures that were above normal in much of North America and Eurasia (see section 3a).

A reanalysis of satellite data has been applied by Robinson (2000) to extend the record of snow cover extent back to November 1966 (Robinson et al. 2001). On average, Northern Hemisphere snow cover extent, including the Greenland ice sheet, is greatest in January (46.6 million km²) with a minimum in August (3.7 million km²). Snow covers more than 33% of lands north of the equator from November to April, reaching 49% coverage in January. In midwinter,

approximately 60% of the continental snow cover lies in Eurasia. Only portions of glaciers and the Greenland ice sheet remain snow covered throughout the year.

From year to year, Northern Hemisphere January snow cover may vary by 8 million km². October cover has varied by 13 million km² and April snow cover by almost 8 million km². Monthly standard deviations range from 1.0 million km² in August to 2.7 million km² in October. The largest monthly anomaly, 8.3 million km², was observed in October 1976.

Snow cover extent during the past 15 years has generally been less than in the preceding 20 years (Fig. 22). Between 1967 and 1987, annual averages of snow cover extent varied near a mean of 26.1 million km². An abrupt transition occurred between 1986 and 1988, and in the ensuing 13 years the mean annual extent has averaged 24.6 million km², a difference significant at the 99% level (using a standard t-test). This decrease in snow cover coincides with a recent rapid rise in global temperatures (see section 3a). Eight of the 10 warmest years on record have occurred since 1990, with the 10 warmest years all occurring since 1983.

Recent decreases in snow cover extent are largest during the late winter to early summer, while fall and early- to midwinter extents show no statistically significant change (Figs. 23a–d). The tendency to less late-season cover in recent years begins in February. Although February snow cover extent exceeded January's values in 8 of the first 20 years of record, this has occurred only once in the past 14 years (Fig. 24). This is consistent with a trend to earlier dates of the last spring freeze as well as reductions in the number of frost days in the MAM season (Easterling 2001, manuscript submitted to *Bull. Amer. Meteor. Soc.*).

A gradual return to conditions of the first 20 years of record appeared to be occurring with a short-term peak in 1995. Since then, snow cover extent has returned to levels observed between 1988 and 1994. These trends have been recorded over both the Eurasian and North American continents. Reductions in

snow cover since the late 1980s occurred over both continents, although larger departures occurred over Eurasia in the early portion of this period, while the opposite has occurred during the last several years.

The decreasing trends observed in the satellite snow cover record are also evident in northern Alaska in situ snowmelt data. The date of snowmelt at the National Oceanic and Atmospheric Administration (NOAA) Climate Monitoring and Diagnostics Laboratory (CMDL) Baseline Observatory in Barrow, Alaska, has been monitored for 35 years, roughly the same period as the satellite snow cover data. Ancillary melt-date data are available, although for shorter periods, from six other North Slope Alaska sites. These data include proxy records from Isaktoak (fowl breeding dates) and Cooper Island (ice melt dates). Analysis of yearly data indicates that these proxy records are correlated with each other and with the Barrow Baseline Observatory data suggesting that snowmelt and icemelt are influenced similarly by variations in climate.

All sites but one (Franklin) show a decreasing linear trend in melt date (Fig. 25). The dashed curve in Fig. 25 represents an ensemble average of all observations normalized to the timing of the Barrow melt. A linear fit of this aggregated station-year record shows an advance in the spring melt of 8 days ±4 days over the 35-yr period (confidence level = 95%) suggestive of a regional trend. The melt tends to progress from the more southerly locations of the Kuparuk River water-

shed, northward toward the coast (e.g., Barter Island), with the latest melt date in the vicinity of Barrow.

The advance in the snowmelt date in northern Alaska is attributed to a combination of an Arctic warming trend (Stone 1997) and changes in synoptic patterns over the past three decades that have diminished winter snowfall and favored warmer conditions in spring (Stone et al. 2001, manuscript submitted to *J. Geophys. Res.*). Brown and Braaten (1998) also attribute decreases in snow cover over northern Canada to major shifts in atmospheric circulation. It is possible these shifts may be related to changes in the Arctic oscillation (Thompson and Wallace 1998).

4. Regional climate highlights

a. North America

1) UNITED STATES TEMPERATURES

The United States experienced its warmest winter and second warmest spring on record in 2000 as above-normal temperatures prevailed across much of the country. Much warmer-than-normal temperatures (top 10% of the historical distribution) covered 20% of the country in January, 50% in February, and more than
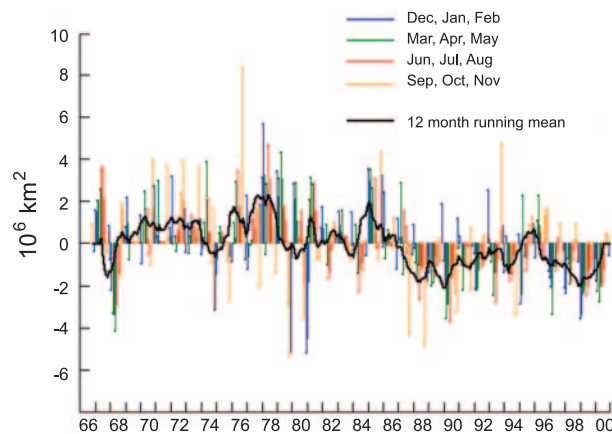
FIG. 22. Anomalies of monthly snow cover extent over Northern Hemisphere lands between November 1966 and December 2000. Also shown are 12-month running anomalies of hemispheric snow extent, plotted on the seventh month of a given interval. Mean hemispheric snow extent is 25.5 million km² for the full period of record. Period of record means were used for missing months (between May and October) in the late 1960s to create a continuous time series from 1966 to the present.
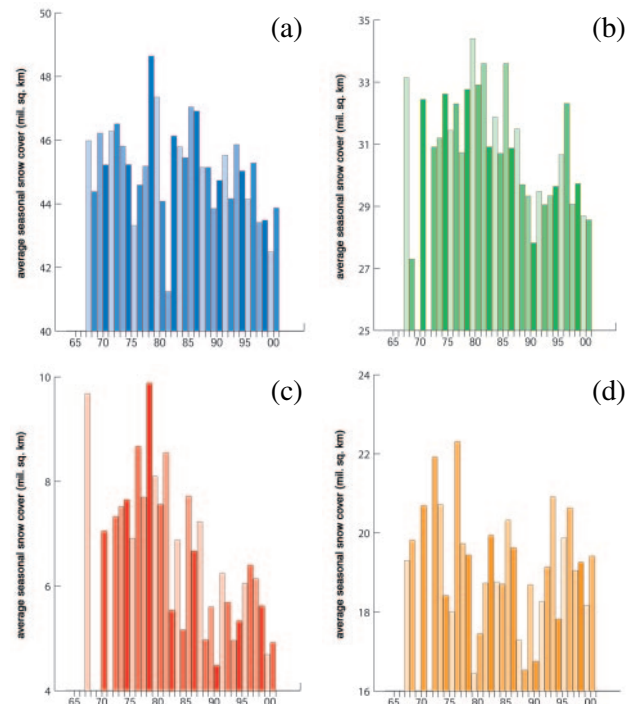
FIG. 23. Extent of (a) winter (DJF), (b) spring (MAM), (c) summer (JJA), and (d) autumn (SON) seasonal snow cover over Northern Hemisphere lands (including Greenland) from the winter of 1966–67 through the autumn of 2000.
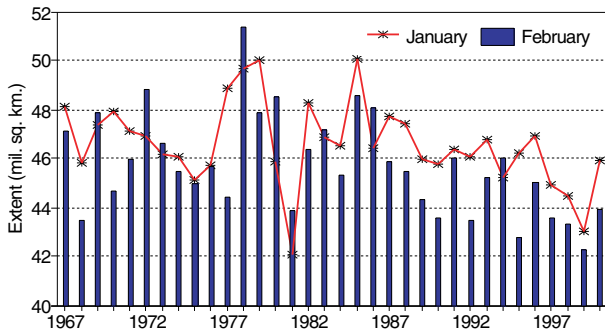
FIG. 24. Extent of January (line) and February (bars) Northern Hemisphere snow cover, 1967–2000.

20% of the country in four of the next six months (Fig. 26) in association with above-normal 500-hPa heights (Figs. 82, 84). Although a persistent trough brought cooler-than-normal conditions to much of the midwest and northeast in June and July, above-normal temperatures persisted in the southern and western United States. As the year progressed, each year-to-date period from March through October (e.g., January–March, January–April, etc.) was the warmest such period in the past 106 years.

The string of record-breaking temperatures came to an abrupt end in November as a deep trough developed over much of the United States bringing cold Arctic air from Canada to the Gulf coast behind a series of strong cold fronts. In stark contrast to the first 10 months of the year, approximately 50% of the country experienced very cold temperatures in both November and December (Fig. 26).

The 2-month period of record-breaking cold temperatures began with an amplification and westward extension of the mean ridge axis across Canada. A pronounced southwestward extension of the mean Hudson Bay trough into the southwestern United States and northern Mexico brought arctic air to much of the nation in November. The eastern two-thirds of the country remained much colder than average in December as the 500-hPa amplified ridge stretched from the extreme western United States to northern Siberia. A very strong surface pressure ridge accompanied this upper-level feature, extending from the central United States to northern Siberia. As this ridge persisted for several weeks, bitterly cold air from northern Siberia continued to flow into Canada and the central and eastern United States (*Climate Diagnostics Bulletin,* November and December 2000).

Very cold temperatures had not covered more than 50% of the United States since 1992 and back-to-back months of very cold temperatures had not occurred since 1976. The two-month arctic outbreak made the November–December 2-month period the coldest such period on record in the United States. For the year, the average temperature in the United States was 54.0°F, the 13th warmest year in the past 106 years.

2) UNITED STATES DROUGHT AND WILDFIRES

Drought conditions often occur as a result of an extended period of below-normal precipitation and
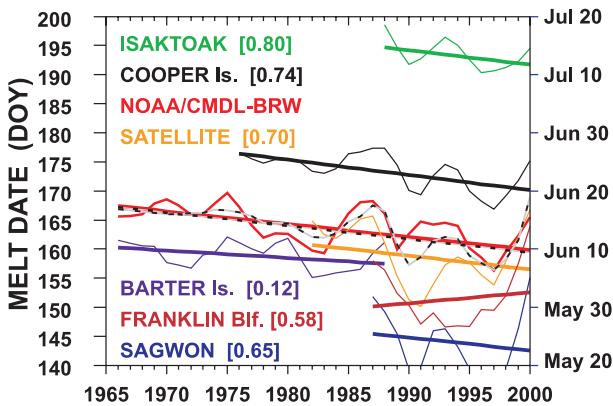

FIG. 25. Snowmelt dates for seven sites along the Alaska North Slope from 1965 to 2000. Yearly data were analyzed to determine trends and correlation coefficients (in brackets), but only 5-yr-smoothed data are presented here. The upper two curves are proxy records. Analysis of yearly data indicates that these proxy records are correlated with each other and with the Barrow Baseline Observatory data suggesting that snowmelt and icemelt are influenced similarly by variations in climate. The series labeled "Satellite" was derived from visible satellite images of a strip of tundra about 150 km south of Barrow.
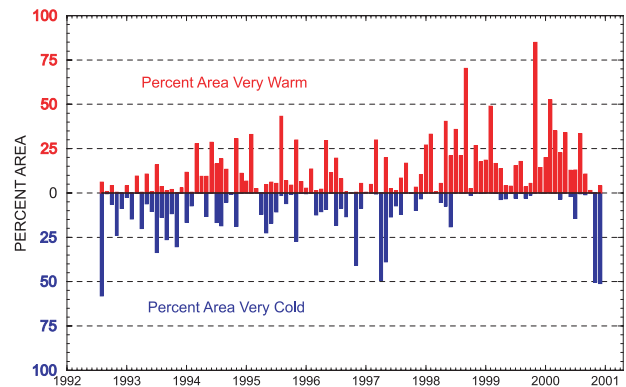

FIG. 26. The percent area of the contiguous United States very warm (upper 10 percentile) and very cold (lower 10 percentile) from August 1992 through December 2000, based on climate division data. The percentiles for each division for each of the 12 calendar months were computed based on data from 1895 through 2000.

above-normal temperatures. Under the continuing influence of La Niña (see section 2), the Gulf coast states endured precipitation deficits for much of the past 2.5 years. Above-normal temperatures also covered much of the United States during this time, most notably in the western half of the country.

The year began with drier-than-normal conditions in the southeastern and western United States. December 1999–February 2000 precipitation totals were below normal to much below normal from the mid-Atlantic states across the southern states and into the Southwest (Fig. 27). Temperatures in California, Nevada, Utah, Arizona, and Colorado averaged from 2° to 4°C above the long-term mean.

Approximately 16% of the country suffered from drought conditions at the beginning of the year, but by August nearly 36% of the country experienced severe to extreme drought conditions, with the largest expansion of drought occurring during the months of June and July. Evaporation during the summer months typically exceeds precipitation in much of the United States. Areas that are already drier than normal at the beginning of the warm season are susceptible to worsening drought conditions throughout the summer months. Although the areal extent of the 2000 drought was not as large as the droughts of the 1930s or 1950s, it is comparable to the 1988 and 1976–77 droughts (Fig. 28).

Hot and dry conditions, combined with low relative humidity and dry thunderstorms, led to thousands of wildfires across the West and Southwest in July and August. Wildfires also had a significant impact along the Gulf coast states, including Texas and Florida. According to the National Interagency Fire Center more than 92 000 wildfires consumed approximately 7.4 million acres across the nation, the most acreage burned in the United States since 1988.

By the end of the year, sufficient precipitation had fallen in many parts of the country to alleviate much of the extreme drought and wildfire threat. Exceptions included the southeastern United States, which remained drier than normal. Heavy precipitation across much of the country during SON resulted in a significant decrease in the areal extent and intensity of the drought, reducing the area affected to about 6% of the contiguous United States by the end of November.

(i) The West Coast, Rocky Mountains, and Texas

Severe long-term drought conditions were confined to southern areas of California and Arizona as
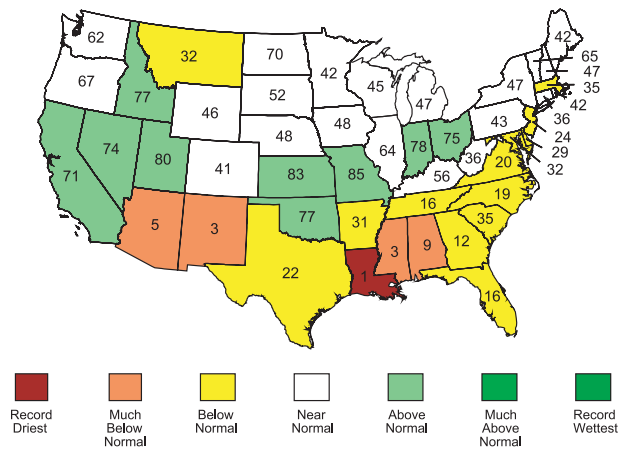
FIG. 27. Statewide rankings of precipitation totals during the winter of 2000 (December 1999 through February 2000). A rank of 1 represents the driest period since 1896. Much-below-normal precipitation is defined as occurring in the lowest 10 of recorded years, which corresponds to a range of ranks from 2 to 10. Below-normal precipitation is defined as occurring in the driest third of recorded winters, or between ranks 11 and 35. Much above normal is likewise the wettest 10 winters while above normal is defined as the remainder of the wettest third of the distribution.

well as west Texas in January. The combination of an early end to the region's monsoon rains the previous August and almost no precipitation since August contributed to extremely dry conditions in the southwestern United States. The drought widened in MAM and JJA 2000 as temperatures remained well above average and precipitation totals were near- to below normal.

For the January to August 2000 period, New Mexico, Utah, and Texas set a record for the warmest such period over the past 106 years (Fig. 29). Many other states came close to setting new records for this
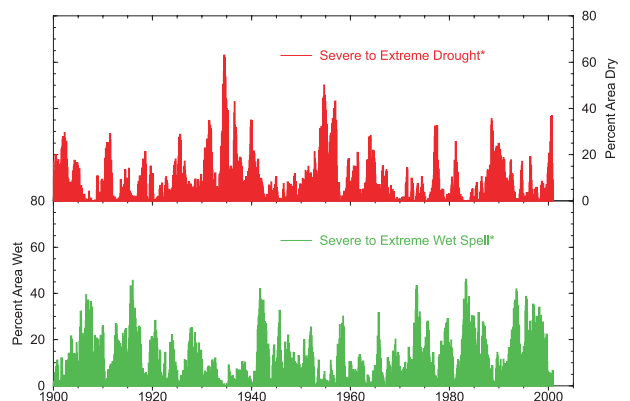
FIG. 28. United States percent area wet and dry from January 1900 through December 2000. Drought and wet spells are based on the Palmer index.
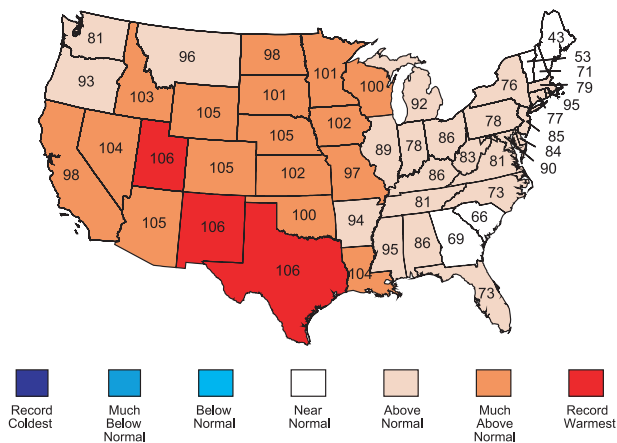
FIG. 29. Statewide rankings of temperature averages for January through August 2000. A rank of 106 represents the warmest such period since 1895. Much above normal temperature is defined as occurring in the top 10 of recorded years, which corresponds to a range of ranks from 97 to 105. Above-normal temperature is defined as occurring in the warmest third of recorded years, or between ranks 72 and 96. Much-below-normal is likewise the coolest 10 year-to-date periods (ranks 2–10) while below normal is defined as the remaining cool third of the distribution, ranks 11–35.

period with average temperatures ranging from 1° to 3°C above the long-term mean. The persistence of above-normal temperatures and increasing precipitation deficits throughout much of the West in the first half of 2000 produced widespread severe to extreme drought from Montana to southwest Texas by August (Fig. 30). This was a contributing factor to the start of thousands of wildfires and the worst national wildfire season in the past 50 years, particularly in the Intermountain West.

Although many factors influence the severity of a wildfire season, short-term drought has been shown to closely correspond to wildfire in the United States (Karl 1986). An overlay of active wildfire location on a map of short-term drought conditions (Fig. 31) shows this strong correspondence. On 18 August 2000, most active wildfires were located in areas experiencing severe to extreme drought.

More than 6.2 million acres of land were consumed by more than 72 000 blazes by the end of August, the peak of the 2000 drought. The most severely impacted states included Idaho, Montana, and Nevada, each with over one half million acres burned. A highly variable large-scale flow pattern across the United States in September was associated with several weak troughs that brought rain and snow to the region and helped diminish the incidence of wildfire.

In October, a 500-hPa trough along the West Coast was associated with heavy rainfall that brought additional drought relief to some parts of the region. New Mexico experienced one of its wettest Octobers on record. Albuquerque received 2.66 in. of rainfall for the month, exceeding the June–September cumulative total. In the southern region of the United States (Texas, Louisiana, Oklahoma, Kansas, Arkansas, and Mississippi), a severe short-term drought brought about by the driest July–September on record, quickly ended two months later as torrential rainfall in parts of the region made November 2000 the wettest November on record.

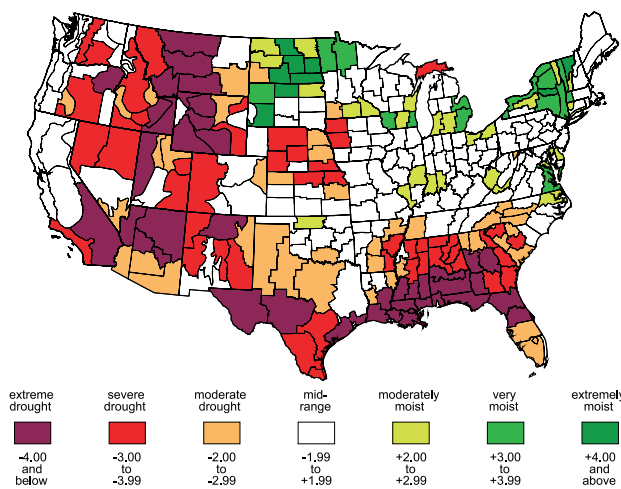Record-breaking temperatures and extremely low rainfall totals in August were associated with positive

FIG. 30. Long-term (meteorological) drought conditions as depicted by the Palmer drought index for August 2000.
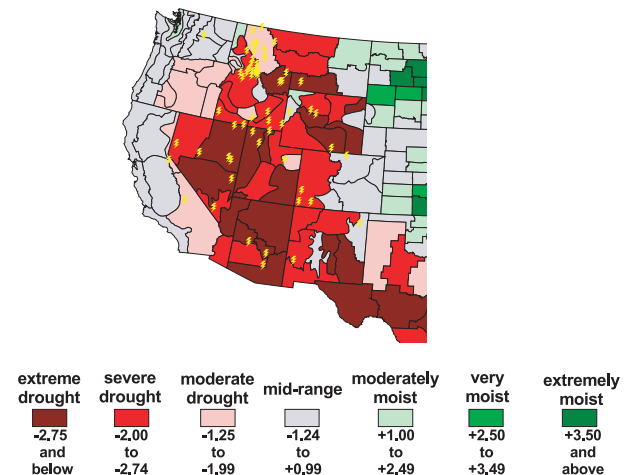

FIG. 31. Overlay of active wildfire locations (18 August 2000) on the July 2000 Palmer short-term drought index map of the western United States.

500-hPa height anomalies across the central and western United States and a slightly amplified ridge across central and southern regions. The drought in the southern plains was highlighted by 84 consecutive days with no measurable precipitation at the Dallas–Fort Worth, Texas, airport, breaking the old record of 58 rain-free days set in 1934 and 1950.

(ii) The Gulf coast, southern Appalachians, and Florida

A prolonged period of below-normal precipitation in the Southeast began with the onset of La Niña in mid-1998. The result of the persistent drier-than-normal conditions was widespread severe to extreme drought in 2000. Lack of precipitation and above-normal temperatures combined to bring the worst drought conditions on record to the Deep South region (Louisiana, Mississippi, Alabama, Georgia, and Florida) by August. Florida was most severely affected, experiencing its driest year on record with a preliminary statewide average total of 40.1 in. of precipitation, 13.8 in. below the 106-yr average (Fig. 32). The year 2000 was the driest since 1955 in Tallahassee, Florida. The preliminary annual precipitation total was 44.5 in., 21.2 in. below normal. Nearly one-fifth of this annual total fell during a 24-hour period in September when Tropical Storm Helene made landfall in the western panhandle of Florida.

The extremely dry conditions also led to numerous wildfires in this region, with major events occurring primarily during the spring and summer months. Wildfires burned across parts of central and south Florida in May 2000 as continued precipitation deficits and warm temperatures in the Southeast provided an ideal environment for additional fires to ignite. By the end of the month, approximately 135 wildfires were burning across the state of Florida alone. May usually denotes the end of the dry season for Florida, but in 2000, the dry season continued well into the summer and early fall months.

Forest fires began to burn across portions of the central and southern Appalachian Mountains in early November. Several localized outbreaks occurred in Kentucky, Tennessee, Virginia, and North Carolina after many locations experienced their driest October on record. Above normal precipitation received in November helped contain the fires and brought short-term drought relief to parts of the South; however, long-term drought conditions covered much of South Carolina, Georgia, Florida, and Alabama at years end.
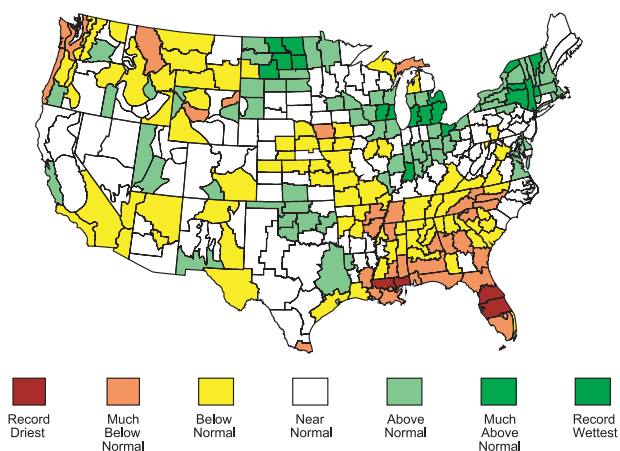
FIG. 32. The 2000 annual precipitation distribution by climate division. Period of record for each division is from 1895 through 2000.

(iii) The high plains, Great Lakes, and Ohio Valley

Although 2000 began drier and warmer than normal in the agricultural belt (central high plains to the southern Great Lakes), the region was spared the anomalous heat and drought that other areas of the country experienced during JJA. Indiana, Kentucky, and Ohio suffered from late winter and early spring drought conditions. Nebraska and Illinois were also included among the drought-stricken areas by May. But as summer began, several heavy precipitation events eliminated most signs of drought in this region (Figs. 33a,b). Cooler temperatures and much-above-average rainfall in June were associated with above-average heights in the western and eastern United States, with below-average heights stretching from the northern plains into northeastern Canada. This created an anomalously strong northwesterly flow into the region, bringing below-average temperatures and much-needed rainfall to the Midwest and Great Lakes regions (*Climate Diagnostics Bulletin,* June 2000).

A number of precipitation records were broken in the Midwest during June and July. Illinois experienced its fourth wettest June in the past 106 years while both Wisconsin and Indiana recorded their 8th wettest June. Much of northwestern Illinois, southern Illinois, southwestern Wisconsin, southeastern Minnesota, and eastern Iowa experienced widespread flash flooding. Rochester, Minnesota, reported 12.52 in. in June, which broke the record for the greatest monthly precipitation total received during any month of the year. Fort Wayne, Indiana. received 8.55 in. of precipita-

(a)

| Record Coldest | Much Below Normal | Below Normal | Near Normal | Above Normal | Much Above Normal | Record Warmest |

(b)

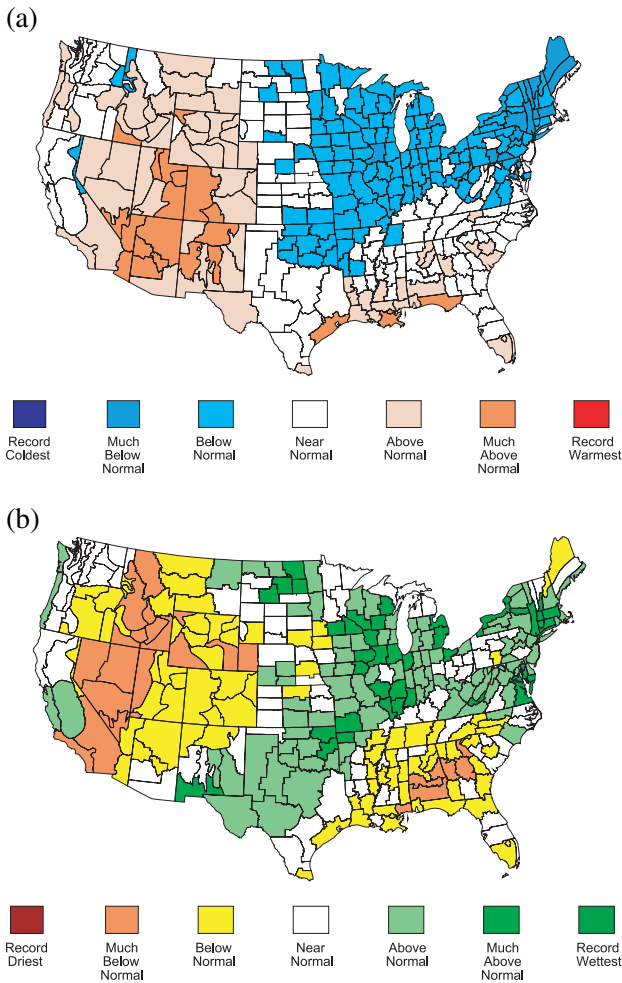| Record Driest | Much Below Normal | Below Normal | Near Normal | Above Normal | Much Above Normal | Record Wettest |

FIG. 33. June through July 2000 (a) temperature and (b) precipitation distributions by climate division. Period of record for each division is 1895–2000.

tion, which set a new record for the month of June. A 24-h precipitation record of 4.39 in., set in July 1912 in Green Bay, Wisconsin, was broken with a total of 4.62 in. on 7 July.

3) ALASKA AND HAWAII

(i) *Alaskan wildfires and thunderstorms over Barrow, Alaska*

Preliminary figures indicate the year 2000 was 1 of the 10 warmest on record in Alaska, with an average temperature more than 1.5°C above the 1961–90 mean. Below-normal precipitation and above-normal temperatures during February–July in central and southern parts of Alaska resulted in numerous wildfires and crop stresses. For the year, approximately 750 000 acres of land were consumed by wildfires, which is about 75% of the annual average (based on the 1990–99 average) 1961–90 mean.

A rare event occurred in Barrow, Alaska, just before midnight on 19 June. A thunderstorm was reported at the airport and was accompanied by 0.17 in. of precipitation received in only a few minutes. Only two additional thunderstorm events have occurred in the vicinity of Barrow since 1978; one on 18 July 1995, and the other on 22 July 1989.

(ii) *Hawaiian drought and record rainfall*

Many of the Hawaiian Islands have suffered from below-normal precipitation totals since early 1998 (also see Bell et al. 2000, their section 4a). This persistent dryness contrasts with precipitation patterns during past La Niña episodes that brought above-normal rainfall to the Hawaiian Islands (Ropelewski and Halpert 1989).

Severe long-term drought persisted through the month of May 2000, with only small improvement during June–October. Portions of Oahu, Molokai, and Maui experienced abnormally dry conditions, which progressively worsened over the past three years. By December 2000, 3-yr precipitation deficits ranged from approximately 37 in. below the 1961–90 mean in Kahului to nearly 48 in. in both Molokai and Honolulu (Figs. 34a–c). The island of Hawaii was not as dry as the other islands throughout the 3-yr period, but was very dry from January through October 2000. Annual deficits at Hilo were almost 24 in. below the 30-yr mean, with a deficit of almost 67 in. for the 3-yr period.

In contrast to the long-term drought experienced throughout the Hawaiian Islands, the southeastern half of the island of Hawaii received record rainfall in early November. Deep tropical moisture from an upper-level low pressure system moved northward across parts of the Hawaiian Islands fueling strong convection and torrential rainfall. The Hilo International Airport reported a 24-h rainfall total of 27.24 in. from 1300 Hawaiian Standard Time (HST) on 1 November to 1300 HST on 2 November, breaking the previous record of 22.30 in. set on 19–20 February 1979. The calendar day total of 16.17 in. on 2 November also set a record for the wettest November day, breaking the previous record by 0.76 in. During one 6-h period, Kapapala Ranch near the city of Pahala reported 22.25 in. of precipitation. For the month, most stations on the island received two to three times their normal amount of precipitation. Kapapala and Pahala had more than five times their normal value. Precipitation received during the month of November did not end the long-term drought conditions in Hawaii, although it did lessen the severity.

4) CANADA

Canada experienced its seventh warmest year since reliable national records began in 1948, as temperatures for the year averaged 0.9°C above normal. The largest deviation from normal occurred in northern British Columbia and in the Yukon Territory where temperatures were 1.7°C above normal. Southern British Columbia was the coolest region, averaging only 0.2°C above normal.

Average precipitation totals in Canada ranked near normal in 2000. Much of British Columbia and Alberta received precipitation totals ranging from 10% to near 30% below normal. The Pacific coast and south British Columbia mountains regions experienced their driest year on record with precipitation totals 26.3% and 21.7% below normal, respectively. Ontario, southwestern Quebec and central portions of the Northwest Territories also received below normal precipitation. Southern Manitoba, northern Quebec, and Newfoundland experienced precipitation departures 10%–20% above normal.

5) The 2000 North Atlantic hurricane season
(i) Overview

The North Atlantic hurricane season runs from June through November and exhibits a peak in activity between mid-August and mid-October, primarily in response to systems developing from African easterly waves. In an average season, 9–10 tropical storms are observed over the North Atlantic, with 5–6 becoming hurricanes and 2 reaching major hurricane status [measured by a category 3, 4, or 5 on the Saffir–Simpson scale (Simpson 1974)]. The 2000 season featured an above-average number of named storms (14), hurricanes (8), and major hurricanes (3). Eight of the 14 storms developed over the tropical Atlantic (between 10° and 20°N) and Caribbean Sea, including 5 of the 8 hurricanes, and all 3 major hurricanes. These areas are known to represent the main development region in other active years as well (Shapiro and Goldenberg 1998). Three other tropical storms formed over the Gulf of Mexico during the 2000 season with one becoming a hurricane. Also consistent with other active years was the small number of named storms (three), which formed outside the Tropics and Gulf of Mexico during the season.

Several indices have been developed to better quantify overall seasonal activity by addressing a combination of factors such as numbers, duration, and intensity of tropical storms and hurricanes. These indices are also useful for diagnosing interannual and interdecadal variations in overall activity, and for partitioning years into active, near-average, and inactive groups. In this section we use a recently developed measure of overall activity (Bell et al. 2000) referred to as the accumulated cyclone energy (ACE) index (Fig. 35). The ACE index is calculated by summing the squares of the estimated 6-hourly maximum sustained wind speed in knots (V_{max}^2) for all periods in which the system is *either a tropical storm or hurricane*. Thus, it is a robust measure of overall activity and does not suffer the shortcomings inherent in attempting to determine the relative activity of a particular season purely by the number of tropical storms or hurricanes alone. The ACE index is a more complete measure of overall activity than the hurricane destruction potential (HDP) parameter commonly used by some researchers (W. Gray 1999, personal communication), which is based on accumulating V_{max}^2 for all 6-hourly periods in which the system is a hurricane only.

Both the ACE index (Fig. 35) and the HDP index (C. Landsea 2000, personal communication) indicate that the 2000 hurricane season featured above-average activity. However, the season exhibited less overall activity than the 1995, 1996, 1998, and 1999 seasons. The ACE index also indicates that the 1995–2000 period is the most active since reliable records began in 1945. This recent increase in the frequency of active years is in sharp contrast to the 1970–94 period, which was marked by many seasons of substantially reduced activity.
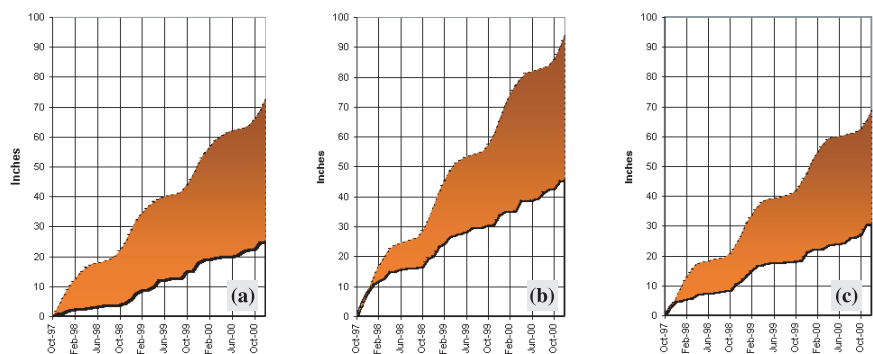

FIG. 34. October 1997 through December 2000 accumulated observed precipitation (solid line) and accumulated 1961–90 mean precipitation (dashed line) for (a) Honolulu, (b) Molokai, and (c) Kahului, Hawaii. Shading depicts the extent of the precipitation deficits.
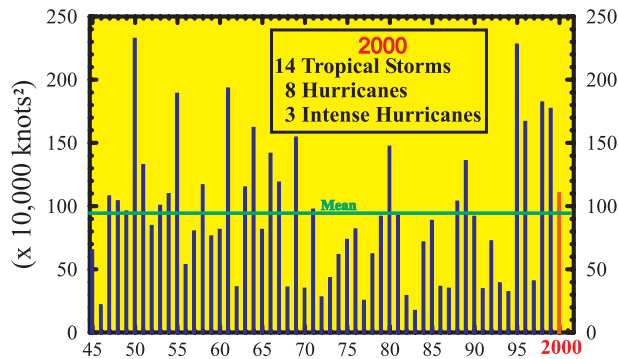
FIG. 35. Accumulated cyclone energy (ACE) index indicating overall Atlantic basin tropical storm and hurricane activity for each Jun–Nov season between 1945 and 2000. The ACE index is calculated by summing the squares of the 6-hourly maximum sustained wind speed in kt ($V_{max}{}^2$) for all named storms during their existence as a tropical storm or hurricane. Seasonal index values have been divided by 10 000 for display.

During the 2000 season all of the named storms over the North Atlantic formed during August–October. Four systems formed in August, seven in September, and three in October. The first storm of the season was a long-lived major hurricane, Alberto, which developed over the tropical Atlantic on 4 August and became extratropical on 23 August. This longevity made Alberto the third-longest-lived tropical system over the North Atlantic since reliable records began in 1945. The last storm of the season developed on 19 October (Tropical Storm Nadine), which contrasts to both the 1998 and 1999 seasons when tropical storms continued to develop into late November.

No hurricanes made landfall in the United States during the 2000 season. Thus, there was considerably less damage and flooding in the United States than was observed in 1999. However, the disturbance that became Tropical Storm Leslie dropped 18 in. of rain in southern Florida, causing massive urban flooding and approximately $700 million in property damage. The primary human loss during the 2000 season occurred in Central America, where Hurricane Gordon killed 19 in Guatemala, and where Hurricane Keith killed 19 in Belize and caused $200 million dollars of damage.

(ii) Atmospheric conditions during the 2000 Atlantic hurricane season: August–October

Tropical storm and hurricane activity over the tropical North Atlantic and Caribbean Sea is strongly influenced by the vertical wind shear between the upper (200 hPa) and lower (850 hPa) troposphere (Gray 1984). Active years feature low vertical shear (below

approximately 8 m s^{-1}) in these regions, while inactive years feature high vertical shear. In addition, tropical cyclogenesis in active years is often associated with African easterly waves, whose evolution is strongly influenced by the structure and location of the African easterly jet (AEJ). The AEJ is centered near 600–700 hPa, and provides the background flow within which the African easterly waves move and evolve (Reed et al. 1977). There are notable differences in both the structure and location of the AEJ between active and inactive years (Bell and Halpert 1998; Halpert and Bell 1997), and these differences represent another fundamental aspect of the coherent atmospheric variability associated with active and inactive hurricane seasons (Bell and Chelliah 1999; Bell et al. 2000).

(a) Vertical wind shear

Eleven of the 14 named storms during the 2000 season occurred during August and September. However, the August–September mean vertical wind shear was above 8 m s^{-1} across the western tropical Atlantic and Caribbean Sea between 10° and 20°N
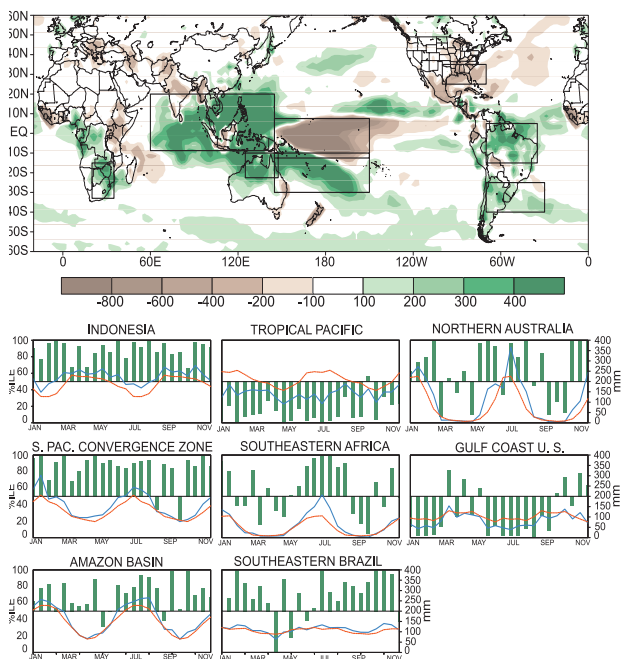
FIG. 36. Magnitude of the August–September 2000 (a) mean and (b) anomalous vertical wind shear. Wind shear is calculated as the difference in wind speeds between 200 and 850 hPa (contour interval is 4 m s^{-1}). Shaded areas in (a) indicate where the vertical wind shear is less than 8 m s^{-1}, and is considered favorable for tropical cyclone formation. Below-average wind shear in (b) is shaded red, while above-average wind shear is shaded blue.

(Fig. 36a), which is generally considered too high to support tropical cyclogenesis. These mean shear values were near to slightly below the long-term average (Fig. 36b), and were consistent with the overall dissipation of the zonally symmetric pattern of upper-level anticyclonic streamfunction anomalies that had dominated the subtropics of both hemispheres since mid-1998 (Bell et al. 2000, see their section 3). These conditions contrast strongly with the significantly below-average mean vertical wind shear typically observed in other active seasons (Landsea et al. 1998; Shapiro and Goldenberg 1998), in association with pronounced upper-level anticyclonic streamfunction anomalies in the subtropics of both hemispheres (Bell et al. 2000).

Since the August–September mean atmospheric conditions were not conducive to tropical cyclogenesis, we focus on the intraseasonal timescale variability to help explain the extremely active August–September 2000 period. One phenomenon that strongly modulates the intraseasonal activity in the Tropics and subtropics of both hemispheres is the MJO. The MJO is a propagating, large-scale pattern of anomalous tropical convection that strongly impacts the upper-level divergence/convergence field at low latitudes as it propagates around the globe. These MJO-related impacts on the upper-level divergence field are monitored and diagnosed regularly by the Climate Prediction Center (2000, personal communication) using a quantity known as the anomalous 200-hPa velocity potential. A time–longitude section of 200-hPa velocity-potential anomalies centered on the equator (Fig. 37a) indicates a highly regular progression of alternating positive and negative anomalies moving around the globe in association with the MJO. Thus, the MJO was quite strong with a quasi-regular periodicity throughout the hurricane season. A similar evolution of the velocity potential anomalies is evident in the 10°–20°N latitude band (Fig. 37b), indicating that the MJO also strongly impacted the upper-level divergence field in the main development region throughout the season.

The structure and amplitude of the subtropical ridges in both hemispheres, and hence the verti-

cal wind shear over the main development region, are also strongly related to the tropical convection on both the ENSO timescale (see section 2) and the intraseasonal timescale. The intraseasonal variations in these circulation features were evident over the main development region throughout the 2000 hurricane season. For example, the 19 August–10 September period featured cyclonic circulation anomalies in the subtropics of both hemispheres (Fig. 38a), which contributed to a large-scale pattern of above-average vertical wind shear across much of the tropical Atlantic and Caribbean Sea (Fig. 39a). Only two tropical systems developed during this 22-day period.

In contrast, the subsequent 11 September–4 October period featured anticyclonic circulation anomalies in the subtropics of both hemispheres (Fig. 38b), which contributed to a large-scale pattern of below-average vertical wind shear across much of the tropical Atlantic and Caribbean Sea (Fig. 39b). This 24-day period featured seven tropical storms in the main development region and the Gulf of Mexico, with five of these systems becoming hurricanes and two becoming major hurricanes. This period of increased activity was then followed during 5–31 October by above-average vertical wind shear across the tropical Atlantic and Caribbean Sea (Fig. 39c). During this 27-day period only two systems formed, both outside the main development region.
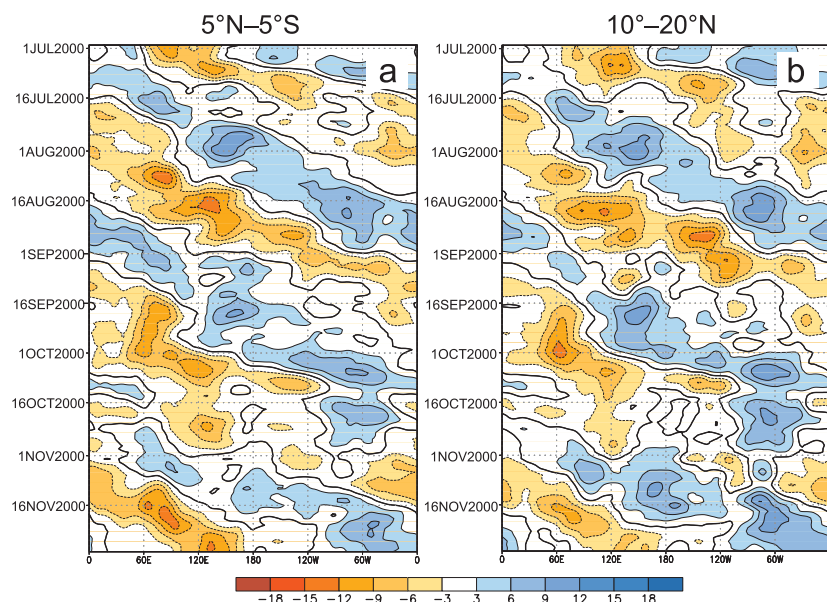

FIG. 37. Time–longitude sections of anomalous 200-hPa velocity potential (10^6 m^2 s^{-1}) averaged over the latitude band from (a) 5°N to 5°S and (b) 10° to 20°N. Contour interval is 3×10^6 m^2 s^{-1}, and the thick contour represents the zero line. Anomalies are departures from the 1979–95 base period means.
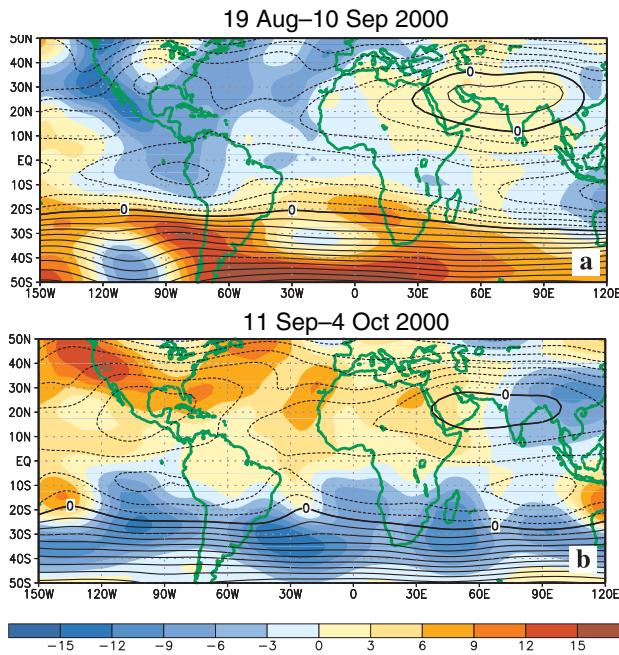
FIG. 38. Anomalous 200-hPa streamfunction (contours) and anomalies (shaded) for (a) 19 August–10 September 2000 and (b) 11 September–4 October 2000. In the Northern (Southern) hemisphere, positive (negative) anomalies indicate an anomalous anticyclonic circulation. Contour interval for the streamfunction is $10 \times 10^6 \ m^2 \ s^{-1}$. Anomalies are departures from the 1979–95 base period means.

FIG. 39. Magnitude of the anomalous vertical wind shear during (a) 19 August–10 September 2000, (b) 11 September–4 October 2000, and (c) 5–31 October 2000. Below-average wind shear is shaded red, while above-average wind shear is shaded blue. Wind shear is calculated as the difference in wind speeds between 200 and 850 hPa. Anomalies are departures from the 1979–95 base period means.

(b) African easterly jet

In addition to the vertical wind shear, the AEJ is an important factor that modulates hurricane activity, primarily during the climatological peak in the season. The AEJ reaches peak strength between the 600 and 700-hPa levels, with the jet core centered near 15°N (Fig. 40a) over the eastern and central tropical Atlantic. The AEJ is important because 1) it provides the background "steering flow" for the easterly waves as they move westward across the tropical Atlantic, and 2) it is an important energy source for the easterly waves which propagate through the cyclonic shear zone (see section 2, Fig. 6b) along the equatorward flank of the jet (Reed et al. 1977).

There is considerable year-to-year variability in the strength, latitudinal position, and westward extent of both the AEJ and the accompanying cyclonic vorticity located along its equatorward flank (Bell and Chelliah 1999; Bell and Halpert 2000). For example, during active years the August–September mean AEJ is generally well-defined and located between 17.5° and 20°N. Indeed, the August–September 2000 period featured an extremely well-defined AEJ (Fig. 40c) with its core centered near 17.5°N. This mean loca-

tion was approximately 2.5° north of its climatological mean position near 15°N, and approximately 5°–7° north of its mean position of 10°–12°N often observed during inactive years (Bell and Halpert 1998).

Also during August–September 2000 strong cyclonic vorticity was present between 10° and 15°N along the entire equatorward flank of the AEJ (Fig. 40d), along with a pronounced westward extension of this high vorticity zone to the central tropical Atlantic. These conditions are notably distinct from the climatological mean conditions (Fig. 40b), and from inactive hurricane years that feature low values of cyclonic vorticity north of 10°N and a confinement of this high vorticity to the eastern tropical Atlantic (e.g., Bell and Halpert 1998, their Fig. 34). Thus, it is evident that during the active 11 September–4 October 2000 period, the combination of a favorable AEJ and low vertical wind shear over the main development re-

gion resulted in an environment conducive to tropical storm and hurricane development. This combination of conditions is similar to that observed in the August–September mean during other active seasons as well, including the 1995, 1996, 1998, and 1999 seasons (Bell and Chelliah 1999; Bell et al. 2000).

b. Asia

1) SOUTHWEST MONSOON

The summer monsoon season in India (June–September) followed a period of drier-than-normal conditions across much of the country. Although precipitation in May was 120% of normal, a lack of rainfall from January through April led to severe drought and shortages of drinking water in the western state of Gujarat. Heat wave conditions covered much of Rajasthan in northwest India for two weeks in April and took numerous lives in Rajasthan, Haryana, and coastal Andhra Pradesh in April and May. Temperatures averaged more than 2°C above normal across India in April, but cooler-than-normal temperatures accompanied the above-normal rainfall in May.

Based on the climatological record, the earliest onset of the southwest monsoon occurs over southern coastal areas of India around 1 June and progresses farther north over the succeeding weeks. The monsoon is normally established across the most northern areas of India by 1 July. The 2000 southwest monsoon began over south Kerala and parts of Tamil Nadu in southern India on 1 June, in keeping with the average onset time. The monsoon rapidly moved northward during the first week of June, but an anomalous ridge of high pressure blocked its advance from 9 to 22 June, and the monsoon remained entrenched over central regions for nearly two weeks. Although nationally, June rainfall was 112% of normal in India, an anomalous 500-mb ridge of high pressure north of 20°N resulted in a weak monsoon epoch throughout much of July. Weak monsoon conditions across northern regions of the country continued in August, while eight southern regions received above-average rainfall.

Total rainfall was 83% of average in August and 75% in September. For the summer monsoon season, precipitation averaged 92% of normal. Much of the
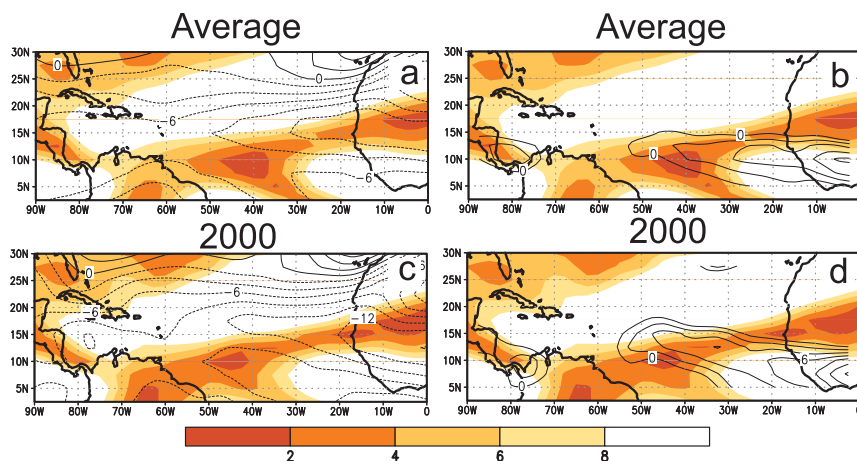

FIG. 40. August–September mean 200–850-hPa vertical wind shear (shaded, m s^{-1}) overlaid with (a), (c) 600-hPa zonal wind (contour interval is 2 m s^{-1}) and (b), (d) 600-hPa cyclonic relative vorticity (contour interval is 2×10^{-6} s^{-1}). (a), (b) The 1979–95 climatological mean conditions and (c), (d) the 2000 mean conditions.

country, 70% of the total area, received near normal (between –20% and +20%) to excess (20% or more above average) rainfall (Fig. 41).

Because central and northern areas of India receive as much as 90% of their total annual rainfall during this 4-month period while southern and northwestern India receive 50%–75% of their annual total, the rainfall received during the summer monsoon season is extremely important to India's vast population. Seasonal rainfall was as much as 20%–50% above normal across much of southern India, while northern parts of the country received near-normal rainfall. Much drier-than-average conditions prevailed across western and central regions of India from Rajasthan and Gujarat to Chhattisgarh in east-central India. Only 598 mm of rainfall fell in western areas of Madya Pradesh, a region which normally receives more than 900 mm of precipitation during the southwest monsoon season. Below-normal monsoon rains in areas already suffering from extended dry conditions worsened the long-term drought outlook.

Although seasonal totals were normal to below normal in much of India, periods of intense rainfall in some parts of the country caused severe flooding typical of the monsoon season. An example is the daily rainfall totals in Bombay (Fig. 42). Precipitation totals approached 2000 mm during the monsoon season, slightly more than the average 4-month total of approximately 1700 mm (17% above normal). However, 57% of the total (1134 mm) fell in the 10-day period 4–13 July, with 350 mm falling in one 24-h period. These torrential rains led to mudslides and flooding

FIG. 41. Cumulative rainfall in India meteorological subdivisions during June–September 2000. Light figures indicate actual rainfall (mm) and bold figures indicate normal rainfall (mm). Percent departures from normal are in parentheses. (Source: India Meteorological Department.)

that killed hundreds of people in the western state of Maharashtra. Other notable incidents included the more than 100 people killed in the southern state of

FIG. 42. (a) Daily and (b) accumulated precipitation (mm) at Bombay, India, for the period 1 June–30 September 2000. Accumulation of climatological precipitation also shown in (b). Base period 1961–90.

Andhra Pradesh and in the northern state of Himachal Pradesh during the month of August from widespread flooding.

Elsewhere, the worst monsoon flooding in decades occurred in parts of Southeast Asia. Monsoon rains began 45 days earlier than usual in Cambodia, and brought devastating floods to parts of the country in July. On average, from 300 to 400 mm of precipitation falls during the month of July in southern Cambodia, but the early onset of heavy rainfall led to large rainfall surpluses. Especially hard hit were areas near the town of Sre Ambel, southwest of Phnom Penh. Monthly rainfall totals exceeded 800 mm, more than 450 mm above normal (Fig. 43).

Flooding in the Mekong delta region of Cambodia and Vietnam during July–November was as severe as any floods experienced in the past 50 years. Although the Mekong River, which runs through central Cambodia and southern Vietnam, typically floods each year between late August and November, the early and heavy onset of monsoon rains in July combined with heavy rain later in the season made the seasonal flooding in 2000 one of the worst in 70 years. The Mekong River at the city of Phnom Penh (location indicated by black dot in Fig. 43a) reached a record high, exceeding 11 m in late September.

2) SEVERE WINTER IN MONGOLIA

Mongolia's climate varies from semiarid in northern and central areas to arid in the south where it borders the Gobi Desert. In all regions of the country, precipitation occurs mainly during the Northern Hemisphere summer. Directly influenced by the Siberian high during winter, daily minimum temperatures often drop below −30°C, but early extremes in temperature coupled with unusually heavy snowfall made the 1999–2000 winter season (DJF) exceptional.

The onset of winter conditions began abruptly during the 1999–2000 season with repeated cold surges starting in September 1999. A time series of 850-mb standardized temperatures and heights (Fig. 44) clearly show the numerous cold outbreaks occurring from September 1999 through February 2000. Conditions were particularly severe throughout the winter months in central and western areas along the Hangai mountain range where minimum daily temperatures dropped below −40°C. Periods of severe cold were interrupted by unusually heavy wintertime precipitation, and the combination of unusually low temperatures and anomalously high precipitation caused much of Mongolia's vast grasslands to become
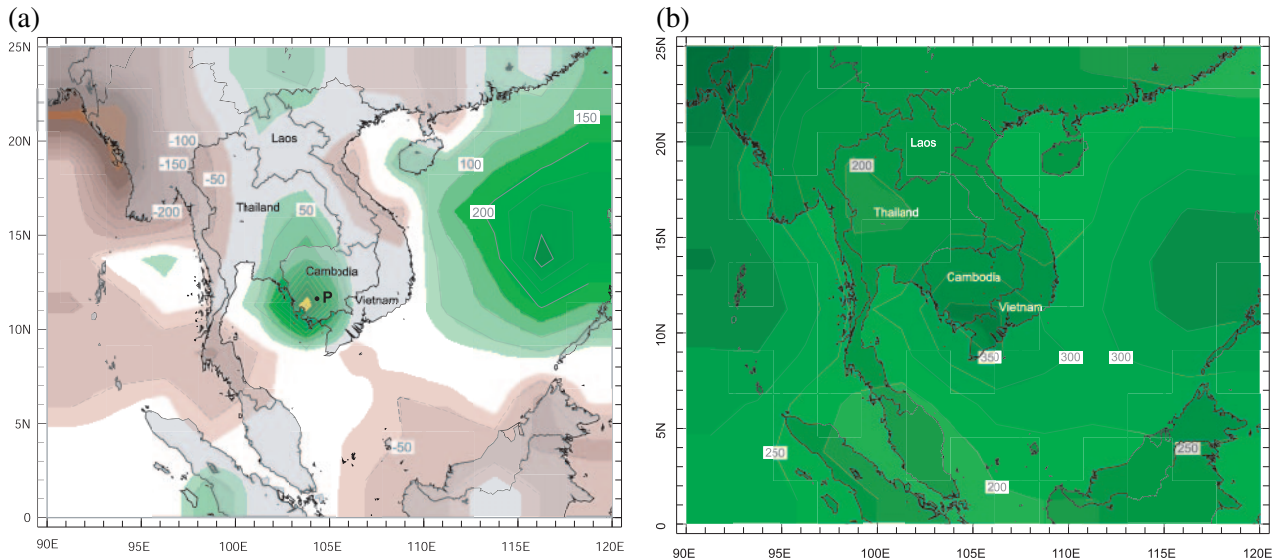
FIG. 43. Precipitation anomaly (mm) for (a) July 2000, and (b) July precipitation climatology (mm) in Southeast Asia. Base period 1961–90 for land regions, 1979–2000 for ocean areas.

capped by ice and snow, greatly stressing livestock, the mainstay of the rural economy.

Repeated snowstorms worsened grazing conditions as the 1999–2000 winter progressed. Temperatures plunged and remained below normal for a prolonged spell from late December 1999 through much of January as the cold Siberian high settled directly over the region. The average January pressure and 850-mb temperatures shown in Fig. 45 clearly indicate the severity of the cold outbreak. Average monthly surface temperatures as low as −37°C in parts of western Mongolia combined with heavy snowfall to create the most severe winter conditions since 1968. The snow depth in some areas of the central province of Dundgobi reached 1 m by February 2000 and led to extremely high mortality rates among livestock. Across Mongolia the extreme winter of 1999–2000 directly impacted over 500 000 people. More than 2.3 million livestock were lost, more than 7% of the national livestock population. The loss of livestock strained food supplies and had a severe economic impact in a country where over 30% of the gross domestic product and one-third of the population is dependent on animal husbandry.

3) WEST ASIA DROUGHT

For the second, and in some areas the third, consecutive year drought plagued much of western Asia from Syria and the Caucasus in the west to Afghanistan and Pakistan in the east. Figure 46a shows this large region of below-average precipitation during the first

six months of 2000 (see climatological normals in Fig. 46b). The period of drier than normal conditions began in July 1998 as below-average precipitation totals were recorded for 24 consecutive months from July 1998 through June 2000 (Fig. 47). Precipitation deficits approached or exceeded 20% in five of the 24 months and early runoff due to an unusually warm winter in 1999–2000 made the drought of 2000 even more severe.

The drought-affected area is primarily an elevated plateau with a semiarid to arid climate. Although widely variable, the bulk of precipitation in the region tends to occur during the cold season. Starting late in the calendar year of 1999 and persisting well into the boreal spring season of 2000, an anomalous anticyclonic circulation developed in the subtropical westerlies. This anomalous circulation dominated the
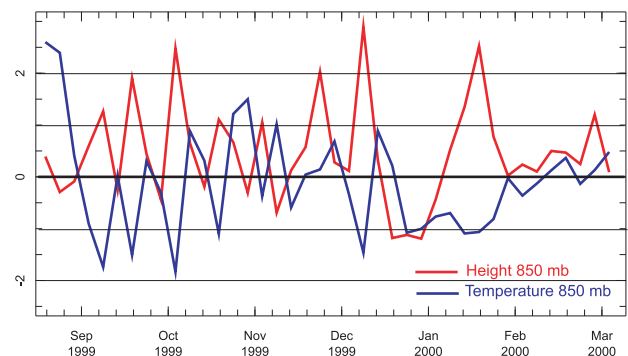

FIG. 44. Pentad standardized 850-hPa temperature (blue) and geopotential height (red) anomalies averaged over the region shown in Fig. 45. Base period 1961–90.
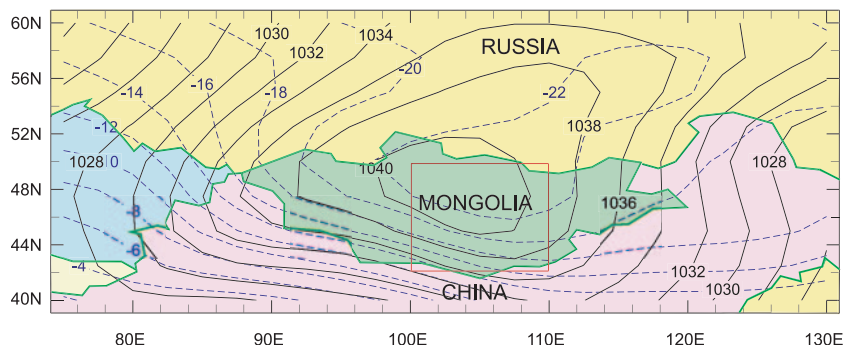
FIG. 45. Average surface pressure reduced to sea level (hPa) and 850-hPa temperature (°C) for January 2000. Boxed region refers to Fig. 44.

upper-level flow during the period of maximum climatological precipitation and led to a continuation of the drought that began more than one year earlier. Figure 48 shows the persistence of this anticyclonic circulation pattern from 40° to 75°E from late November 1999 through March 2000.

For many areas, drought conditions in 2000 were the worst in 30 years. While rainfall in many locations was less than 20% of the long-term average through
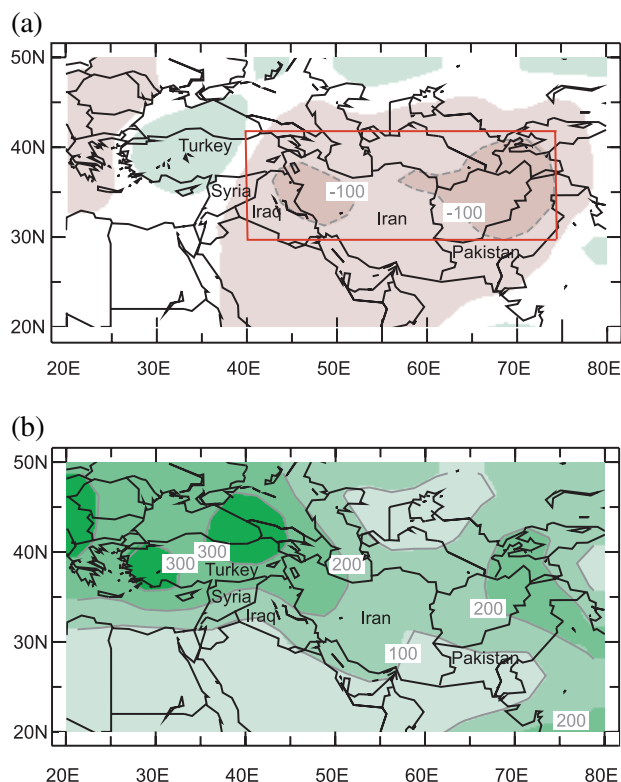

FIG. 46. (a) Precipitation anomaly (mm) for the period January–June 2000, and (b) January–June precipitation climatology (mm). Base period 1961–90 for land regions, 1979–2000 for ocean areas. Boxed region refers to Fig. 47.

June 2000, some parts of Iran reported no measurable rainfall for 30 consecutive months. Southwest Pakistan endured one of the worst droughts in the nation's history. The impact of back-to-back droughts was devastating, affecting over 50 million people according to some estimates. Drinking water became scarce with shallow wells either drying up or becoming contaminated. Crop failures became widespread and loss of livestock was prevalent. In Afghanistan, the United Nations Food and Agriculture Organization estimated a doubling of food deficits in 2000 from the record levels set in 1999.

c. Africa

1) THE 1999–2000 SOUTHERN AFRICA RAINY SEASON

The onset of the primary rainy season in southern Africa occurs during October with rainfall totals generally peaking between December and March. The 1999–2000 rainy season was characterized by significant rainfall across much of southern Africa (Figs. 49a,b) despite a late onset in October and November 1999 and an early withdrawal in April 2000 (Fig. 49d). The overall wetness across southern Africa was consistent with the ongoing La Niña episode, which also resulted in above-normal rainfall in the eastern part of the region during the 1998–99 season. In La Niña years, southeastern Africa typically receives above-average rainfall, while it is typically drier than normal during El Niño episodes (Ropelewski and Halpert 1987, 1989; Hastenrath 1995; Dai et al. 1997; Thiaw et al. 1999).
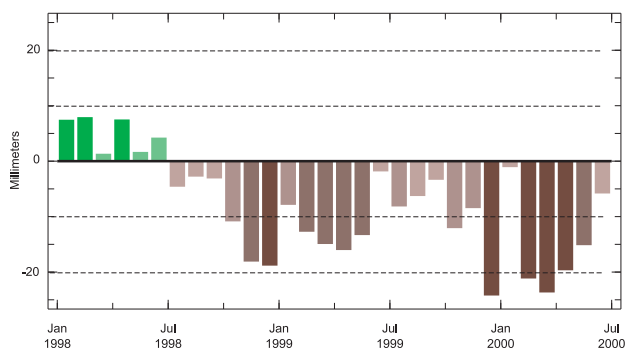

FIG. 47. Monthly average precipitation anomaly (mm) for boxed region in Fig. 46 for the period January 1998–July 2000.

Above-average seasonal rainfall in southern Africa occurred as a result of significant enhancement of the global monsoon system featuring an anomalous atmospheric circulation across the Indian Ocean and southern Africa. The low-level atmospheric circulation for the 1999–2000 rainy season featured easterly winds that averaged 4–8 m s^{-1} from the east-central Indian Ocean westward into Madagascar and across portions of interior southern Africa (Fig. 50a). Over the Indian Ocean, this easterly flow was found along the equatorward flank of the Mascarene high pressure system. The anomalous circulation during DJF when the season is at its prime was characterized by easterly wind anomalies across the central Indian Ocean and an area of low-level convergence over eastern southern Africa. In February 2000, a broad anomalous easterly flow extended across the central Indian Ocean into Madagascar (Fig. 50b) with anomalous poleward flow over the Mozambique Channel. This circulation pattern in association with intense convection over Indonesia provided favorable conditions for tropical cyclone activity over southern Africa.

Southern Mozambique received more than twice its normal January–June rainfall in 2000. Rainfall surpluses greater than 500 mm, as shown in Fig. 51, occurred in southern Mozambique while precipitation anomalies from 300 to 500 mm stretched into Zimbabwe and parts of Botswana and Zambia.

Flooding occurred in stages starting in January. A time series of daily precipitation for Tzaneen New Agatha in northern Transvaal province South Africa (Fig. 52) is typical of the flood-affected regions and reflects the episodic nature of the flooding. Rainfall was well above average after the start of 2000 and minor flooding was reported along the Maputo and Incomati Rivers in southern Mozambique in January. An unusual southern shift to the equatorial trough during early February produced another round of heavy rainfall, triggering more severe flooding, especially along the Incomati and Limpopo Rivers. Some locations received a season's rainfall in less than a week during early February. In a single day, 328 mm of rainfall was recorded in Maputo, Mozambique.

The presaturated conditions of early February set the stage for devastating floods later in the month when tropical cyclone Leon-Eline made landfall in south-central Mozambique on 22 February. With anomalously weak westerlies at upper levels and unusually strong high pressure to the south of the Mozambique Channel, the storm continued its westward track producing over 250 mm of rain in sections of central and
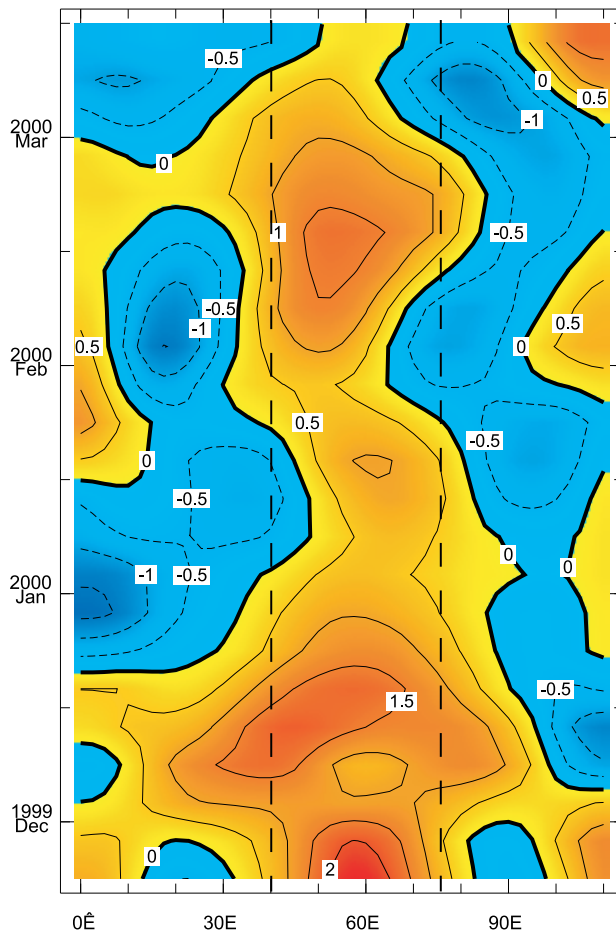

FIG. 48. Pentad time–longitude plot of standardized 250-hPa geopotential height anomaly at 35°N for the period 24 November 1999–29 March 2000. Vertical dashed lines indicate east–west boundaries of drought-affected area.

southern Mozambique before traveling west to southern Zimbabwe on 23 February.

Torrential rains from the dissipating storm inundated northern South Africa, southern Zimbabwe, and Botswana, the headwaters of the Limpopo and Save Rivers. The already flooded rivers rose even higher, causing numerous fatalities and tremendous destruction of homes, bridges, and roadways from northern South Africa into southern Mozambique as the waters raced through low-lying areas. Locally heavy rains during March produced some additional flooding, though in general the floodwaters were receding. Tropical Cyclone Huddah made landfall in northern Mozambique during April, but the heaviest rainfall was primarily north of the previously flooded areas.

An exception to the above normal rainfall and flooding in southern Africa occurred in an area includ-

ing northern Mozambique and northern Madagascar. This region received significantly below-normal precipitation, with rainfall deficits from 200 mm to more than 300 mm and rainfall totals 5%–10% of normal (Fig. 51). Near- to below-normal rainfall was also observed over Malawi, much of Zambia, and southern Tanzania, where rainfall totals were 20%–70% of normal. The climatologically dry areas of coastal Namibia and the west coast of South Africa also experienced near- to below-normal rainfall.

2) DROUGHT IN THE GREATER HORN OF AFRICA

Following two years of erratic rainfall throughout much of the Greater Horn, the failure of the early 2000 rainy season helped trigger food shortages and livestock losses not seen since 1984–85. Twenty-two months of below-normal precipitation during the past three years (Fig. 53) produced widespread drought with pastoral areas of northern Kenya and southern and southeastern Ethiopia most severely affected. Drought also had an impact in Sudan, Somalia, Tanzania, and Eritrea.

Precipitation deficits for the first six months of 2000 (Fig. 51) exceeded 100 mm across a large part of the Greater Horn. The combination of drought and civil strife left an estimated 20 million people facing food shortages in the Greater Horn during 2000, 10 million in Ethiopia alone.

In the areas most affected by the drought, the annual distribution of rainfall is generally bimodal. The primary rainy season in northern and central Kenya extends from February to May with a secondary season from October to January. In Ethiopia, the annual cycle is similar in the southern regions, where the drought was most severe, while in western areas the primary season is generally May to October. Crop growing seasons parallel the annual cycle of precipitation.

During early 2000, rainfall in much of the Greater Horn was generally characterized by late onset and little accumulation. Anomalous large-scale subsidence suppressed precipitation and by the end of April the cumulative 2000 rainfall was less than 25% of the long-term average in sections of southern Ethiopia and north-central Kenya.

Severe drought resulted and crop failures became widespread by June with losses especially high in Kenya where the spring growing season accounts for up to 80% of annual food production. Short season cereal production in central and western areas of Ethiopia slumped as well. Irregular and insufficient rainfall also had a serious impact on range vegetation, which resulted in the loss of large numbers of livestock. Failed crops posed an additional problem of inadequate grain production for animal feed. By midyear a large-scale relief effort was under way to provide food supplies in an effort to avoid widespread famine.

3) JUNE–SEPTEMBER 2000 WEST AFRICA RAINFALL

Rainfall in the Sahel (see region bounded by box in Fig. 54) is closely related to the intertropical convergence zone, which begins a northward movement in March and reaches its northernmost position near 15°N in August. Although rainfall typically varies widely across the region, with long-term average totals reaching 1300 mm in the
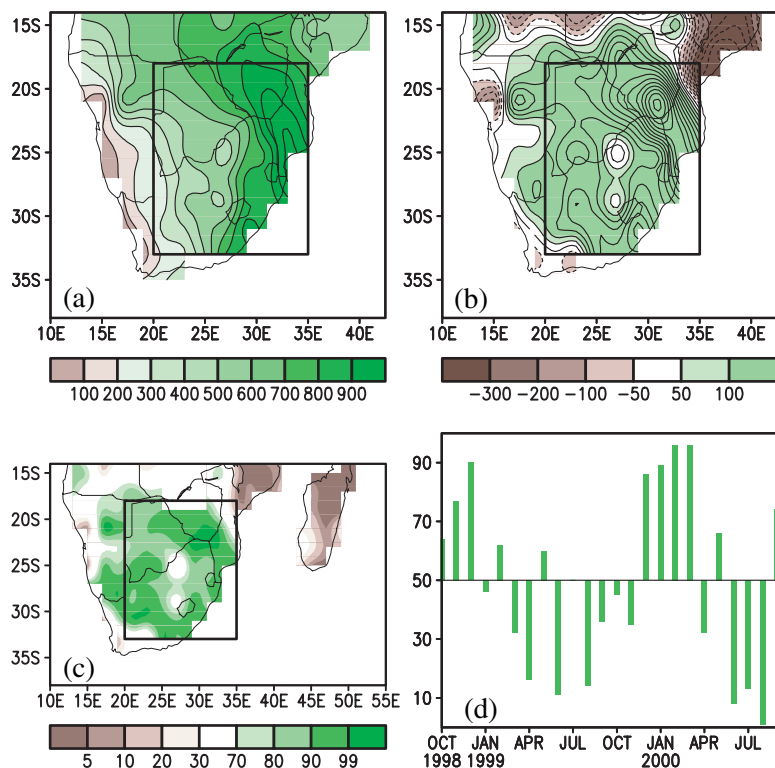

FIG. 49. October 1999–April 2000 (a) total precipitation (mm), (b) precipitation anomalies (mm), and (c) precipitation percentiles based on a gamma distribution fit to the 1961–90 base period. (d) Monthly time series of precipitation percentiles, based on precipitation totals averaged over the boxed region depicted in (a)–(c).
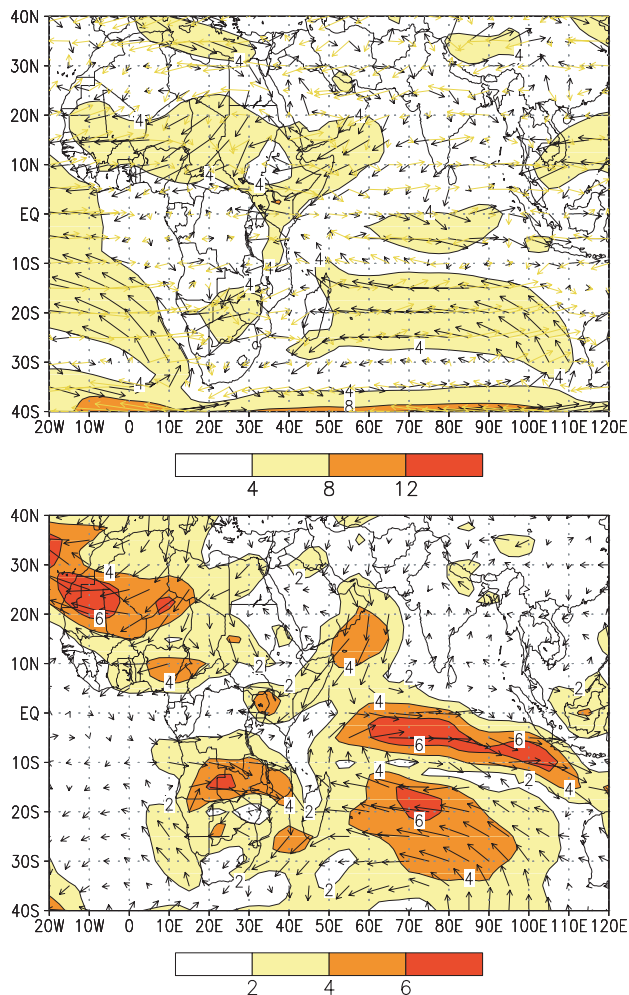
FIG. 50. The 850-hPa total wind for (a) October 1999–April 2000 and (b) DJF 1999–2000 wind anomalies. Anomalies (m s⁻¹) are departures from the 1979–95 base period means.
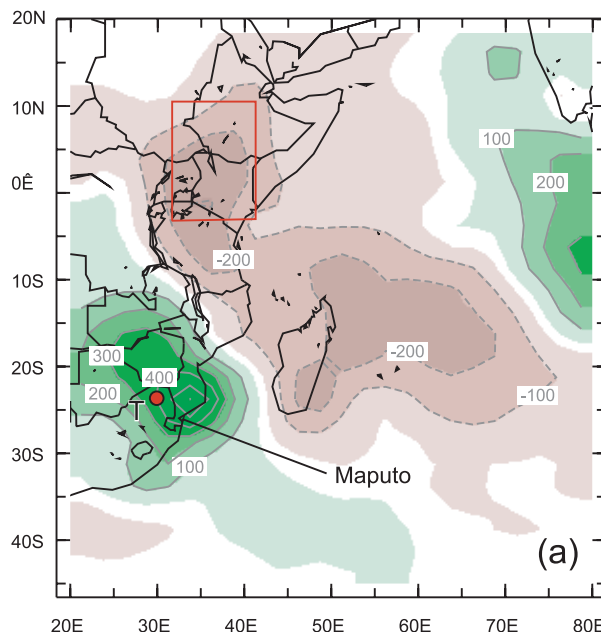

FIG. 51. Precipitation anomaly (mm) for the period January–June 2000. Base period 1961–90 for land regions, 1979–2000 for ocean areas.

Guinean Highlands in the southwest, 700 mm in the southeast, and 100–300 mm in the north, approximately 90% of Sahel's mean annual rainfall is received in the June–September period.

Following an extremely wet rainy season in 1999, rainfall in 2000 was near the 1961–90 average (Fig. 54a). Area-averaged totals ranged from 500 to 700 mm in the south, 300–500 mm in central Sahel, and 100 to 300 mm in the north. Although precipitation in 2000 (Fig. 55) was generally near normal, wetter-than-normal conditions were experienced in western Chad just northeast of Lake Chad (Fig. 54b), with rainfall anomalies ranging between 50 and 150 mm. The western part of the Guinea region was extremely dry, with rainfall totals from 500 to 700 mm, more than 400 mm below the 1961–90 mean. The eastern part of the Guinea region was also slightly drier

than average, with rainfall deficits from 100 to 300 mm below the climatological mean.

The regional conditions that contributed to near-normal Sahel rains in 2000 were linked to the gradual return to normal of the global-scale monsoon system consistent with the weakening of the cold ENSO episode in the middle of the year (see section 2a). The atmospheric circulation during the 2000 season featured a moderately strong southerly and southwesterly flow of Atlantic tropical moisture into the Sahel at 925 hPa. The northward penetration of moisture was deeper in the eastern part of the Sahel, as strong northeasterly winds across northwestern Africa pushed the moisture farther south in western Sahel. The westerly winds in the western Sahel were suppressed by easterly wind anomalies averaging 1–2 m s⁻¹ over southern Mauritania and northern Senegal (Fig. 56a).

Despite the relaxation of the low-level westerlies between 10° and 15°N, in general the monsoonal flow was slightly enhanced at 850 hPa (Fig. 56b). But although there was a slight enhancement of the monsoonal flow at 850 hPa, the midlevel jet axis and the associated cyclonic vorticity did not extend farther north to favor the development of African wave disturbances (Fig. 57). As a result, precipitation in 2000 was less than in 1999.
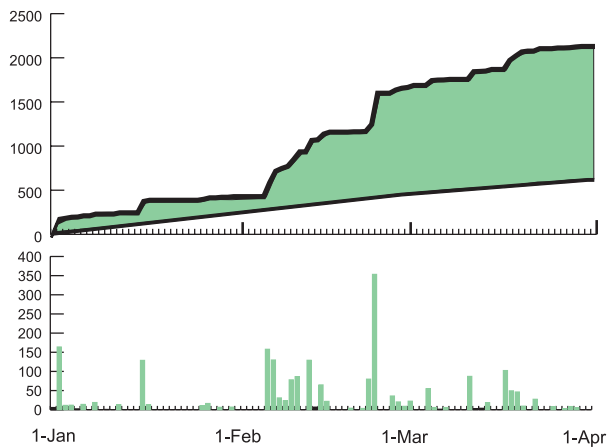
FIG. 52. Daily and accumulated precipitation (mm) at Tzaneen New Agatha, South Africa, for the period 1 January–31 March 2000. Accumulation of climatological precipitation also shown. Base period 1961–90. Station location shown by red dot in Fig. 51. (Data courtesy of the South African Weather Bureau.)

d. *Temperature and precipitation extremes in Europe*

1) SOUTHEASTERN EUROPE HEAT WAVE

An extremely dry year in much of southeastern Europe was highlighted by a summer of water shortages brought about by months of below-normal precipitation and record summer heat. The year began with January precipitation more than 35% below normal and deficits in some areas greater than 50%. Slightly drier-than-normal conditions that persisted through late winter and early spring were interrupted by periods of heavy precipitation in early spring. In Romania and Hungary, precipitation deficits, which were present early in 2000, were replaced by floods during April as rainfall and unseasonably high temperatures accelerated snow melt in the Carpathian Mountains. Along the Tisza River in Hungary, water levels reached the highest levels ever measured in
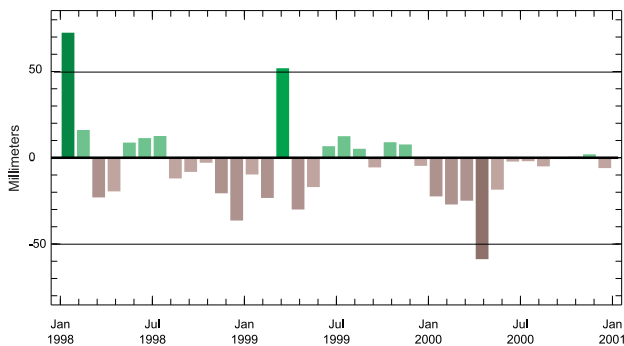
FIG. 53. Monthly precipitation anomaly (mm) for the boxed region in Fig. 51.

some locations requiring the evacuation of nearby towns.

Much drier-than-normal conditions returned in May and intensified into severe drought across much of southern Europe and the Balkans by June. (Average precipitation for the 4-month period May through August is shown in Fig. 58a, and the precipitation anomalies for 2000 are included in Fig. 58b.) Rainfall was well below average throughout much of southeastern Europe with many areas receiving less than 50% of the long-term average precipitation for the 4-month period. Timisoara, Romania, indicated by the red dot in Fig. 58b, experienced one of their driest May–August periods on record and their driest summer (JJA) since 1952.

Average May through August precipitation totals (Fig. 59) were the lowest in the past century for a large part of southern Europe (boxed region in Fig. 58b). Precipitation deficits greater than 20 mm (Fig. 60) were recorded in May, June, and August with a 4-month seasonal deficit of 73 mm, more than 40% below normal for the region.
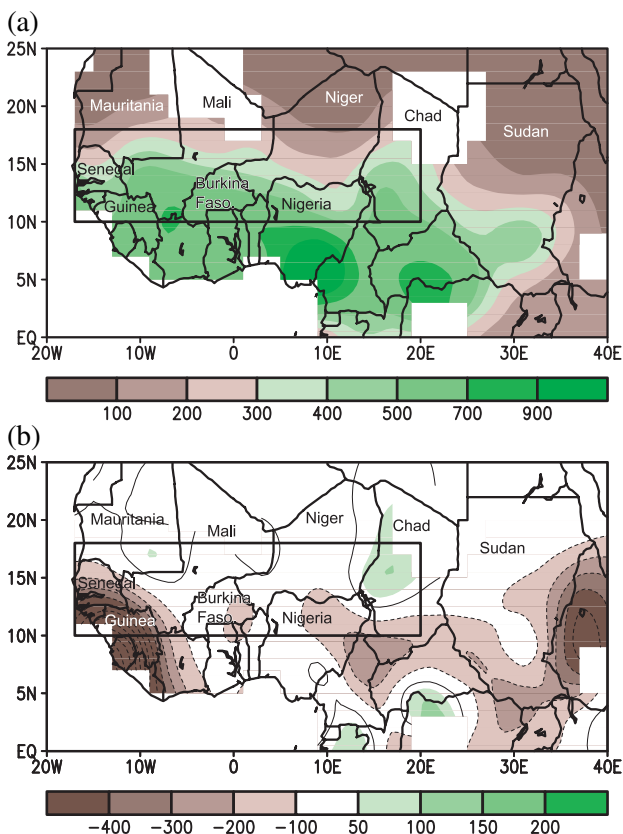

FIG. 54. June–September 2000 (a) total precipitation (mm) and (b) anomalies (mm) for the Sahel. The boxed region denotes the approximate boundaries of the Sahel.

The prolonged period of below-average precipitation was associated with recurrent and anomalous ridging in the upper-level flow across eastern Europe, which was established in May and persisted throughout much of the boreal summer. The pentad-averaged standardized 250-hPa geopotential height anomalies for the area most severely affected (43°–48°N,15°–25°E) show the persistence of this pattern throughout much of the May–August period (Fig. 61).
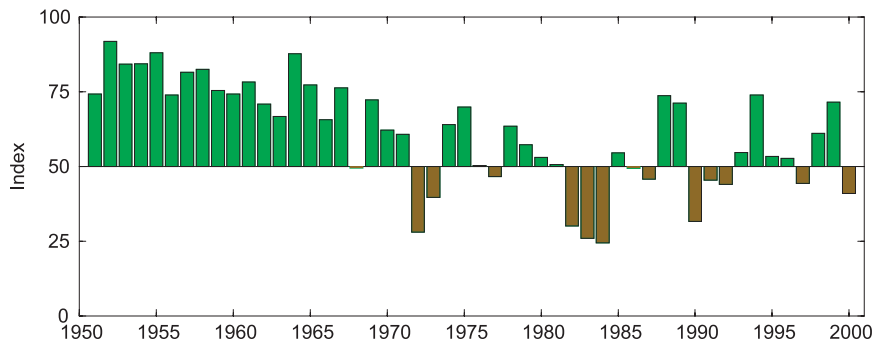

FIG. 55. Percentile index (average gamma percentiles of station precipitation within region) for the Sahel during June–September. Percentiles are computed for the 1961–90 base period.

After a very warm start to July, the ridging pattern temporarily collapsed allowing cooler air to move southward and triggered severe thunderstorms in some areas during midmonth. Rainfall brought minor relief to some drought-stricken areas and contributed to smaller precipitation deficits for the month. The cooler conditions were short lived as unusually hot and dry weather returned in August.

Before the ridging collapsed in mid-July, a record-breaking heat wave worsened the already dry conditions and led to heat related fatalities and numerous wildfires. Century-old records were broken during the first week of July. Temperatures reached as high as 44°C in locations across Turkey, Greece, Romania and Italy with some locations in Sardinia and the Greek Islands exceeding 48°C. The hot conditions buckled train tracks in Romania and were blamed for over 40 fatalities throughout the region. The hot, dry conditions contributed to numerous wildfires as well. Wildfires were also unusually widespread from the Balkans to Italy, and Greece experienced its worst fire season in decades.

2) Precipitation extremes in the United Kingdom and western Europe

Several regions in the United Kingdom experienced extreme rainfall and flooding in 2000. Drier than normal conditions in the first three months of the year in much of the United Kingdom gave way to record rainfall in April in central England. Normally the driest of the nine precipitation regions of the United Kingdom, central England received more April rainfall than the mountainous region of northwest Scotland, which typically receives approximately three times more annual precipitation. This heavy rainfall contributed to a record-breaking April total of

143 mm across England and Wales, the greatest value in the 235-yr England and Wales precipitation (EWP) series (Alexander and Jones 2001).

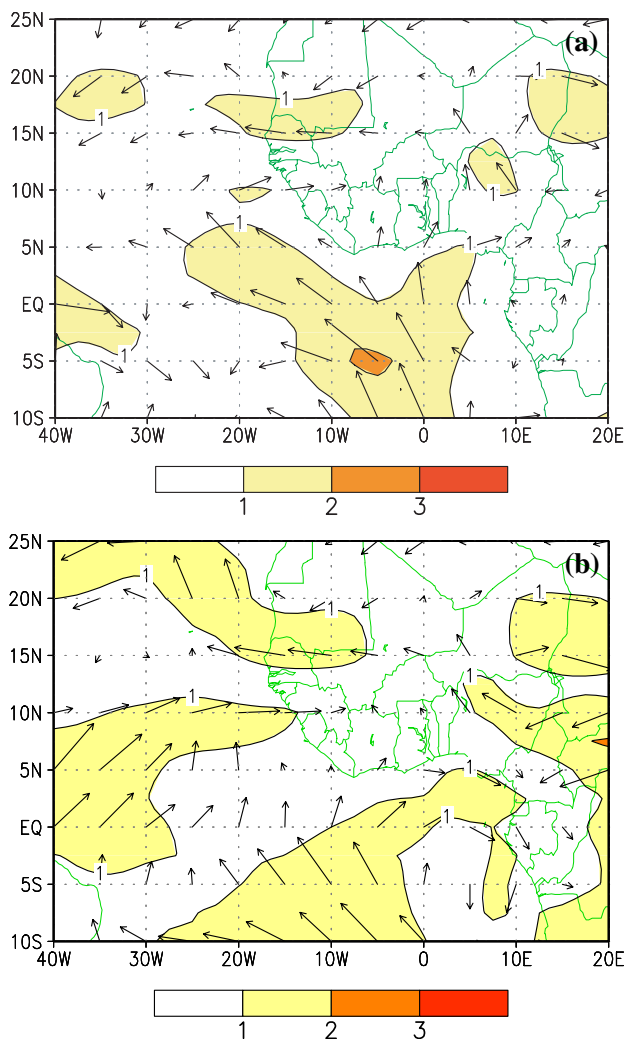FIG. 56. Anomalous wind speed (m s⁻¹) and anomalous vector wind during Jun–Sep 2000 at (a) 925 and (b) 850 hPa. Anomalies are departures from the 1979–95 base period.
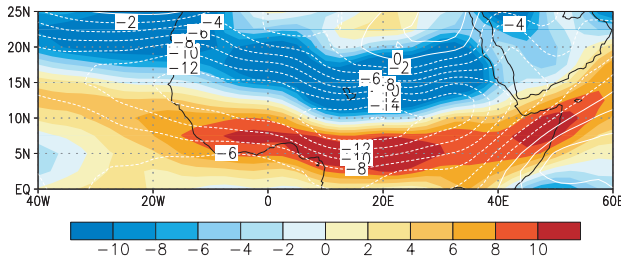
FIG. 57. August–September 2000 mean 600-hPa zonal wind (contours, m s^{-1}), overlaid with 600-hPa relative vorticity (shaded, 2×10^{-6} s^{-1}).

Summer (JJA) precipitation totals were below normal across most regions of the United Kingdom, continuing a 130-yr trend to drier conditions as shown for southeast England in Fig. 62. Although below-normal rainfall was prevalent across the country, northeast England received record-breaking daily values on 3 June. This was preceded by several above-average rainy days and led to flooding in the northeast of England.

Following the dry summer season, a period of storminess began in September and lasted for several months. Fronts associated with a deep low anchored
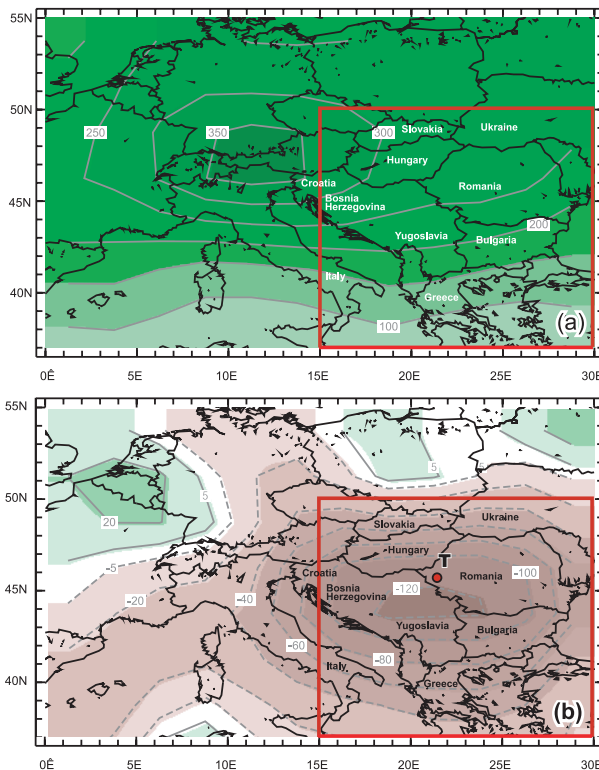
FIG. 58. (a) Climatological precipitation (mm) for May–August, and (b) precipitation anomaly (mm) for the same period in 2000. Base period 1961–90 for land regions, 1979–2000 for ocean areas.

between Greenland and Iceland led to a series of potent wave depressions, which tracked across the United Kingdom and western Europe at the close of October causing widespread flooding and major disruption across the region. The high saturation of the soil together with a continuing period of prolonged rainfall led to the flooding of several coastal southern English counties at the beginning of October. The wet weather continued into November contributing to the wettest autumn (SON) since records began in 1766. The anomalous weather was evident throughout the country with only the normally wet regions receiving near-average rainfall (Fig. 63). The anomalous wet spell continued into December making October–December the wettest 3-month period in EWP history.

Torrential October rainfall also led to floods and mudflows and contributed to numerous deaths in the Southern Alps in an area stretching from the Rhone valley in France to the Po valley in northern Italy. The town of Locarno, located in southern Switzerland near the Italian border, received more than 285 mm of rainfall from 11 to 16 October. This led to the overflow of Lake Maggiore and flooding throughout much of the surrounding area. A mudslide, brought about by heavy rainfall, also swept away much of the tiny town of Gondo, Switzerland.

Nine-day precipitation totals were greater than 200 mm along much of the border region between Italy and Switzerland (Fig. 64). In the agriculturally rich Po Valley, heavy rainfall began on 14 October and continued for the next three days. More than 500 mm of rainfall was recorded near Milan in the 3-day period from 15 to 17 October. Two-day rainfall totals in Turin, Italy, exceeded 115 mm.
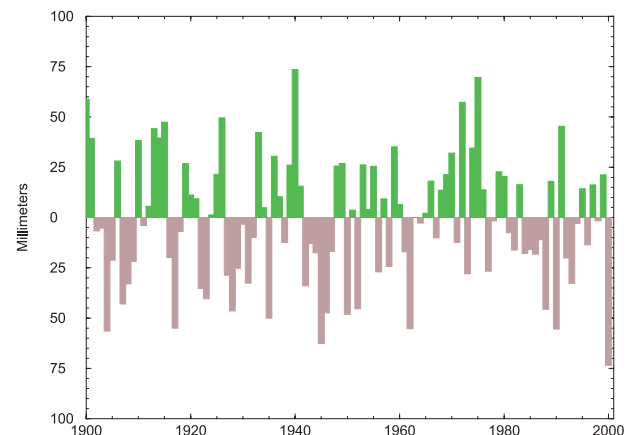

FIG. 59. Average May–August precipitation anomalies (mm) for the boxed region in Fig. 58b for the period 1900–2000. (Source: Global Historical Climatology Network.)
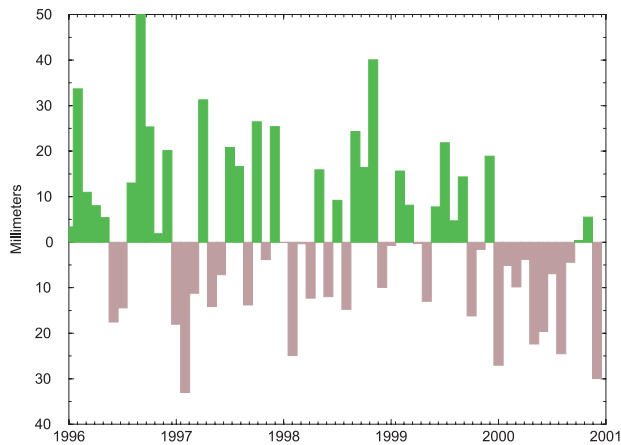
FIG. 60. Monthly precipitation anomalies (mm) for the boxed region in Fig. 58b for the period January 1996–December 2000. (Source: Global Historical Climatology Network.)

This extreme regional rainfall event brought the Po River to historic heights, causing it to break over its banks in some parts of Italy requiring the evacuation of thousands of people. Roads were closed, dozens of bridges were destroyed, and many rail services from Italy to France and Switzerland were suspended.

Later in the month, torrential rainstorms caused major flooding in eastern Spain. Some stations recorded monthly totals greater than 500 mm and measurements between 200 and 300 mm were widespread. Some coastal areas received more than 275 mm of rainfall in the four days from 22 to 25 October.

These storms, which led to extensive flooding in some eastern cities, occurred during an extended period of below-normal rainfall and brought drought relief to some parts of Spain that had experienced below normal precipitation for much of the past two years. Rainfall deficits during the first nine months of 2000 worsened drought conditions, which began in 1998 and were most severe in eastern and southeastern areas of the Spanish peninsula.

An analysis of precipitation data from the Global Historical Climatology Network (Vose et al. 1992) revealed a 1998 precipitation deficit of 171 mm below the 1961–90 average in Spain. Below-normal precipitation continued in 1999 (–112 mm) and extended through the first nine months of 2000. Seven of the first nine months of 2000 were drier than normal, leading to a 9-month total that was 65 mm less than the 30-yr average.
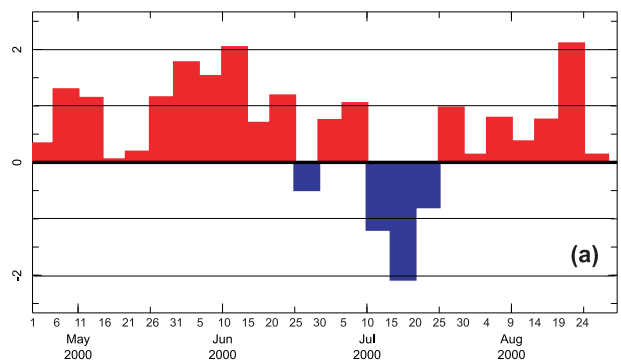

FIG. 61. Pentad average standardized 250-hPa geopotential height anomaly for the period 1 May–28 August 2000 for the region 43°–48°N, 15°–25°E.

The standardized precipitation index (SPI) (Fig. 65) illustrates the severity of the long-term drought in the east and southeastern catchment areas of Spain. The progression of one-month to 24-month SPI values beginning in September 1998 and continuing through August 2000 shows the worsening drought conditions in this region. The index decreased almost continuously from +0.13, reached very low levels in October 1999, and fell to –2.39 by the end of the biennium. According to Spain's National Institute of Meteorology, total mean precipitation during the biennium (614 mm) in this region was so low that the probability of reoccurrence is 0.0084. A similar period of precipitation deficits occur on average only once every 118 years.

e. South America

Annual precipitation totals exceeded 1961–90 normals across much of South America in 2000 (Fig. 66). The largest anomalies were recorded in northeast Brazil and the Amazon Basin with above-normal precipitation also falling in much of the southern half of the continent and near-normal conditions in extreme northern South America. Annual anomalies exceeded 250 mm throughout the Amazon Basin with extreme northeastern Brazil receiving precipitation more than 550 mm above the 1961–90 average.
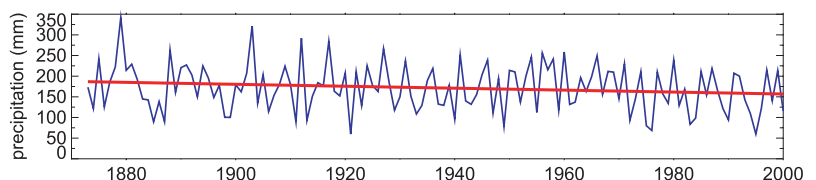

FIG. 62. Monthly southeast England summer (JJA) precipitation totals. Also fitted with a least squares trend line. The downward trend is significant at the 95% level of confidence. (Source: U.K. Met Office.)
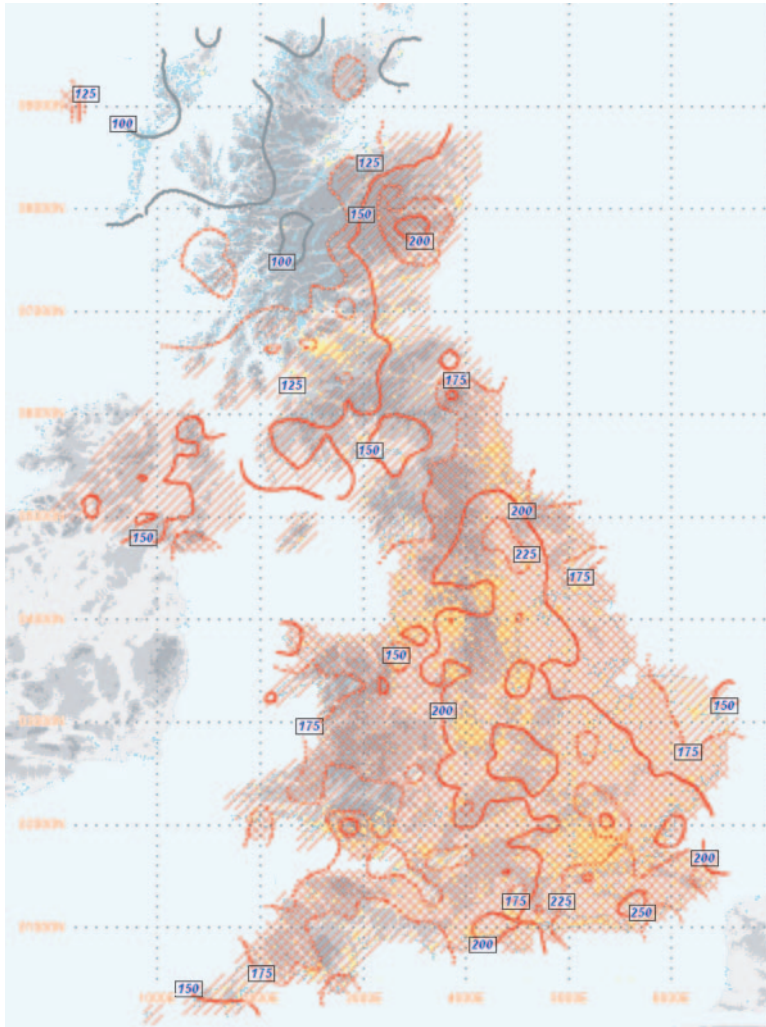
FIG. 63. Autumn (SON) precipitation anomalies for the United Kingdom based on percentages of the 1961–90 climatological average. (Source: U.K. Met Office.)

with an average exceedance of 185% during the 3-month period. Five days of torrential rainfall in extreme eastern areas led to the worst flooding in 25 years, destroying thousands of homes and contributing to the deaths of dozens of people. Some of the poorest areas of Brazil were most severely impacted as water levels exceeded 12 ft above street level in places.

Storms associated with the presence of La Niña also brought above-normal precipitation to the sub-Andean sector of northwest Argentina in early 2000. Torrential rains led to the most severe flooding in Argentina since the devastating floods that accompanied the 1997–98 El Niño episode. The Argentina–Bolivia–Paraguay border region received an average of more than 280 mm of precipitation in March, 165 mm above normal, making March 2000 one of the wettest such months on record.

Northern areas of Argentina as well as Paraguay also experienced a prolonged cold outbreak in July. Daily minimum temperatures below 0°C occurred frequently between 10 and 20 July in this region, which typically experiences minimum temperatures near 10°C. The time series of daily minimum temperatures for Mariscal, Paraguay (Fig. 67), is typical of the anomalously cold weather experienced in the area during the July 2000 cold outbreak.

Winter weather in Paraguay is generally affected by the frequency and structure of cold fronts originating from the south. These occur most frequently in June and July. The anomalous cold of 2000 was due to several outbreaks of polar air associated with a large area of negative height anomalies over the southern half of the continent. Frequent blocking in the vicinity of the Weddell Sea contributed to a prolonged influx of cold air into Paraguay and the surrounding region (*Climate Diagnostics Bulletin,* July 2000). All-time low temperatures were recorded at nine locations in Paraguay, and the lowest temperature ever observed in the country (−7.5°C) was recorded on 13 July at Pratts Gill. This prolonged cold spell led to the coldest July on record in Paraguay. However, the JJA season was not as cold as the winter seasons of

Wetter than normal precipitation patterns over the Amazon basin and northern South America are typically associated with La Niña conditions, particularly in the DJF and MAM seasons. Precipitation was 12% above average in northeast Brazil during the January–May period of 2000, normally the wettest months of the year. Although three of the five months (February, March, and May) were drier than normal, average anomalies greater than 75 mm in January and April contributed to a 5-month total (1040 mm) more than 100 mm above the 30-yr mean. Monthly totals were also above average during much of the remainder of the year. Precipitation in 2000 totaled 732 mm, more than 300 mm above average.

Rainfall was particularly heavy in the July–September period, with monthly totals exceeding the climatological average by more than 140% in each month

1996 and 1998 as temperatures in June and August were near normal to above normal throughout the country.

f. Australia and New Zealand

1) TEMPERATURE: AUSTRALIA

Australia is notable as the only continent, other than Antarctica, to record an average annual temperature below normal in 2000 as the presence of La Niña (see section 2a) contributed to generally cooler- and wetter-than-normal conditions. Annually averaged maximum temperatures (Fig. 68) were generally below normal in central and northern regions of the continent, while slightly warmer-than-normal temperatures were widespread in southeastern and extreme southwestern Australia. Although the annually averaged mean temperature was 0.22°C below the 1961–90 average, some noteworthy warm spells occurred, particularly across the southern half of the continent.

Southeastern Australia experienced unusually hot weather in February, November, and December. In Melbourne, the average February maximum (30.1°C) was the second highest in 150 years of record keeping. Several places in Victoria and Tasmania had their hottest February on record. Victoria had a record warm November, with nearly every station in the state experiencing a record warm mean minimum temperature for the month. Records were also broken throughout much of South Australia, New South Wales (NSW), and Tasmania. The previous November record was exceeded by almost 2°C in Melbourne. December temperatures were also well above normal throughout the southern states.

Conversely, maximum temperatures were generally well below normal in the January–June period over northern and western Australia, extending at times into central Australia. Over inland western Australia, average anomalies in the February–April period (Fig. 68) were as low as −4°C in places. This unusual coolness continued a trend that began during the last two months of 1999.

In contrast to the relatively cool first half of the year, warmer-than-normal conditions were prevalent during July–September. September was exceptionally warm over a broad belt of central and eastern Australia centered along 30°S. Anomalies in this area exceeded 4°C during the Olympic Games. Many parts of NSW, Queensland, and southern sections of the Northern Territory experienced record or near-record daily maxima in late September.
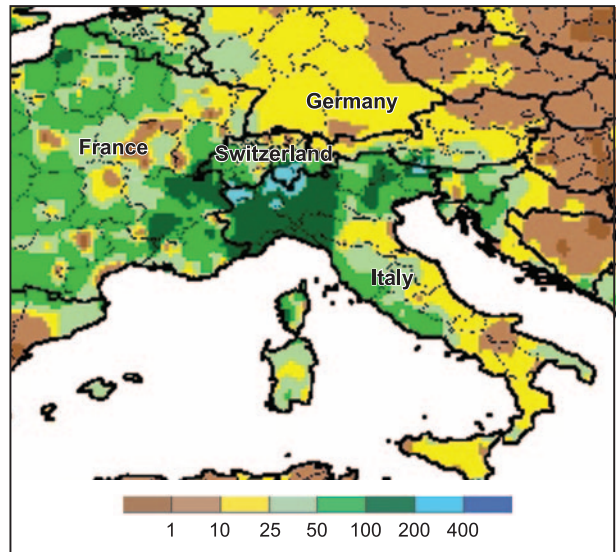

FIG. 64. Accumulated precipitation (mm) for the period 8–16 October 2000. (Courtesy of the U.S. Department of Agriculture.)

Exceptionally low maxima returned to northern Australia in the last three months of the year, coinciding with the early onset of the northern wet season. In December, maximum temperatures were more than 5ºC below average over an extensive area of eastern Northern Territory and western Queensland.

2) PRECIPITATION: AUSTRALIA

The cooler-than-normal temperatures in northern and western sections of Australia were related to unusually heavy rainfall, especially during the first four and the last three months of the year. The average continent-wide rainfall for 2000 totaled 714 mm,
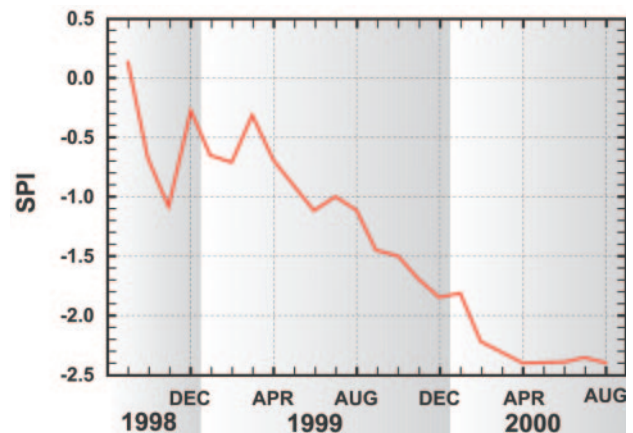

FIG. 65. One- to 24-month standardized precipitation index (SPI) values for the period September 1998 through August 2000. (Courtesy of Spain's Institute of Meteorology.)
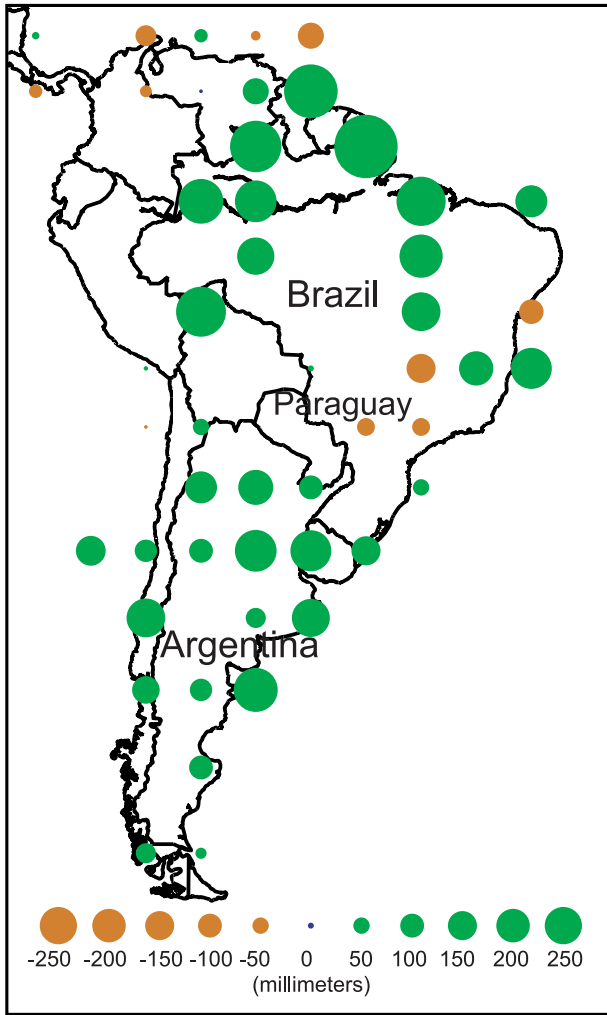
FIG. 66. Annual in situ precipitation anomalies (mm) for 2000. Precipitation anomalies were calculated for each station based on 1961–90 normals and averaged into 5° × 5° grid cells. Calculation of grid cell anomalies required at least 10 months of data. (Source: Global Historical Climatology Network.)

FIG. 67. Daily minimum temperatures (°C) at Mariscal, Paraguay, for the period 1 June–31 August 2000. (Source: National Climatic Data Center, DATSAV3 database.)

largely attributable to the dominance of La Niña early in the year (see section 2a), while the return to weak La Niña conditions later in the year was accompanied by another burst of unusually heavy rainfall in northern Australia.

Heavy rain events, which accompanied La Niña, brought widespread flooding to many areas in 2000. During the second and third weeks of February, extremely heavy rains with totals from 200 to 400 mm fell across normally arid central Australia and inland Queensland in association with an unusually well developed and southward displaced monsoonal trough. The torrential rainfall led to large flows in the ephermal inland-flowing rivers. Flooding in some parts of southwest Queensland was among the worst ever. The large volumes of water flowing inland led to partial filling, two to three months later, of Lake Eyre, a large, usually dry salt lake in South Australia that only rarely contains significant amounts of water.

Heavy rains also affected north Queensland during the last week of February due to an active monsoon coupled with Tropical Cyclone Steve. Major flooding and wind damage occurred in northeast Queensland as the cyclone tracked inland. Tropical Cyclone Steve then followed a remarkable, long-lived path (Fig. 70), moving west across the Northern Territory and Western Australia, then across inland areas of southern Western Australia, leaving a trail of widespread and sometimes severe flooding. Many pastoral stations in inland western Australia received their average yearly rainfall in just a few days, with some totals exceeding 200 mm within 24 h.

second only to the average of 784 mm recorded in 1974.

The most significant rainfall surpluses occurred in sparsely populated areas of northwestern and central Australia. Much of northwest Australia experienced their wettest year on record, and at least half the country had rainfall in the highest 10% of recorded falls (Fig. 69). A new Australian record for total annual rainfall at an observing station was set in 2000. Bellenden Ker, situated at an elevation of 1550 m in mountainous country adjoining the wet "Trade Wind coast" region of northeast Queensland, recorded an annual total of 12 461 mm, exceeding the previous record for a calendar year (11 852 mm) set at the same station just one year earlier. These excessively wet conditions are
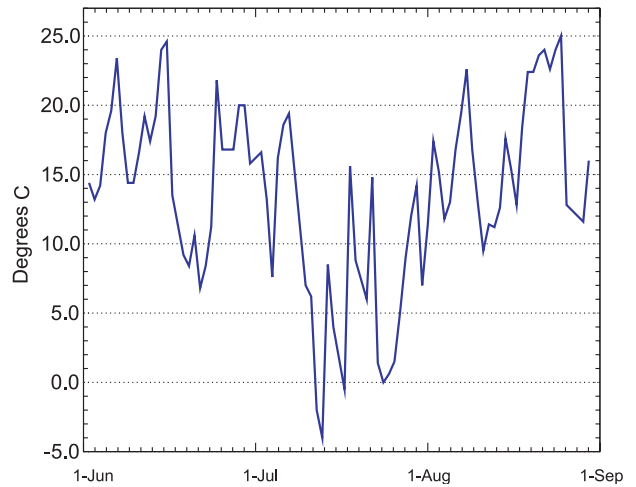
Widespread heavy rain drenched most of eastern Australia in November, due to a combination of persistent trough activity and tropical moisture that extended as far as the southern states. On 17 November, localized heavy rainfall occurred in the Mackay-Sarina area, with up to 470 mm in 24 h. In NSW, widespread amounts of 100–300 mm fell in one week over central and eastern areas of the territory and resulted in major flooding along many rivers.

Although precipitation was much above normal on a continent-wide scale, annual rainfall was less than normal in parts of the east, southeast, and southwest (Fig. 69). The most heavily populated areas of Australia, along the east and southeast coasts, received near-normal to below-average rainfall in 2000. Sydney and Brisbane were notably dry. Sydney's total of 822 mm was 67% of normal, while precipitation in Brisbane (660 mm) was only 57% of normal. Agricultural areas in southwestern Australia (slightly inland from the coast) recorded near-average rainfall in 2000, but much of this rain fell in the first quarter of the year, while rainfall during the growing season (April–November) was well below average.

Drought conditions developed along much of the eastern seaboard, and by late October severe 9-month rainfall deficits had developed in some areas of southeast Queensland and northeast NSW. The dry conditions, coupled with heavy vegetation from the previous wet season, and unusually warm, windy weather in September and October, led to a very bad bushfire season. In NSW, more than 250 000 ha of bushland were consumed in six weeks between Sydney and the Queensland border. Homes were frequently threatened and losses occurred. The fires continued well into October, before rain near the end of the month eased the danger.

3) New Zealand

In New Zealand, the maturing La Niña pattern early in the year was reflected by an unusually cool austral summer. With the weakening of La Niña in autumn, warmer-than-average sea surface tem-
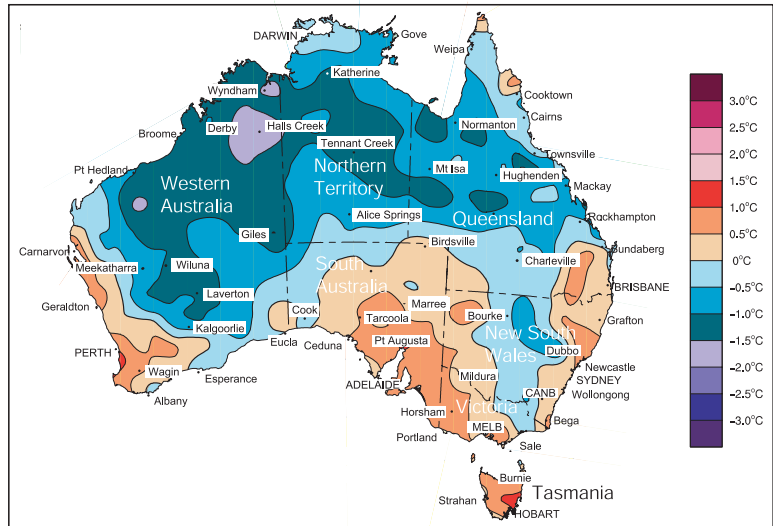

FIG. 68. January–December 2000 average maximum temperature anomalies.

peratures around the country and a tendency for ridging east of New Zealand became the primary controlling factors on the country's weather. The late austral summer and early autumn period was extremely dry in many areas with record low rainfall totals in a number of places in February. The year 2000 featured average to slightly below-average rains over much of the country, although some areas, notably parts of the northern and southern North Island, received only about 80% of their normal rainfall. By contrast, the relatively low rainfall areas of Canterbury and Otago, on the east coast of the South Island, experienced a wet year, with total rainfall for the year as much as 35% above normal.
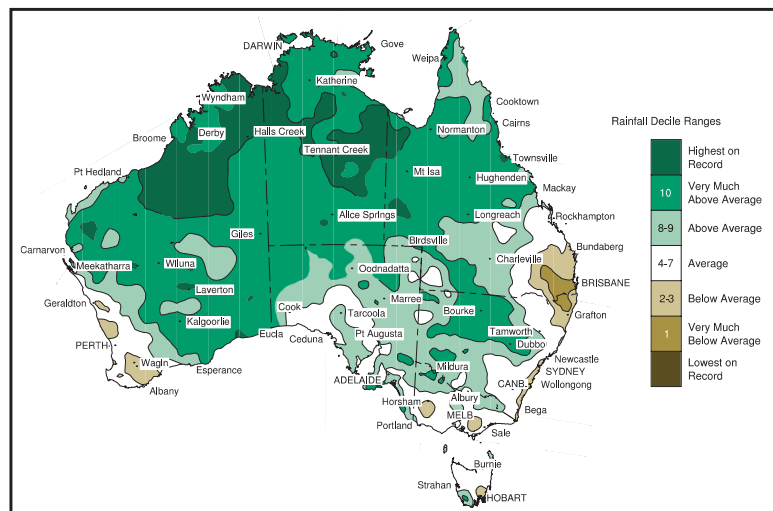

FIG. 69. January–December 2000 precipitation deciles.

FIG. 70. Path of Tropical Cyclone Steve in February 2000.

A rainfall event of particular note occurred in October, with extensive flooding in the central North Island. As much as 750 mm fell in 72 h on the Tararua Range area, followed by another 300 mm about one week later. Also in October, a fierce southerly storm caused widespread damage, particularly to parts of the eastern South Island where winds reached hurricane force (mean wind speeds up to 120 km h^{-1}).

The average temperature across New Zealand was near normal in 2000, 0.2°C above the 1961–90 average. The austral summer of 1999–2000 (DJF) was cooler than normal, especially in the far north of the North Island, and in the east of the South Island. The national average summer temperature was almost 2°C lower than in the summers of 1997–98 and 1998–99, though only 0.4°C below the 1961–90 normal. In contrast the winter (JJA) was exceptionally warm. Overall, it was the second warmest winter since reliable measurements were established in the 1850s, second only to the winter of 1984. The major cities of Wellington and Christchurch had their warmest mean winter temperatures since records began in the mid-nineteenth century.

5. Trace gases

a. Antarctic ozone

Ozone data over the Antarctic was collected via the solar backscatter ultraviolet instrument (SBUV/2) that measures total column ozone (from the surface to the top of the earth's atmosphere) on board the *NOAA-14* polar-orbiting satellite. Balloon-borne ozonesonde measurements were also collected by NOAA's Climate Monitoring and Diagnostics Laboratory. Although stratospheric ozone is measured throughout the world, the greatest changes in ozone concentration during recent decades have occurred in the Antarctic.

The ozone hole over the Antarctic does not develop until sunlight reaches the polar stratosphere near the end of the austral winter. For the past two decades significant decreases in ozone levels over Antarctica have been measured during the August through November period. Ozone levels near 300 Dobson units (DU) fall to levels near 150 DU as sunlight returns during the late austral winter and early spring to initiate photochemical reactions, which result in large losses of ozone.

The cold atmospheric conditions of the long polar night lead to the development of the polar vortex, a strong westerly circulation around the pole that is a large area isolated from the atmosphere to the north. As temperatures within the vortex fall below –78°C, large clouds composed mostly of nitric acid and water are ideal surfaces for chemical reactions involving chlorine.

Throughout the dark winter months, ordinarily inert compounds containing chlorine react on the surfaces of polar stratospheric cloud particles to form photochemically active chlorine compounds such as chlorine peroxide in the lower stratosphere. As sunlight returns to the arctic during the late winter and early spring, these compounds react in the presence of sunlight to destroy ozone, lowering ozone concentrations throughout the Antarctic stratosphere.

Although ozone destruction also occurs in the Arctic during the boreal spring, ozone loss is not as intense or as widespread. The polar vortex over the arctic is not as strong and temperatures are not as cold as those within the Southern Hemisphere polar vortex, so the production of large reservoirs of photochemically active chlorine compounds is not as common.

The ozone hole is defined geographicaly as the area wherein the total ozone amount is less than 220 Dobson units. The ozone hole has steadily grown in size (up to 27 million km^2) and duration (from August through early December) over the past two decades. Measurements from the SBUV/2 instrument (Fig. 71) illustrate the cyclical nature of the ozone hole. In 2000, the size of the hole began to grow quickly in mid-August until it reached a size greater than 27 million km^2 in early September. Although the areal extent of this ozone hole was the greatest ever recorded, the ozone hole disappeared about one month earlier than in 1999 and much earlier than the most recent 10-yr average.

The vertical structure of ozone over Antarctica in 2000 was obtained from ozonesondes flown over the South Pole. A vertical profile based on 65 ozone profiles is shown in Fig. 72. In the lower stratosphere (15–25 km above the surface), ozone concentrations remained relatively constant throughout the autumn (MAM) and much of the winter months (JJA) with signs of somewhat higher ozone amounts descending from higher altitudes. By August, ozone amounts in the stratosphere began to gradually decline. This likely reflected the chemical loss of ozone near the periphery of Antarctica where sunlight was already present, and subsequent transport of ozone depleted air over the South Pole. By September ozone concentration began to quickly drop. This is reflected in decreasing total column amounts (Fig. 73). By late September, ozone was completely removed from a region between 15–20 km above the surface.

Ozone concentrations began to decrease about one week earlier in 2000 than in previous years. Total column ozone fell near 100 Dobson units by 25 September. This minimum approached, but did not exceed, the record low values (90 DU) measured since 1993.

Total ozone amounts began to recover earlier than generally observed in the past decade, exceeding 265 DU by 3 November (Fig. 73). This primarily reflects a large influx of ozone at altitudes above 20 km. Recovery of the ozone hole in 2000 may have been related to warmer stratospheric temperatures and the less circular shape (stronger wavenumbers 2 and higher) of the Antarctic polar vortex. This would allow greater exposure to processed air early in the ozone hole season producing early depletion, and weakening of the vortex later in the spring. The net result is an influx of ozone from lower latitudes and higher altitudes (also see section 3b).

b. Trends in greenhouse gases

While most of the atmosphere consists of nitrogen and oxygen (~99% of dry air), these gases are transparent to infrared radiation. Water vapor, which varies from 0% to 2%, carbon dioxide and other trace gases such as methane, carbon monoxide, nitrous oxide, and halogenated compounds absorb some of the thermal radiation emitted from the earth's surface. These radiatively active gases are known as greenhouse gases because they trap thermal radiation, which provides the mechanism for warming the earth to an inhabitable temperature.

1) CARBON DIOXIDE

Carbon dioxide (CO_2) is the most abundant carbon cycle greenhouse gas and has a direct impact on the
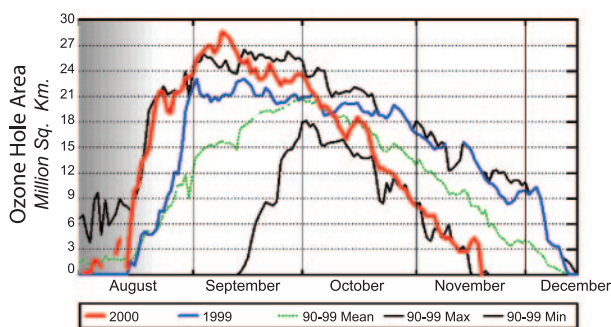

FIG. 71. Areal extent of the Antarctic ozone hole based on data collected from NOAA's SBUV/2 instrument. Data are included for 2000 (red line), 1999 (blue line), mean ozone hole area for each day over the 1990–99 period (green line), maximum ozone hole area (upper black line) and minimum ozone hole area (lower black line) for each day throughout the 1990–99 period.

earth's climate through the absorption of infrared radiation. For the 10 000 yr preceding the industrial revolution, the atmospheric abundance of CO_2 was nearly constant at ~280 ppm (ppm = parts in 10^6 by mole fraction). This abundance represented a balance among large seasonal fluxes (on order of 100 Gt C yr^{-1}, where 1 Gt = 10^{15}g) between the atmosphere and biosphere (photosynthesis and respiration) and the atmosphere and the ocean (physical exchange of CO_2). Since the late 1800s, atmospheric CO_2 has increased by approximately 30%, primarily due to emissions from combustion of fossil fuels (currently about 7 Gt C yr^{-1}) and, to a lesser extent, deforestation (0–2 Gt C yr^{-1}). High-precision measurements of atmospheric CO_2, beginning in 1958, show the average increase of CO_2 in the atmosphere corresponds to ~55% of the CO_2 emitted by fossil fuel combustion (Keeling et al. 1995), but this
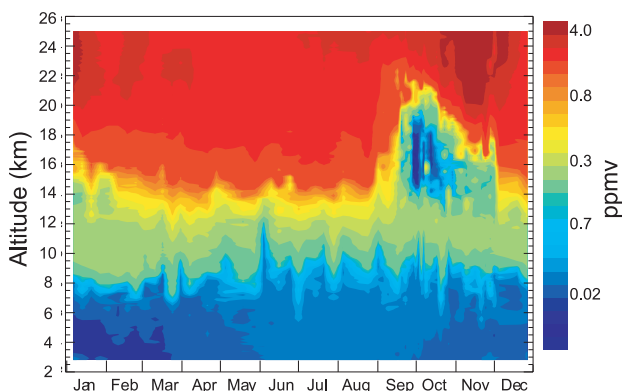

FIG. 72. Time–height cross section of ozone mixing ratio at the South Pole for the year 2000 showing the ozone hole in September–November. (Courtesy: S. Oltmans, B. Johnson, and H. Vomel, NOAA/CMDL.)
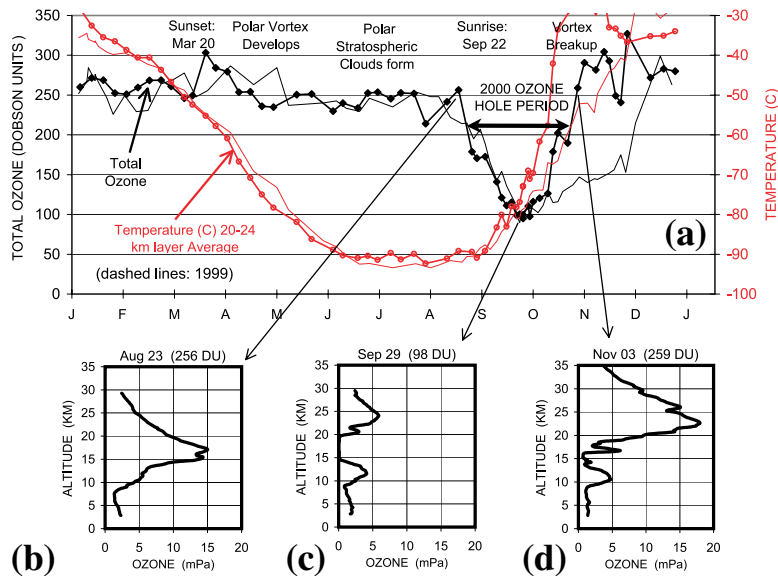
FIG. 73. (a) Total ozone (black curve) and temperature (red curve) from ozonesondes flown at the South Pole in 2000. (b) Ozone profile for 23 August prior to the development of the ozone hole, (c) profile on 25 September when total column ozone is a minimum, and (d) profile from the period after the vortex has broken down and ozone has returned to Antarctica. (Courtesy: B. Johnson and S.Oltmans, NOAA/CMDL.)

fraction varies from ~20% to ~90% (Conway et al. 1994; Ciais et al. 1995). The remaining fossil fuel CO_2 is removed from the atmosphere by the oceans and the terrestrial biosphere.

The net increase in atmospheric CO_2, determined from a globally distributed network of air sampling sites, is plotted for 1980–99 in Fig. 74 (red line). Global emissions of carbon resulting from fossil fuel combustion (available from the Carbon Dioxide Information and Analysis Center) are also plotted (black line). Note the variability of the increase in carbon during the 20-yr period. The increase was a relatively small fraction of fossil-fuel emissions in 1992, but nearly 90% of the fossil emissions of carbon remained in the atmosphere during 1998.

The difference between fossil-fuel emissions and the atmospheric increase is the net global sink. Clearly, the variations in the atmospheric increase are much larger than the variations in fossil fuel emissions. However, these variations arise from relatively small imbalances between the large one-way atmosphere–ocean and atmosphere–terrestrial biosphere fluxes. Most attempts to explain the interannual variability of the atmospheric CO_2 increase have focused on short-term climate fluctuations (e.g., ENSO and post-Pinatubo cooling) but the mechanisms, especially the role of the terrestrial biosphere, are not well

understood. For example, it has been speculated that the high CO_2 growth rate in 1998 was related to unusually warm temperatures. However, an analysis of 1999 CO_2 measurements indicates a return to average or a lower-than-average growth rate in 1999, even though global temperatures in 1999 were only slightly lower than in 1998.

Understanding the relative contributions of the ocean and biosphere to the net global carbon sink has important environmental policy implications. High-precision measurements of atmospheric CO_2 abundance alone are insufficient to calculate this partitioning. One approach uses measurements of the carbon-isotopic composition of CO_2. Results of the analysis using isotopic data are shown in Fig. 74 as green (biosphere) and blue (ocean) shaded areas. During the 1990s, on average, about half of the net carbon sink went into each reservoir, but the amount of fossil CO_2 that goes into each reservoir varies from year to year. For example, the biosphere was a relatively large sink in 1996, but it was a small net source of carbon to the atmosphere in 1998. The ocean sink was of comparable magnitude in those two years. A better understanding of the processes that remove CO_2 from the atmosphere and how these processes respond to climate fluctuations will enable better predictions of future CO_2 levels, which will in turn decrease the uncertainty associated with models of future climate.

2) METHANE

Methane (CH_4) contributes about 20% of the direct radiative forcing attributable to anthropogenic greenhouse gases. Methane also influences the earth's climate indirectly through chemical reactions with other greenhouse gases such as tropospheric ozone (O_3), stratospheric water vapor (H_2O), and the hydroxyl radical (OH). The indirect effects are estimated to add ~40% to the direct climate effect of methane (Lelieveld et al. 1993).

High-precision measurements of atmospheric methane provide climate modelers with current and historical rates of CH_4 increase, while also providing a useful constraint on the CH_4 budget. In Fig. 75a, smoothed, globally averaged CH_4 mole fractions from the NOAA/CMDL air-sampling network are plotted as a function

of time. Methane concentrations have increased throughout this nearly 20-yr period, but the rate of increase has slowed in the past 10 years. Dlugokencky et al. (1998) have explained the decreasing growth rate as an "approach to steady state," meaning global emission rates and the CH_4 atmospheric lifetime are both nearly constant. The long-term trend can also be explained by increasing emission rates and decreasing CH_4 lifetime (Karlsdottir and Isaksen 2000).

Figure 75b shows annual CH_4 increases that are determined from the deseasonalized trend shown in Fig. 75a. This rate of increase is the net difference between total CH_4 emissions and losses, and it is equal to about 3% of total emissions during the 1990s. Superimposed upon the long-term decreasing CH_4 trend are significant interannual variations in CH_4 growth rates; (the largest variations were in 1991 and 1998). Some of this year-to-year variability can be associated with significant natural events and serves to test our understanding of specific terms in the methane budget.

The increase in CH_4 growth rate during 1991 occurred immediately after the eruption of Mount Pinatubo. Dlugokencky et al. (1996) attributed this to the effects of SO_2 and ash injected during the eruption on CH_4 chemical loss rates. During 1998 the imbalance between CH_4 sources and sinks more than doubled relative to the previous three years. This was also the warmest year on record. Dlugokencky et al. (2001) found that the warm conditions during 1998
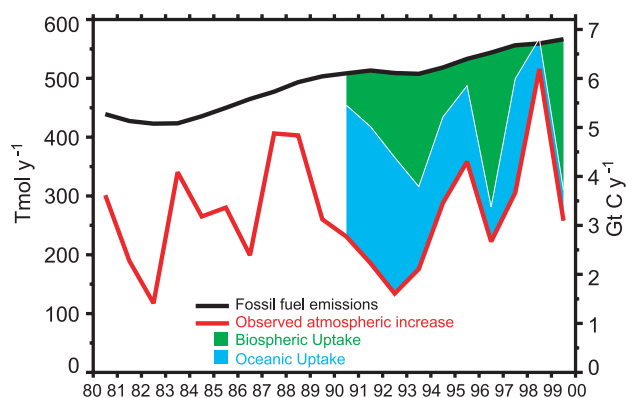
likely meant more CH_4 emissions from natural wetlands, a CH_4 source that is strongly temperature dependent. While the measurements of CH_4 in the contemporary atmosphere cannot be used to predict the future atmospheric abundance of this important greenhouse gas, a warmer climate in the future has the potential to cause an increase in atmospheric methane.

3) CARBON MONOXIDE

Although carbon monoxide (CO) does not strongly absorb terrestrial infrared radiation, its influence on the earth's climate comes through atmospheric chemical reactions with other compounds. Because it reacts with the hydroxyl radical (which influences the lifetimes of CH_4) as well as tropospheric O_3 (also a greenhouse gas) emissions of CO can be considered equivalent to emissions of CH_4 (Prather 1996). It is also believed that emissions of CO may contribute more to radiative forcing over decadal timescales than emissions of anthropogenic N_2O (Daniel and Solomon 1998).

Zonally averaged CO mole fractions (blue circles) for the latitude band 53°–90°N are plotted as a function of time in Fig. 76a. A deseasonalized trend curve (solid blue line) and a function (dashed red line) are also plotted. The function represents the average trend and seasonal cycle for CO in this northern high-lati-
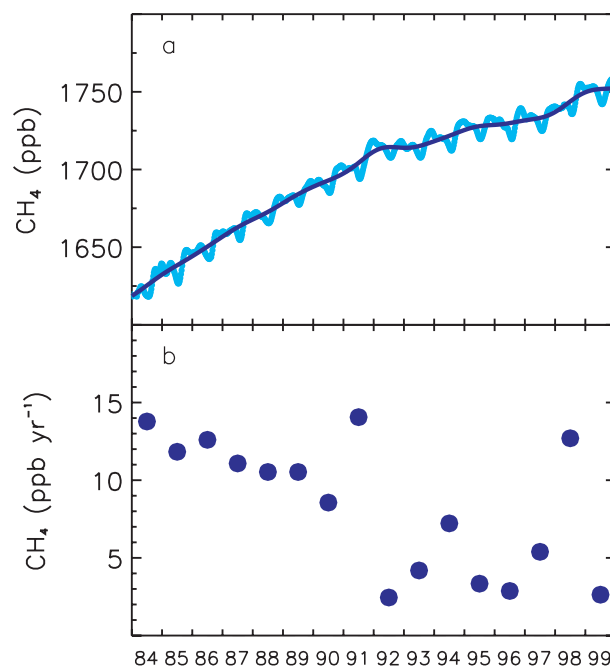

FIG. 74. Global CO_2 emissions due to fossil fuel use (black line) from the Carbon Dioxide Information and Analysis Center and observed global atmospheric CO_2 increase (red line) determined from NOAA/CMDL cooperative air sampling network measurements. Shaded areas are estimates of terrestrial (green) and oceanic (blue) sinks for CO_2 based on atmospheric measurements of CO_2 abundance and isotopic composition. (Courtesy: T. J. Conway, NOAA/CMDL.)

FIG. 75. (a) Globally averaged methane mole fractions. The solid line is the deseasonalized trend. (b) Global, annual increase in CH_4 mole fraction. (Courtesy: E. Dlugokencky, NOAA/CMDL.)

tude region for 1991–99. While there is a small negative trend in CO, its time series is dominated by interannual variability.

The most significant feature occurred in 1998, as shown most clearly in Fig. 76b as plots of residuals from the function (blue circles minus red curve). These residuals represent differences from the average trend and seasonal cycle for CO during this time period. The signal for CO in 1998 is clearly the largest in the measurement record. Bruhwiler et al. (2000) and Kasischke et al. (2000) have studied the potential causes of this anomaly in atmospheric CO during 1998. They found that large forest and peatland fires in North America and Siberia during late summer and early autumn released an estimated 164 Tg CO, and that these emissions are responsible for the anomalous CO observed during 1998.

4) HALOCARBONS AND NITROUS OXIDE

The long-lived halocarbons and nitrous oxide that are released into the troposphere by human activities contribute to stratospheric ozone depletion and climate
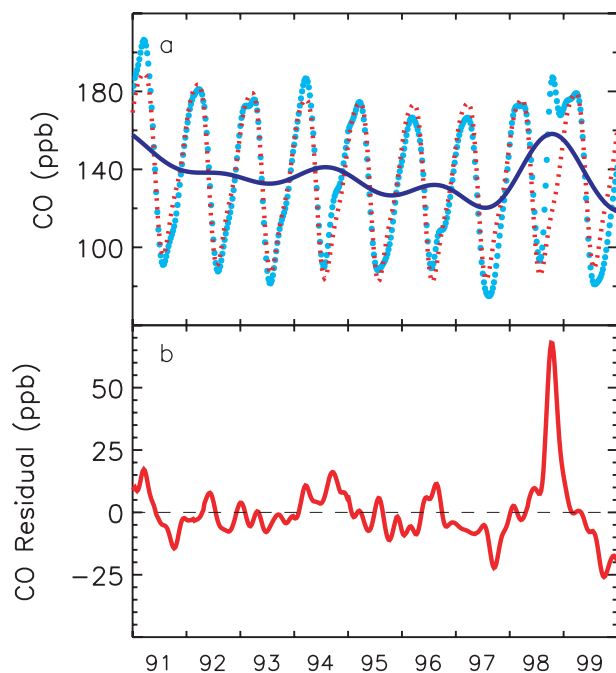

FIG. 76. (a) Zonally averaged CO mole fractions for the high-northern latitude zone 53°–90°N. The deseasonalized trend is plotted as a solid blue line. The dashed red line is a function consisting of a series of four harmonics and a quadratic polynomial used to represent the average long-term trend and seasonal cycle for CO during 1991–99. (b) Difference (residuals) between the CO zonal averages and the function. (Courtesy: P. C. Novelli, NOAA/CMDL.)

forcing. Nitrous oxide (N_2O) has a much greater greenhouse warming potential on a per molecule basis (by a factor of ~310) than carbon dioxide over a 100-yr time horizon but is present at mixing ratios almost 1000 times less. It is responsible for about 7% of total climate forcing from all of the greenhouse gases (Houghton et al. 1995). The production of the long-lived chlorine- and bromine-containing halocarbons from developed countries have been restricted by the 1987 Montreal Protocol and its subsequent amendments. The elimination of these controlled substances in developing countries is scheduled for 2010. The two primary chlorofluorocarbons, CFC-11 (CCl_3F) and CFC-12 (CCl_2F_2), which accounted for 50% of the total chlorine in the troposphere, had growth rates of ~5% per year in the 1970s and 1980s before the Montreal Protocol restrictions started in the early 1990s (Elkins et al. 1993).

The most striking observation is the rapid decline of methyl chloroform (CH_3CCl_3), a solvent used in degreasing metals, in the troposphere as shown in Fig. 77. This decline is due to its short atmosphere lifetime (5.2 yr) caused primarily by its reaction with the tropospheric hydroxyl radical (Montzka et al. 2000). In spite of the restrictions imposed by the Montreal Protocol, tropospheric levels of CFC-12 and the halons (H-1211, $CBrClF_2$, and H-1301, $CBrF_3$) are still increasing at slow rates (Fig. 77). Bromine-containing chemicals, like the halons, are 50 times more effective at destroying stratospheric ozone than chlorine on a per atom basis, but are present in the atmosphere at lower concentrations. The continued increase of these compounds in the atmosphere is the result of large reservoirs still in use (refrigerators, air conditioners, fire extinguishers, etc.) and legal production in developing countries.

The CFC replacement compounds, the hydrochlorofluorocarbons (HCFCs), which still contain some chlorine, but are shorter lived in the atmosphere than the CFCs, are experiencing rapid growth in the troposphere (Fig. 77). The decline in CH_3CCl_3 is the primary driver for the decrease of ~5% of total effective equivalent chlorine (chlorine + 50 times bromine or EECl) after its peak sometime between mid-1992 and mid-1994 (Montzka et al, 1999). Its decline currently compensates for the increases of CFC-12, HCFCs, and the halons in the troposphere.

Measurements from NOAA's network of in situ monitoring instruments indicate that mean global mixing ratios for tropospheric N_2O at the beginning of 2000 are about 315 parts per billion (ppb) (Fig. 78). On average, the growth rate since 1987 is approximately 0.8 ppb yr^{-1}, but in recent years the growth rate
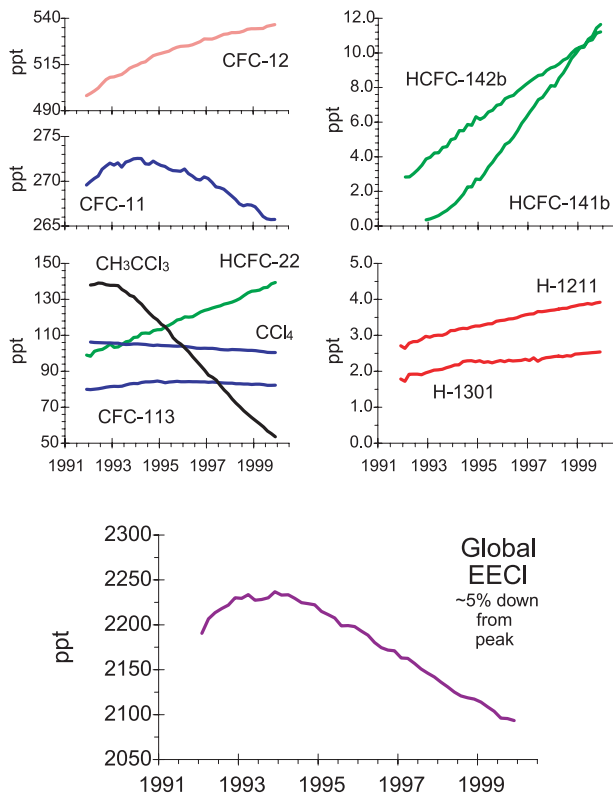
FIG. 77. Global trends of halocarbons and effective equivalent chlorine in the troposphere from the NOAA/CMDL network. Mixing ratios (reported as dry mole fractions in parts per trillion, ppt) of CFC-12, CFC-11, CH_3CCl_3, and CCl_4 from in situ instruments and CFC-113, HCFC-22, HCFC-141b, HCFC-142b, halons H-1211, and H-1301 from flask sample versus time [updated data from Elkins et al. (1993); Butler et al. (1998); Montzka et al. (1999)]. (Courtesy: S. Montzka and J. Butler, NOAA/CMDL.)

FIG. 78. Tropospheric trends of nitrous oxide (N_2O) from in situ gas chromatographs from the NOAA/CMDL network. Values of mixing ratios of (a) monthly mean at individual stations, (b) hemispheric and global means, and (c) growth rates are shown. Values are reported as dry mole fractions in parts per billion (ppb). (Courtesy: T. Thompson and B. Hall, NOAA/CMDL.)

has increased to almost 1 ppb yr^{-1}. The reason for the changing growth rate is unknown.

5) STRATOSPHERIC WATER VAPOR

Although water vapor concentrations in the stratosphere are several orders of magnitude smaller than those in the troposphere, recent modeling work (Forster and Shine 1999; Dvortsov and Solomon 2001) has shown that water vapor changes in the stratosphere can play a significant role in both stratospheric and tropospheric temperature changes. There is strong evidence for increasing water vapor in the stratosphere over recent decades (Rosenlof et al. 2001; Oltmans et al. 2000). This can be seen in the 20-yr record of water vapor profiles recorded at Boulder, Colorado (Fig. 79). Water vapor has increased by approximately 20%, although the rate has not been constant throughout the period, with declining concentrations in recent years (Rosenlof et al. 2001).
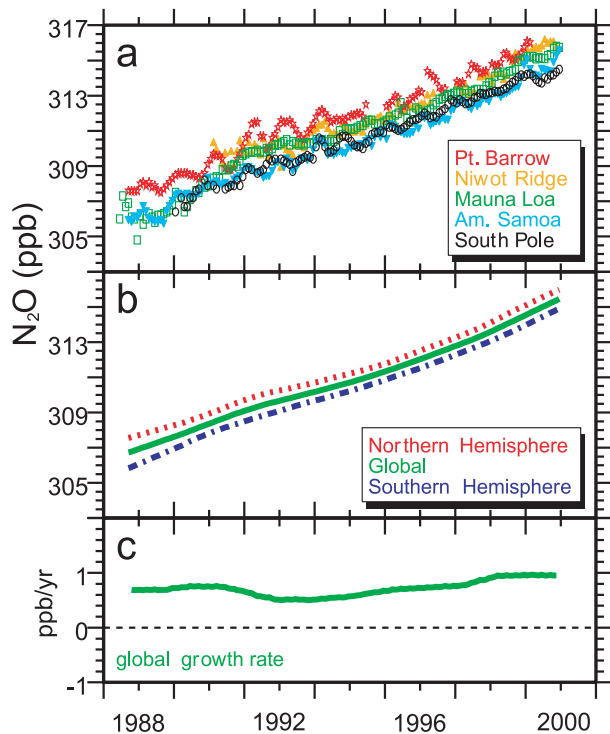
Although some increase in stratospheric water vapor is expected due to rising methane levels in the atmosphere, this accounts for no more than one-half of the increase. Methane is a source of water vapor in the stratosphere by its conversion through photochemical oxidation. The equatorial tropical tropopause is a source of dry air to the stratosphere and is in effect a sink for stratospheric water vapor. Changes in the flux of air through the tropopause may thus be important in the stratospheric increase. The cause of the increase beyond that expected from methane is not presently known.

c. *Shortwave atmospheric transmission above*
the marine boundary layer over the mid-Pacific

The temperature of the earth is affected by the transmission of both longwave and shortwave energy. Although considerable research and monitoring efforts have gone into the study of longwave energy with respect to its relationship to climate change, shortwave energy has received considerably less attention. As a result, there are less well-defined theories for possible global trends that might affect the climate of the earth.

Nonetheless, sustained measurements of shortwave transmission under clear skies have been carried out at the NOAA Mauna Loa Observatory since 1958 and have revealed several important events in the baseline atmosphere of the mid-Northern Hemisphere Tropics (Dutton and Bodhaine 2001 and references therein). Of particular interest are the effects of major volcanic eruptions, annual variability driven by the annual oscillation of Asian dust transport over the mid-Pacific, and the long-term stability of the transmission. The latter is useful in assessing any possible trends in the amount of solar radiation reaching the earth's surface. Because the Mauna Loa observatory is located at an elevation of 3.4 km, this record is indicative of the solar transmission in the stratosphere and upper two-thirds of the troposphere.

At the beginning of the Mauna Loa solar transmission record (1958–62), there was no change in the annual mean transmission. A baseline transmissivity level, 0.9335, was clearly established during this 5-yr period. But in 1963 the eruption of the Agung volcano in the Southern Hemisphere resulted in a significant depression of values to near 0.915 for more than a year. A series of subsequent smaller eruptions prevented the transmission from returning to the baseline levels until 1978 when, for a few months, the values slightly exceeded the earlier baseline. Since the explosive volcanic eruptions of El Chichón in 1982 and Mount Pinatubo in 1991, the transmission level has not reached and maintained the background level of the late 1950s.

Recovery to the previously established background levels appeared to be under way in the late 1990s until the transport of an unusually large annual springtime aerosol event to Hawaii in 1999. The subsequent months of 1999 did not show a complete recovery from the springtime, and the year 2000 began with depressed transmission and another unusually extended spring depression, although not as deep as 1999. However, in the last two months of 2000 the transmission quickly increased to the highest levels since the anomalous maximum in 1978. The level of transmission at the end of 2000 is consistent with the recovery toward historic baseline levels that appeared to be occurring during the mid- to late 1990s (Fig. 80). However, the December 2000 levels had not yet been sustained to the point of assuring a full recovery to the 1950s baseline.

The specific cause of the anomalous springtime aerosol event over Hawaii in 1999 and again in 2000 has not been identified, although there have been scattered reports of excessive aerosols in the eastern Asia source region during the period of interest. The typical enhanced tropospheric aerosol optical depths measured over Mauna Loa in 2000 were less than 0.07 in the midvisible and often less than 0.05, so detection and monitoring of these sustained events (for months) in the vicinity and downwind of Hawaii would not be easily achieved by current satellite sensors. Careful and prolonged investigations of the aerosol source regions would be necessary to explain the continuously varying nature of the aerosol loading and resultant atmospheric transmission over Hawaii.
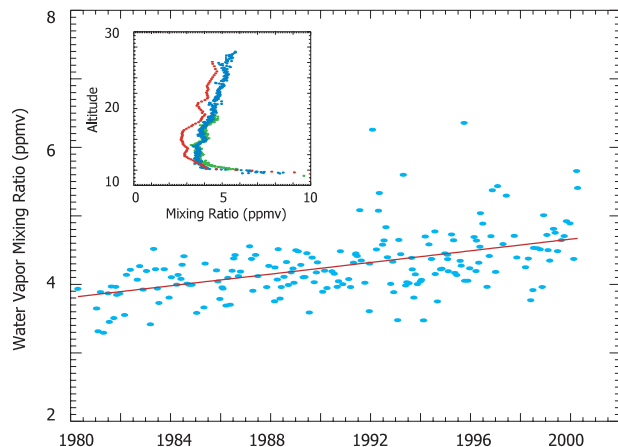

FIG. 79. Time series of water vapor mixing ratio at 20–22 km over Boulder, CO, showing a 20% increase in water vapor in the stratosphere over a 20-yr period. (Courtesy: S. Oltmans and H. Vomel, CIRES and NOAA/CMDL.)
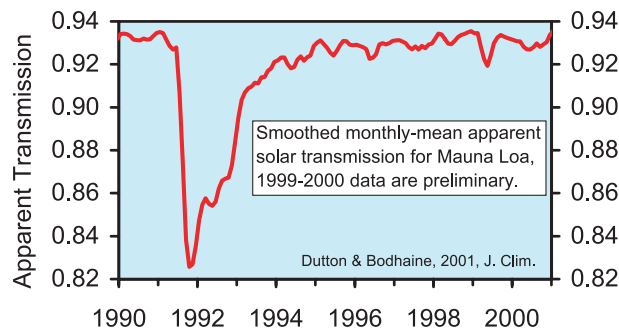

FIG. 80. Solar transmission record from the NOAA/CMDL Mauna Loa Observatory, HI. The effects of the 1991 Mount Pinatubo volcanic eruption are clearly observable as are some large spring Asian aerosol transport events in 1999 and 2000. (Courtesy: E. Dutton and B. Bodhaine, NOAA/CMDL).

6. Seasonal summaries

Fig. 82. December 1999–February 2000 (top) Northern Hemisphere and (bottom) Southern Hemisphere 500-hPa geopotential heights (contours, interval is 9 dam) and anomalies (shading). Anomalies are departures from the 1979–95 base period means.
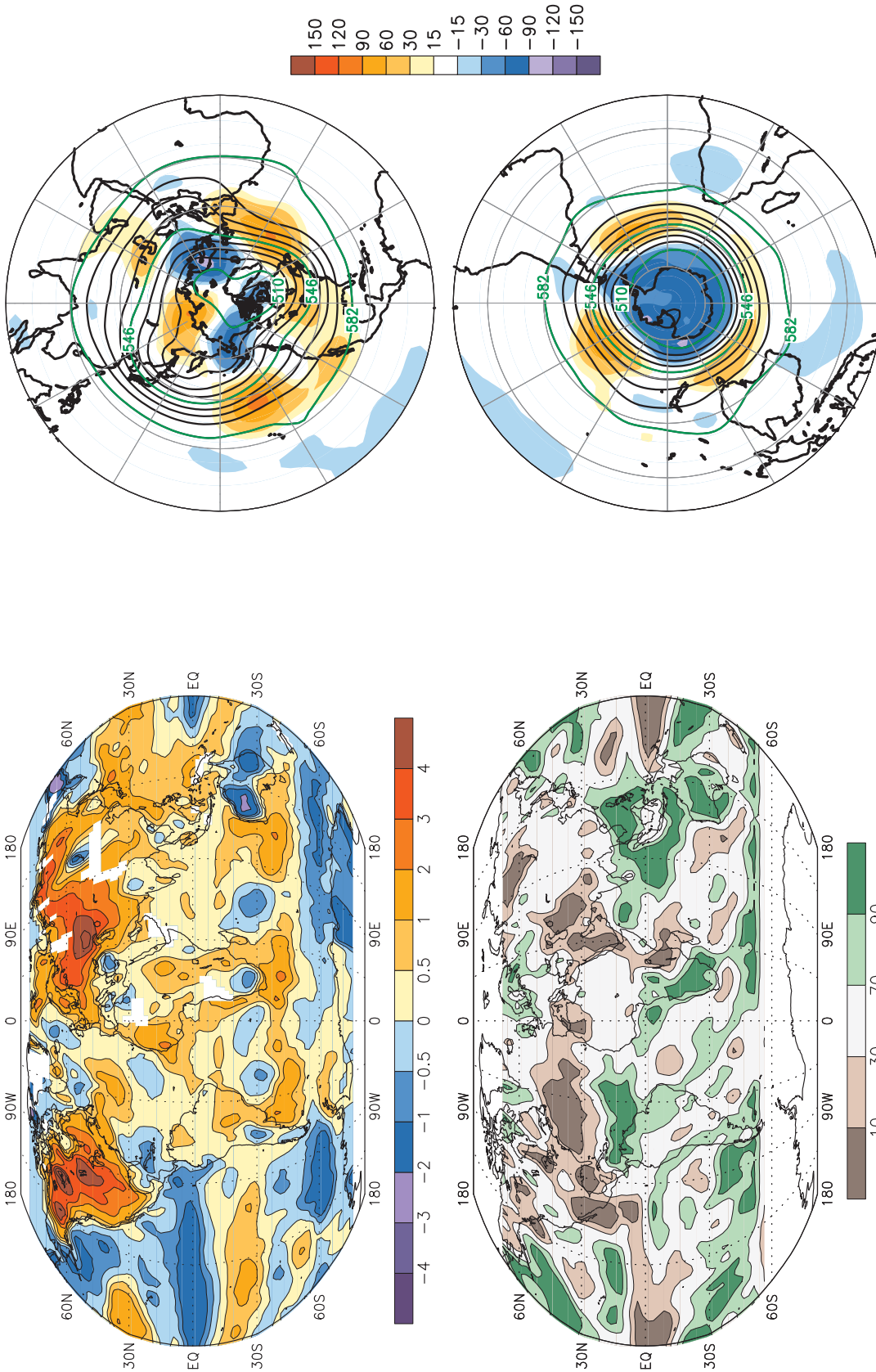

Fig. 81. December 1999–February 2000 surface temperature anomalies (top, °C) and precipitation percentiles based on a gama distribution fit to the 1979–95 base period (bottom). Temperature anomalies (1961–90 base period) are based on station data over land and sea surface temperature data over water. Precipitation data are obtained from a merge of rain gauge observations and satellite-derived precipitation estimates (Janowiak and Xie 1999). The analysis is omitted in data-sparse regions (white areas).

Fig. 84. March–May 2000 Northern Hemisphere (top) and Southern Hemisphere (bottom) 500-hPa geopotential heights (contours, interval is 9 dam) and anomalies (shading). Anomalies are departures from the 1979–95 base period means.
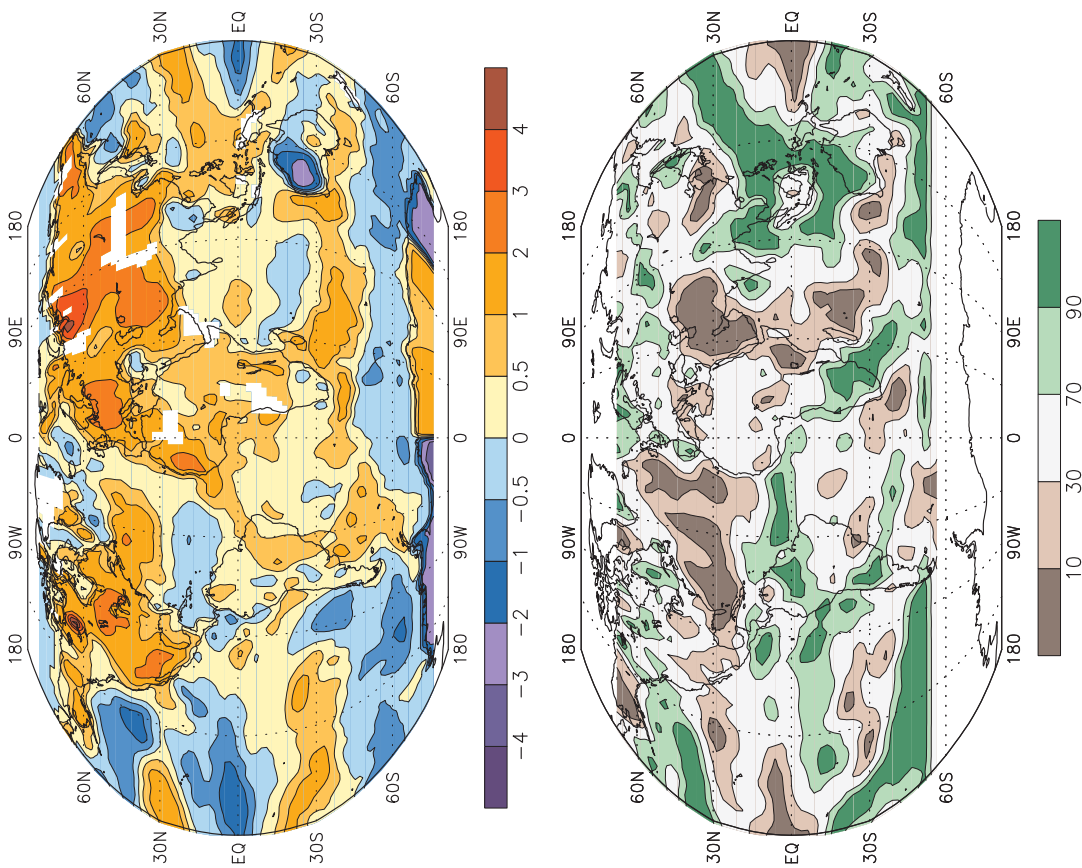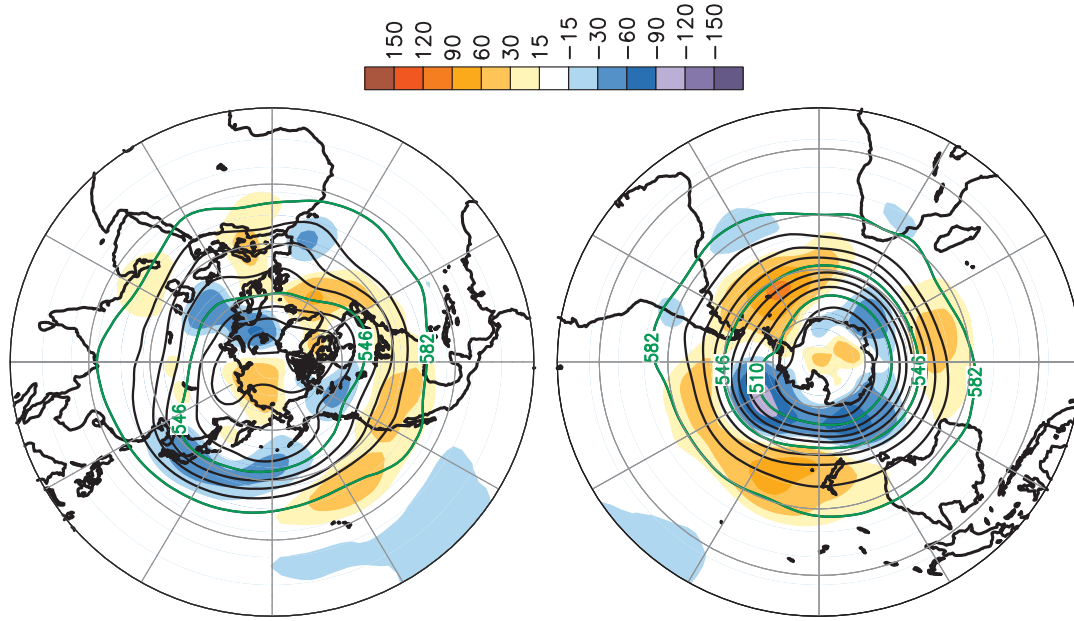

Fig. 83. March–May 2000 surface temperature anomalies (top, °C) and precipitation percentiles based on a gamma distribution fit to the 1979–95 base period (bottom). Temperature anomalies (1961–90 base period) are based on station data over land and sea surface temperature data over water. Precipitation data are obtained from a merge of rain gauge observations and satellite-derived precipitation estimates (Janowiak and Xie 1999). The analysis is omitted in data-sparse regions (white areas).

Fig. 86. June–August 2000 Northern Hemisphere (top) and Southern Hemisphere (bottom) 500-hPa geopotentials heights (contours, interval is 9 dam) and anomalies (shading). Anomalies are departures from the 1979–95 base period means.
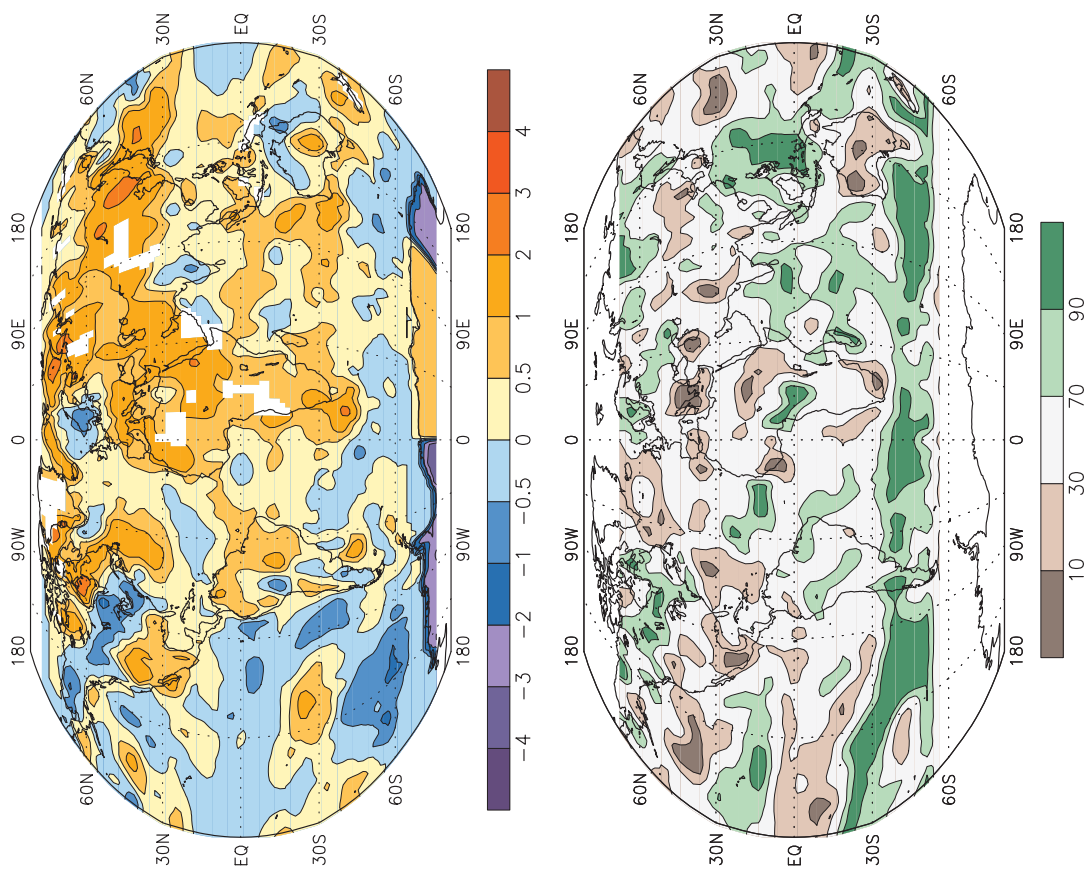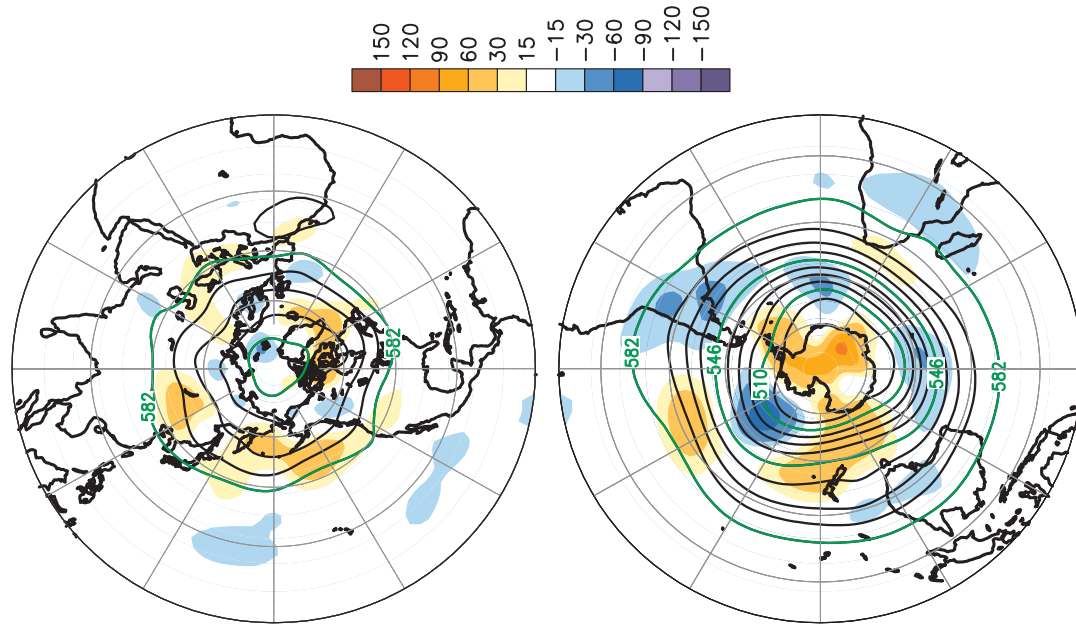

Fig. 85. June–August 2000 surface temperature anomalies (top, °C) and precipitation percentiles based on a gamma distribution fit to the 1979–95 base period (bottom). Temperature anomalies (1961–90) base period) are based on station data over land and sea surface temperature data over water. Precipitation data are obtained from a merge of rain gauge observations and satellite-derived precipitation estimates (Janowiak and Xie 1999). The analysis is omitted in data-sparse regions (white areas).

FIG. 88. September–November 2000 Northern Hemisphere (top) and Southern Hemisphere (bottom) 500-hPa geopotentials heights (contours, interval is 9 dam) and anomalies (shading). Anomalies are departures from the 1979–95 base period means.
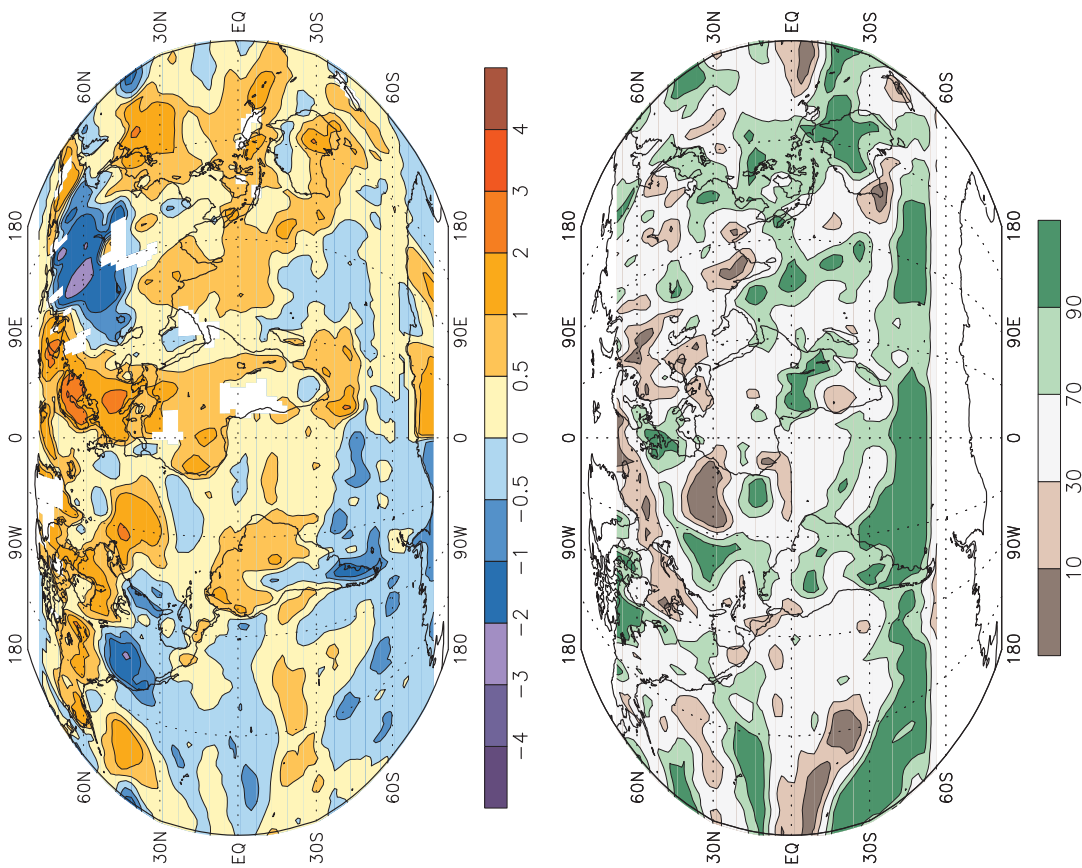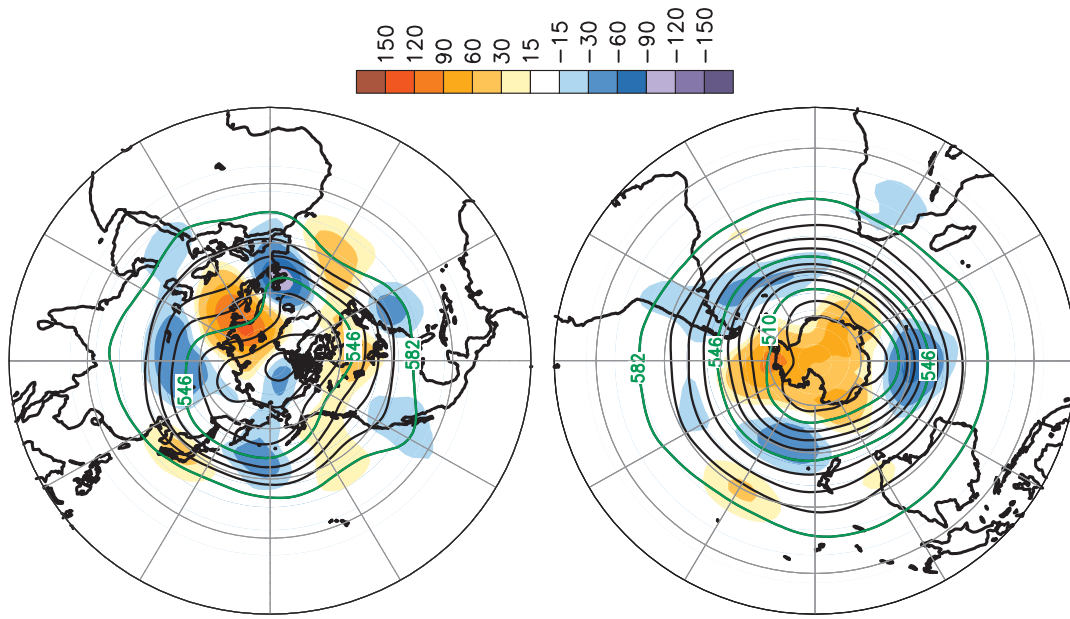

FIG. 87. September–November 2000 surface temperature anomalies (top, °C) and precipitation percentiles based on a gamma distribution fit to the 1979–95 base period (bottom). Temperature anomalies (1961–90 base period) are based on station data over land and sea surface temperature data over water. Precipitation data are obtained from a merge of rain gauge observations and satellite-derived precipitation estimates (Janowiak and Xie 1999). The analysis is omitted in data-sparse regions (white areas).

Appendix: Contributors

Atmospheric Environment Service, Environment Canada, Ottawa, Canada
- D. Phillips

National Climatic Data Center/NESDIS/NOAA
- T. Wallis
- T. Peterson
- T. Ross

Climate Monitoring and Diagnostics Laboratory/ERL/ NOAA
- J. Butler
- T. Conway
- E. Dlugokencky
- B. Johnson
- S. Montzka
- P. Novelli
- S. Oltmans

Deutscher Wetterdienst, Hamburg, Germany
- G. Rosenhagen

Instituto Nacional de Meteorologia, Barcelona, Spain
- R. Diaz-Pabon

World Meteorological Organization, Geneva, Switzerland
- L. Malone

References

Alexander, L. V., and P. D. Jones, 2001: Updated precipitation series for the U.K. *Atmos. Sci. Lett.,* in press.

Behringer, D. W., M. Ji, and A. Leetmaa, 1998: An improved coupled model for ENSO prediction and implications for ocean initialization. Part I: The ocean data assimilation system. *Mon. Wea. Rev.,* **126,** 1013–1021.

Bell, G. D., and M. S. Halpert, 1998: Climate assessment for 1997. *Bull. Amer. Meteor. Soc.,* **79** (May), S1–S50.

——, and M. Chelliah, 1999: The African easterly jet and its link to Atlantic basin tropical cyclone activity and the global monsoon system. *Proc. Twenty-third Annual Climate Diagnostics Workshop,* Miami, FL, NCEP/NOAA, 215–218.

——, ——, C. F. Ropelewski, V. E. Kousky, A. V. Douglas, R.C. Schnell, and M. E. Gelman, 1999: Climate assessment for 1998. *Bull. Amer. Meteor. Soc.,* **80** (May), S1–S48.

——, and Coauthors, 2000: Climate assessment for 1999. *Bull. Amer. Meteor. Soc.,* **81** (June), S1–S50.

Brown, R. D., and R. O. Braaten, 1998: Spatial and temporal variability of Canadian monthly snow depths, 1946–1995. *Atmos.– Ocean,* **36,** 37–54.

Bruhwiler, L. M., E. S. Kasischke, E. J. Dlugokencky, and P. Tans, 2000: Boreal biomass burning during 1998 and anomalous northern hemispheric CO. *Eos, Trans. Amer. Geophys. Union,* **81,** 260.

Butler, J. H., S. A. Montzka, A. D. Clarke, J. M. Lobert, and J. W. Elkins, 1998: Growth and distribution of halons in the atmosphere. *J. Geophys. Res.,* **103,** 1503–1511.

Ciais, P., P. P. Tans, and M. Trolier, 1995: A large northern-hemisphere terrestrial CO_2 sink indicated by the $^{13}C/^{12}C$ ratio of atmospheric CO_2. *Science,* **269,** 1098–1102.

Conway, T. J., P. P. Tans, L. S. Waterman, K. W. Thoning, D. R. Kitzis, K. A. Masarie, and N. Zhang, 1994: Evidence for interannual variability of the carbon cycle from the NOAA/ CMDL global air sampling network. *J. Geophys. Res.,* **99,** 22 831–22 855.

Dai, A., I. Y. Fung, and A. D. Del Genio, 1997: Surface observed global land precipitation variations during 1900–88. *J. Climate,* **10,** 2943–2961.

Daniel, J. S., and S. Solomon, 1998: On the climate forcing of carbon monoxide. *J. Geophys. Res.,* **103,** 13 249–13 260.

Dlugokencky, E. J., E. G. Dutton, P. C. Novelli, P. P. Tans, K. A. Masarie, K. O. Lantz, and S. Madronich, 1996: Changes in CH_4 and CO growth rates after the eruption of Mt. Pinatubo and their link with changes in tropical tropospheric UV flux. *Geophys. Res. Lett.,* **23,** 2761–2764.

——, K. A. Masarie, P. M. Lang, and P. P. Tans, 1998: Continuing decline in the growth rate of the atmospheric methane burden. *Nature,* **393,** 447–450.

——, B. P. Walter, K. A. Masarie, P. M. Lang, and E. S. Kasischke, 2001: Measurements of an anomalous global methane increase during 1998. *Geophys. Res. Lett.,* **28,** 499–502.

Dvortsov, V. L., and S. Solomon, 2001: Response of the stratospheric temperature and ozone to past and future increases in stratospheric humidity. *J. Geophys. Res.,* **106,** 7505–7514.

Dutton, E. G., and B. A. Bodhaine, 2001: Solar irradiance anomalies caused by clear sky transmission variations above Mauna Loa: 1958–99. *J. Climate,* in press.

Easterling, D. R., T. R. Karl, E. H. Mason, P. Y. Hughes, D. P. Bowman, R. C. Daniels, and T. A. Boden, 1996: United States Historical Climatology Network (U.S. HCN) monthly temperature and precipitation data. ORNL/CDIAC-87, NDP-019/R3. 280 pp.

Elkins, J. W., T. M. Thompson, T. H. Swanson, J. H. Butler, B. D. Hall, S. O. Cummings, D. A. Fisher, and A. G. Raffo, 1993: Decrease in the growth rates of atmospheric chlorofluorocarbons 11 and 12. *Nature,* **364,** 780–783.

Forster, P. M. de F., and K. P. Shine, 1999: Stratospheric water vapor changes as a possible contributor to the observed stratospheric cooling. *Geophys. Res. Lett.,* **26,** 3309–3312.

Gadgil, S. J., P. V. Joseph, and N. V. Joshi, 1984: Ocean-atmosphere coupling over monsoon regions. *Nature,* **312**, 141–143.

Gray, W. M., 1984: Atlantic seasonal hurricane frequency: Part I: El Niño and 30-mb quasibiennial oscillation influences. *Mon. Wea. Rev.,* **112,** 1669–1683.

Groisman, P. Ya., and D. R. Easterling, 1994: Variability and trends of precipitation and snowfall over the United States and Canada. *J. Climate,* **7,** 184–205.

Halpert, M. S., and G. D. Bell, 1997: Climate assessment for 1996. *Bull. Amer. Meteor. Soc.,* **78** (May), S1–S49.

Hastenrath, S., 1995: Recent advances in tropical climate prediction. *J. Climate,* **8,** 1519–1532.

Houghton, J. T., L. G. Meira Filho, B. A. Callander, N. Harris, A. Kattenberg, and K. Maskell, Eds., 1995: *Climate Change, 1995: The Science of Climate Change. Contribution of Working Group 1 to the Second Assessment Report of the Intergovernmental Panel on Climate Change*, Cambridge University Press, 572 pp.

Janowiak, J. E. and P. Xie, 1999: CAMS-OPI: A global satellite-rain gauge merged product for real-time precipitation monitoring applications. *J. Climate,* **12,** 3335–3342.

Jones, P. D., C. K. Folland, E. B. Horton, L. V. Alexander, T. J. Osborn, K. R. Briffa, D. E. Parker, and N. A. Rayner, 2001: Adjusting for sampling density in grid box land and ocean surface temperature time series. *J. Geophys. Res.,* **106,** 3371–3380.

Karl, T. R., 1986: The sensitivity of the Palmer drought severity index and Palmer's Z-index to their calibration coefficients including potential evapotranspiration. *J. Climate Appl. Meteor.,* **25,** 77–86.

——, R. W. Knight, and B. Baker, 2000: The record breaking global temperatures of 1997 and 1998: Evidence for an increase in the rate of global warming? *Geophys. Res. Lett.,* **27,** 719–722.

Karlsdóttir, S., and I. S. A. Isaksen, 2000: Hanging methane lifetime: Possible cause for reduced growth. *Geophys. Res. Lett.,* **27,** 93–96.

Kasischke, E. S., and Coauthors, 2000: Contributions of 1998 fires in the boreal forest to atmospheric concentrations of carbon monoxide and methane. *Eos, Trans. Amer. Geophys. Union,* **81,** 260.

Keeling, C. D., T. P. Whorf, M. Wahlen, and J. Vanderplicht, 1995: Interannual extremes in the rate of rise of atmospheric carbon dioxide since 1980. *Nature,* **375,** 666–670.

Kistler, R., and Coauthors, 2001: The NCEP–NCAR 50-year reanalysis: Monthly means CD-ROM and documentation. *Bull. Amer. Meteor. Soc.,* **82,** 247–267.

Landsea, C. W., G. D. Bell, W. M. Gray, and S. B. Goldenberg, 1998: The extremely active 1995 Atlantic hurricane season:

Environment conditions and verification of seasonal forecasts. *Mon. Wea. Rev.,* **126,** 1174–1193.

Lelieveld, J., P. J. Crutzen, and C. Brühl, 1993: Climate effects of atmospheric methane. *Chemosphere,* **26,** 739–768.

Mo, K. C., and V. E. Kousky, 1993: Further analysis of the relationship between circulation anomaly patterns and tropical convection. *J. Geophys. Res.,* **98,** 5103–5113.

Montzka, S. A., J. H. Butler, J. W. Elkins, T. M. Thompson, A. D. Clarke, and L. T. Lock, 1999: Present and future trends in the atmospheric burden of ozone-depleting halogens. *Nature,* **398,** 690–694.

——, C. M. Spivakovsky, J. H. Butler, J. W. Elkins, L. T. Lock, and D. J. Mondeel, 2000: New observational constraints for atmospheric hydroxyl on global and hemispheric scales. *Science,* **288,** 500–503.

National Research Council, 2000: Reconciling observations of global temperature change. National Academy Press, Washington, DC, 85 pp.

Oltmans, S. J., H. Vömel, D. J. Hofmann, K. H. Rosenlof, and D. Kley, 2000: The increase in stratospheric water vapor from balloonborne, frostpoint hygrometer measurements at Washington, D.C. and Boulder, Colorado. *Geophys. Res. Lett.,* **27,** 3453–3456.

Peterson, T. C., and R.S. Vose, 1997: An overview of the Global Historical Climatology Network temperature database. *Bull. Amer. Meteor. Soc.,* **78,** 2837–2849.

Prather, M. J., 1996: Natural modes and time scales in atmospheric chemistry theory, GWPs for CH_4 and CO, and runaway growth. *Geophys. Res. Lett.,* **23,** 2597–2600.

Quayle, R. G., T. C. Peterson, A. N. Basist, and C. S. Godfrey, 1999: An operational near-real-time global temperature index. *Geophys. Res. Lett.,* **26,** 333–335.

Reed, R. J., D. C. Norquist, and E. E. Recker, 1977: The structure and properties of African wave disturbances as observed during Phase III of GATE. *Mon. Wea. Rev.,* **105,** 317–333.

Reynolds, R. W., and T. M. Smith, 1994: Improved global sea surface temperature analyses using optimum interpolation. *J. Climate,* **7,** 929–948.

Robinson, D. A., 2000: Weekly Northern Hemisphere snow maps: 1966–1999. Preprints, *12th Conf. on Applied Climatology*, Asheville, NC, Amer. Meteor. Soc., 12–15.

Robinson, D. A., A. Bamzai, and B. Ramsay, 2001: Evaluating Northern Hemisphere snow cover during the satellite era: Variations in extent and associations with temperature. Preprints, *12th Symp. on Global Change and Climate Variations,* Albuquerque, NM, Amer. Meteor. Soc., 36–39.

Ropelewski, C. F. and M. S. Halpert, 1987: Global and regional scale precipitation patterns associated with El Niña/Southern Oscillation. *Mon. Wea. Rev.,* **115,** 1606–1626.

——, and ——, 1989: Precipitation patterns associated with the high index phase of the Southern Oscillation. *J. Climate,* **2,** 268–284.

Rosenlof, K. H., and Coauthors, 2001: Stratospheric water vapor increases over the past half century. *Geophys. Res. Lett.,* **28,** 1195–1198.

Shapiro, L. J., and S. B. Goldenberg, 1998: Atlantic sea surface temperatures and tropical cyclone formation. *J. Climate,* **11,** 578–590.

Simpson, R. H., 1974: The hurricane disaster potential scale. *Weatherwise,* **27,** 169–186.

Smith, T. M., and R. W. Reynolds, 1998: A high-resolution global sea surface temperature climatology for the 1961–90 base period. *J. Climate,* **11,** 3320–3323.

——, ——, R. E. Livezey, and D. C. Stokes, 1996: Reconstruction of historical sea surface temperature using empirical orthogonal functions. *J. Climate,* **9,** 1402–1420.

Spencer, R. W., and J. R. Christy, 1992: Precision and radiosonde validation of satellite gridpoint temperature anomalies, Part I: MSU channel 2. *J. Climate,* **5,** 847–857.

Stone, R. S., 1997: Variations in western Arctic temperatures in response to cloud radiative and synoptic-scale influences. *J. Geophys. Res.,* **102,** 21 769–21 776.

Thiaw, W. M., A. B. Barnston, and V. Kumar, 1999: Predictions of African Rainfall on the Seasonal Time Scale. *J.Geophys. Res.—Atmos.,* **104,** 31 589–31 597.

Thompson, D.W. J., and J. M. Wallace, 1998: The Arctic oscillation signature in the wintertime geopotential height and temperature fields. *Geophys. Res. Lett.,* **25,** 1297–1300.

Vose, R. S., R. L. Schmoyer, P. M. Steurer, T. C. Peterson, R. Heim, T. R. Karl, and J. Eischeid, 1992: The Global Historical Climatology Network: Long-term monthly temperature, precipitation, sea level pressure, and station pressure data. Rep. ORNL/CDIAC-53, NDP-041.

WMO, 1983: Guide to climatological practices. WMO-No. 100.